UNIVERSITÀ DEGLI STUDI DI PADOVA

Second Cycle Degree in Environmental Engineering
ICEA Department

Master Thesis

Luca Moresco

PHOTODEGRADATION OF A HYDROCARBONS CONTAMINATED SOIL: A LAB SCALE STUDY

Supervisors
Prof. Roberto Raga
Prof. Roberta Bertani

Academic Year 2013-2014

LIST OF CONTENTS

LIST OF TABLES

LIST OF FIGURES

1. INTRODUCTION AND THESIS OBJECTIVES

1.1 INTRODUCTION

In recent years, increasing ecological problems, connected with the presence of hydrocarbons in the environment, are observed. A serious issue is the remediation of soil contaminated with hydrocarbons derivatives originated by accidents or in places where specific working activities use hydrocarbons (i.e. oil-refineries, military bases, machine-shops, oil-pumps, place for machine demolition).

Hydrocarbons are found in the environment as hydrophobic pollutants like crude petrol, diesel, lubricants and fuels.

Most of the publications are addressed to the problem of removing hydrocarbon pollutants for the aquatic environment (Rosenberg et al., 1992; Turchi et al., 1993; Turchi and Mehos, 1992; Berry and Mueller, 1994). The removal of hydrocarbons from soil is still a rarely discussed problem.

The conventional methods currently used for hydrocarbons removal (such as combustion, extraction, biological methods) are not perfect. Their disadvantages are: low efficiency, long time of the process, secondary pollution of environment and high costs. Hence, it is necessary to search for alternative complementary methods in order to remove hydrocarbons from the environment.

Recently, there have been many publications connected with the application of semiconductors as photocatalysts and different light sources as activators of the process of organic pollutants degradation (Kaneko and Okura, 2002; Canle et al., 2012).

This study is related to an Italian soil which has been contaminated by an unknown mixture of petroleum hydrocarbons supplied by RE.AL. Spa, a company that deals with contaminated sites remediation, environmental investigation and ecological emergency.

1.2 THESIS OBJECTIVES

The aim of this study is to investigate the availability of photocatalytic methods for hydrocarbons degradation in the soil.

In particular the thesis involves the evaluation of many experimental parameters (such as reaction time, TiO_2 amount, pH, influence of H_2O_2) in order to optimize the process which was previously preliminarily tested (Burigo, 2014) demonstrating that photocatalysis mediated by TiO_2 nanoparticles and UV lamps was able to reduce the hydrocarbons content in the contaminated soil.

A further topic of the thesis is to check the possible formation of by-products, which could be, in principle, more dangerous than the starting pollutants.

Moreover, he results will be compared with those of other oxidative degradation processes.

The final target is to propose an efficient process to apply in addition to other methods for soil remediation in order to reach the law limits.

It is to remember that D.Lgs 152/2006, Part IV, V, Annex 5 (Table 1) reports the limits of concentration of > C_{12} hydrocarbons in soil matrix (50mg/kg for green areas; 750 mg/kg for industrial areas).

2. PHOTOCATALYSIS

2.1 PROCESS DESCRIPTION

In chemistry, photocatalysis (Kaneko and Okura,2002) is a reaction occurring with light, which is sped up due to the presence of a photocatalyst. This latter, reduces the activation energy of a given photoreaction.

The system considered to carry out the process in this case study, consists in a mixture of semiconductor nanoparticles, contaminated soil and water, which is then exposed to UV lights, to let the reaction occurring faster.

From the photocatalyst exposure to light, excited states are generated which are able to start chain processes such as redox reactions and molecular transformations.

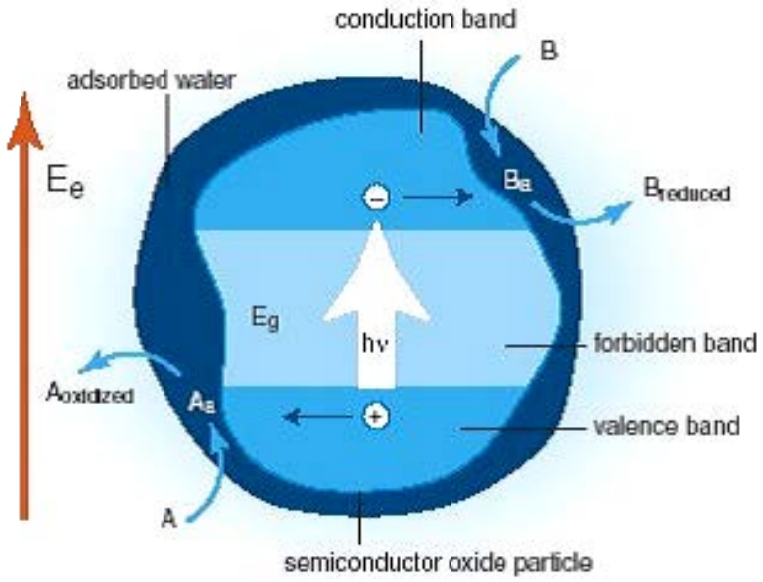

Figure 2.1. Photoexcitation of a semiconductor particle [Licciulli et al. 2006].

Figure 2.1 shows the general reaction scheme of a photocatalytic process.

The most general semiconductors utilized are metal oxides as ZnO and TiO_2, or sulphides as ZnS.

Because of the electronic structure, which is characterized by a complete valence band (VB) and an empty conduction band (CB), they can behave as sensitizers for photo-induced redox processes.

The difference between the lowest CB level and the highest VB one is called “energy gap” and it corresponds to the minimum light required to let the material be a conductor.

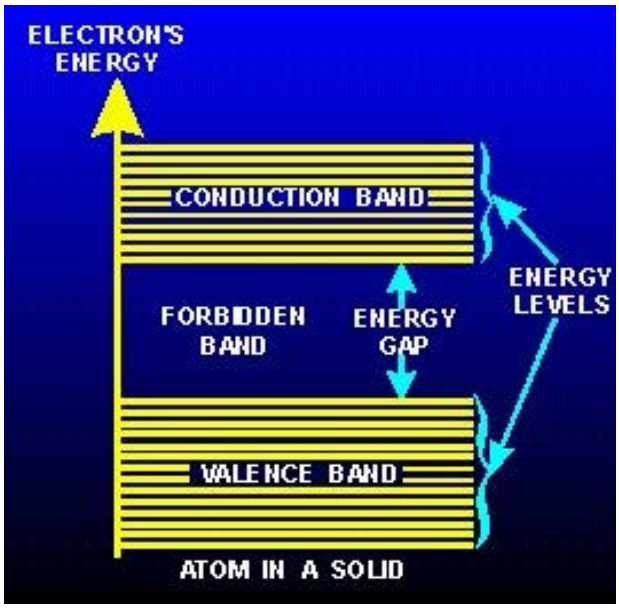

Figure 2.1.1. Energy gap and valence and conduction band of a semiconductor. [Licciulli et al. 2006].

The formation of the mobile energy carriers is possible due to three mechanisms:

- The thermal excitation: if the energy gap is < 0.5 eV , the process may promote an electron from the VB to the CB;
- The photoexcitation: the electron promotion from the VB to the CB may occur thanks to an absorption of a photon, as long as hν > Eg;
- The doping: with additional elements able to reduce the energy gap with the oxidation or the reduction of the absorbed specie on the semiconductor surface.

If the photon has an energy hν > Eg, an electron, e^-, is promoted from the VB to the CB leaving behind a positive lacuna h^+. In the semiconductors some of these pairs e^- - h^+ diffuses among the particle catalytic surface and take part to the photochemical reaction with the absorbed molecules: the donor D and the acceptor A.

The following reactions show how lacunas h^+ can oxidize donor molecules (1), while CB electrons can reduce electron acceptor.

$$D + h^+ \rightarrow D^{\bullet +} \quad (1)$$

$$A + e^- \rightarrow A^{\bullet -} \quad (2)$$

A peculiar property of metal oxides semiconductors is the strong oxidant capacity of the lacuna h^+, which can react with the absorbed water on their surface. This leads to the formation of an highly reactive •OH radical as reported in the following reaction (3)

$$H_2O + h^+ \rightarrow {}^{\bullet}OH + H^+ \quad (3)$$

Both the lacuna h^+ and the hydroxyl radicals are strongly oxidants, therefore they can be used to oxidize the majority of the organic contaminants.

Also the oxygen present in the air has a fundamental role, in fact it acts as electron acceptor to form super-oxide ions, as described as follows (4).

$$O_2 + e^- \rightarrow \bullet O_2^- \quad (4)$$

Super-oxide ions are highly reactive particles which can oxidize organic compounds, and this is the reason why, for instance, TiO_2 is really important for the air and water depuration.

Thermodynamically, the level of the potential of the acceptor specie must be lower than the CB of the semiconductor, otherwise the level of the potential of the donor must be higher to the one of the VB of the semiconductor in order to yield an electron or emptying a h^+. The bands boundaries for several semiconductors are reported in Figure 2.1.2.

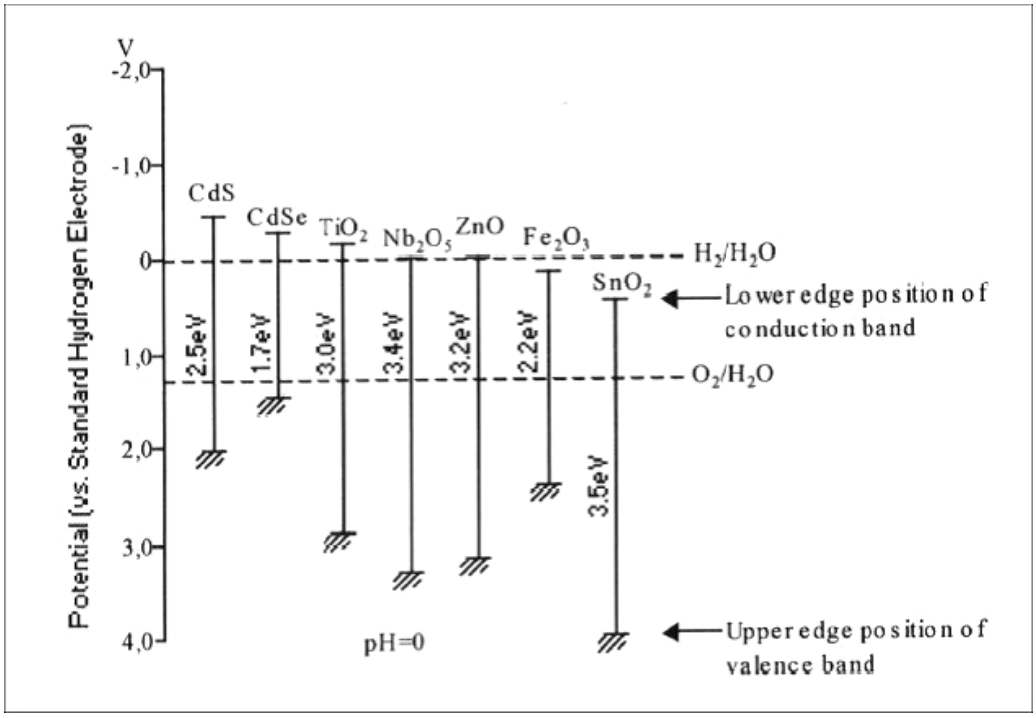

Figure 2.1.2. Bands boundaries for several semiconductors. [Licciulli et al. 2006].

Summarizing , in a photocatalytic process the reactions involved are:

$$\text{semiconductor} + h\nu \rightarrow e^- + h^+ \quad (5)$$

$$e^- + h^+ \rightarrow \text{heat} \quad (6)$$

$$e^- + O_2 \rightarrow \bullet O_2^- \quad (7)$$

after the super-oxide radical generation:

$$\bullet O_2^- + H_2O \rightarrow HO_2 + OH^- \quad (8)$$

$$HO_2 + e^- \rightarrow HO_2^- \quad (9)$$

At the end hydroxyl radicals are formed:

$$OH^- + h^+ \rightarrow \bullet OH \quad (10)$$

The process can be schematized as follows (Figure 2.1.3).

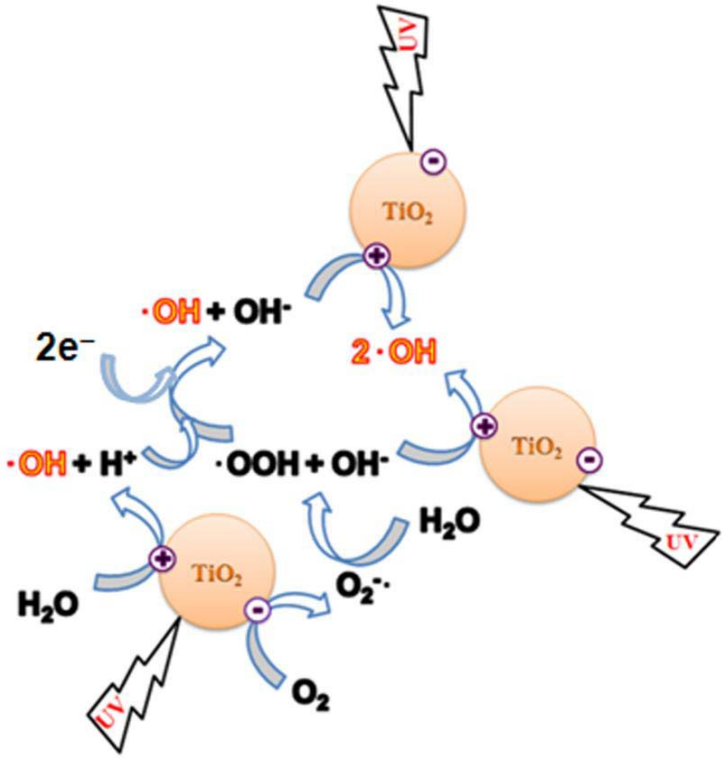

Figure 2.1.3. Schematization of the photocatalytic process [Lazar et al., 2012].

The process of charge transfer is very important in the analysis of the whole process efficiency. Also, beside this aspect, the process efficiency depends on the ability of adsorption of substances to be degraded on the photocatalyst particle surface.

The latter, is a critical point because the extremely reactive radicals formed have a short lifetime, so that they are characterized by a short radius of diffusion in the eventual solution present.

At the same time,it is important that the desorption of the oxidized molecules is fast to let the active sites become free to accommodate new molecules.

Also the success of the process is due to the energy of the incident photons and not on their intensity, meaning that even few of them having the necessary energy are able to stimulate the photocatalytic activity (Tobaldi, 2009).

As for the process kinetic, it follows a Langmuir – Hinshelwood one, where the reaction rate R is proportional to the extent of overlap of the absorbed species θ, according to the following equation:

$$R = \frac{dc}{dt} = k * \theta = \frac{k * KC}{1 + KC}$$

Where:

- k = reaction constant;
- K = adsorption coefficient;
- C = reactant concentration.

When the reactant concentration is low the term KC is negligible (with respect to 1) and the reaction can be modeled as a pseudo 1st order kinetic.

2.2 THE CATALYST : TiO_2

Titanium dioxide is the most investigated semi-conductor material for the photocatalysis applications and it is the one considered in this case study.

The TiO_2 used here is commercial P25 developed by the company Evonik Degussa. The nominal size of the nanoparticles is about 21 nm and agrees with the features included in the product card present in Evonik database. The specific surface area is about 50±15m^2/g (Evonik).

An ideal catalyst must have some minimum requirements (Kaneko and Okura, 2002):

- high crystallinity;
- larger surface area, that correspond to a higher rate of surface reaction of e^- and h^+.

If the specific surface increases, without changing the surface properties, also the rate of reaction increases because the amount of substrates adsorbed on the photocatalyst is higher. Titania is an oxide semiconductor that has a high reactivity and it can be chemically activated by sunlight too. In fact through the direct absorption of the incident photons, it may participate in photochemical surface processes. This high photocatalytic activity, due to its chemical and physical characteristics, has been the subject of numerous studies from as early as 1972 in Japan, but the analysis of the process has intensified especially in recent years. In particular, TiO_2 was the most effective catalyst, compared to other employees, in the degradation of many contaminants of interest.

The practical importance of titanium dioxide is demonstrated by its use in electro-chemical processes and as a pigment for paints and polymers. The optical and electronic properties of TiO_2 have numerous applications in gas sensors, antireflection coatings for solar cells and energy conversion processes in photo - chemistry.

Peculiarities of this semiconductor are that it is relatively inexpensive to produce in large amounts, available in nature, chemically stable, not harmful, biocompatible and with a more efficient photoactivity (Kaneko and Okura, 2002). During the photocatalysis the titania maintain its properties, in fact the process takes place without the support is degraded, and a continuous and constant effectiveness over time is guaranteed.

The titanium dioxide exists in three different crystal structures, rutile, anatase and brookite (Figure 2.2), and an amorphous phase. Brookite has an orthorhombic structure, the other two forms instead have a tetragonal structure containing three distorted octahedra, in particular the structure of tetragonal rutile contains two molecules of TiO_2 for primitive cell. Rutile and anatase are the most common forms in nature.

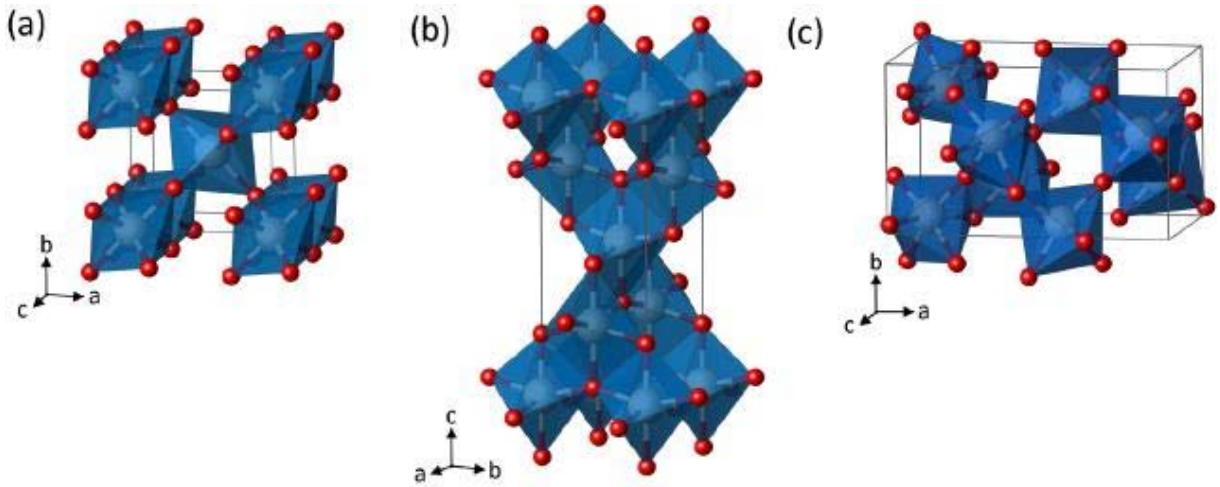

Figure 2.2. TiO_2 crystalline structures (a) rutile , (b) anatase, (c) brookite [Lazar et al., 2012].

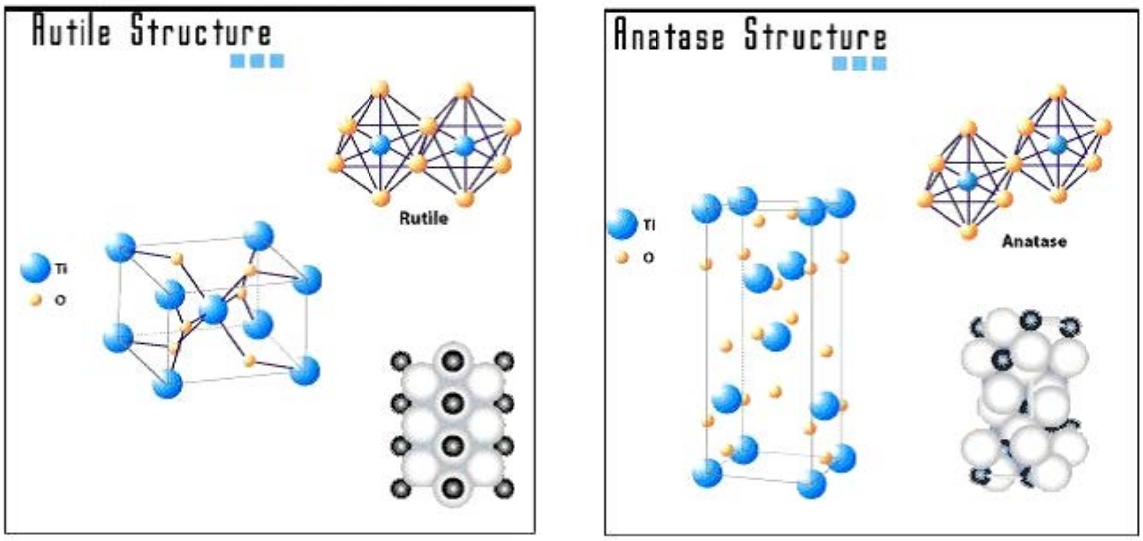

Figure 2.2.1. Crystalline structure of the rutile (left) and anatase (right) [Lazar et al., 2012].

In Figure 2.2.1, the larger spheres represent the atoms of titanium while the smallest the oxygen atoms .

Each titanium atom is surrounded by a slightly distorted octahedron of oxygen atoms.

TiO_6 octahedra are the basic structural unit of the various polymorphic structures.

The major structural differences between the different forms are in the number of shared octahedra , for instance two in rutile , three in brookite and four in anatase.

Rutile is the thermodynamically most stable crystalline form and is the most industrially used while anatase is metastable and among the three forms is the most active as a photocatalyst and is therefore the most technologically used.

Optical absorption measurements have shown that anatase has a higher absorption threshold of rutile. In particular, for rutile the energy gap Eg is equal to 3.3 eV while for anatase is equal to 3.18 eV . Rutile has a density of 4.2 g /mL , anatase of 3.9 g / mL .

Thanks to its ability to combine the high refractive index with the high degree of transparency in the region of the visible spectrum, titanium oxide semiconductor is the best studied in the field of chemical conversion and storage of solar energy despite that absorbs only 5% of the incident solar radiation.

In fact, comparing the refractive index of rutile and of anatase with that of other materials it is clear that the greater is the difference between the index of the material and that of air, the greater will be the reflection of light .

The refractive index (n) is defined as the ratio between the speed of light in vacuum and in the material and for rutile worth 2.76 while for anatase worth 2.52.

Table 2.2. Typical physical and mechanical properties of titania.

Property	Value
Density	4 gcm^{-3}
Porosity	0%
Modulus of rupture	140MPa
Compressive strength	680MPa
Poisson's ratio	0.27
Fracture toughness	3.2 $Mpa.m^{-1/2}$
Shear modulus	90GPa
Modulus of elasticity	230GPa
Microhardness (HV0.5)	880
Resistivity (25°C)	10^{12} ohm.cm
Resistivity (700°C)	$2.5x10^{4}$ ohm.cm
Dielectric constant (1MHz)	85
Dissipation factor (1MHz)	$5x10^{-4}$
Dielectric strength	4 $kVmm^{-1}$
Thermal expansion (RT-1000°C)	9 x 10^{-6}
Thermal conductivity (25°C)	11.7 WmK^{-1}

Despite the performance of pure anatase as photocatalyst, according to the literature, the mixture of anatase and rutile exhibits a greater photocatalytic activity, thanks of the combination of the respective energy gaps (Kaneko and Okura,2002; Kim et al., 2012).

Increasing of the efficiency of photocatalytic titanium oxide is one of the main goals of scientific research that has as its object this particular material. It is possible, in fact, acting on different aspects involved in the overall photocatalytic process as, for instance, the capacity of absorption and desorption of the molecules on the photocatalyst, the rate of charge transfer at the interface and the absorption spectrum of the material.

Titanium dioxide may also be doped with different elements metal ions such as alkaline earth metals Ca^{2+}, Sr^{2+} and Ba^{2+}, transition metals V^{+}, Cr^{+}, Mn^{+}, Fe^{+} (Yamashita H., Harada et al. 2001), Fe^{3+}, Cr^{6+}, Mn^{2+}, Cr^{3+}, CO_2 +, CO_3^{+}, Mo^{5+} (Brezová, Blazkova et al. 1997; Dvoranová, Brezová et al. 2002; Carp, Huisman et al., 2004) and Al^{3+} (Teodorescu, Blanchin et al . 1999), Ga^{3+}, In^{3+} (Wang, Cheng et al. 1999), Ag^{+} (Herrmann, Tahiri et al. 1997), Ru^{3+} (Choi, Termin et al. 2002), Nd^{5+} (Wang, Cheng et al. 1999) , Sb^{5+} (Moon, Takagi et al., 2001) and rare earths (La^{3+}, Ce^{3+}, Er^{3+}, Pr^{3+}, Gd^{3+}, Nd^{3+}, Sm^{3+}) (Carp, Huisman et al. 2004). Also, titanium dioxide can be doped with N and with C in order to let it be active in presence of visible light (380-760 nm),

or better, by extension, the sunlight (360-830nm) (Noguchi et al., 2005; Cong et al., 2006; Palanivelu et al., 2007; Chen et al., 2007., Xu Q.C. et al., 2011; Wang et al., 2014).

In the photocatalytic process the water absorbed on the surface of titanium dioxide is oxidized from lacunas and it forms hydroxyl radicals (•OH). After this, the radicals react with organic matter. If oxygen is present in this reactive process, the radicals, which are among the organic compounds and oxygen molecules, start a chain reaction (reactions ranging from (1) to (4) are repeated). Finally, the organic materials decompose into carbon dioxide and water.

On the other hand the electron deoxidizes and generates super-oxide ions ($\bullet O_2^-$) as shown in the following reaction (11).

$$OH^- + h^+ \rightarrow \bullet OH$$

$$O_2 + e^- \rightarrow \bullet O_2^- \qquad (11)$$

The TiO_2 surface is covered with hydroxyl groups when it is in contact with water, in fact, when the water is dissociated on the surface of pure titania, forms two distinct hydroxyl groups. (Figure 2.2.2).

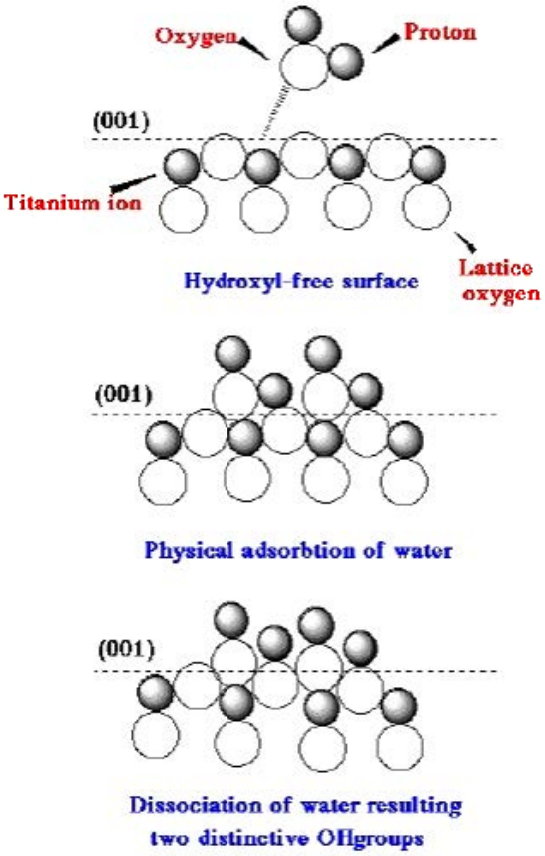

Figure 2.2.2. Hydroxyl groups produced on the TiO_2 surface [Lazar et al., 2012].

Another very interesting property of titania is super-hydrophilicity, which manifests itself on the surface of the material after exposure to UV light. The super-hydrophilicity and hydrophobicity are the two main ways to achieve self-cleaning materials. The wettability of a solid with water, where the air is the surrounding medium, depends on the relationship existing between the surface tensions at the interface (air-water, water-solid, solid-to-air). The relationship between these voltages, determines a contact angle θ.

If θ is zero the wetting is complete, if it has a value of 180° the coverage is incomplete. To obtain hydrophilic surface θ must decrease resulting in a higher adhesion.

Water-repellency possessed by the surfaces of plants has long been known. Recently, the correlation between microstructure, wettability and pollutants, in particular, using the lotus leaves, has been studied. This area with its micro-irregularities shows contact angles higher than 130°, then the adhesion of water is particularly low.

By transferring the microstructure of materials used for practical applications, it is possible to develop super-hydrophobic surfaces. When water is in contact with these surfaces is contracted immediately into droplets. Particles of pollutants adhere to the surface of the droplets and are removed when they roll.

If TiO_2 in the anatase crystalline form is exposed to UV light, contact angles < 1° are obtained. These materials have the rare property to attract rather than repel it .

This characteristic is called super - hydrophilicity in which practically water stays flat on the surface instead of forming droplets. If the exposure stops, the super-hydrophilic behavior remains for about two days.

In addition, the UV illumination of titania leads to the formation of potent agents with the ability to oxidize and decompose many types of bacteria and organic and inorganic materials.

2.3 ENVIRONMENTAL APPLICATIONS OF PHOTOCATALYSIS : WATER & AIR DEPURATION

2.3.1 Water depuration

The presence of organic compounds in industrial wastewater is a serious environmental problem. These substances are generally removed with the use of absorbent or coagulant treatments, but, according to the new laws need to be matched by other processes.

An alternative to the conventional methods is represented by advanced oxidation processes (AOPs) based on the generation of highly reactive species such as hydroxyl radicals (•OH) which result from the photocatalytic process.

The literature concerning the water depuration by means of photocatalysis using TiO_2 is very wide and the case studies can be summarized as follows (Table 2.3.1).

Table 2.3.1. Literature case studies regarding water treatment using TiO_2 mediated photocatalysis.

Contaminant	Photocatalytic system	Reference
Dyes		
Reactive violet 5	UV/Anatase powder (Sigma Aldrich)	Chung et al., 2009
Blue 9, Red 51& Yellow 23	Solar/TiO_2 (Evonik Degussa P25)	Dias et al., 2009
Methyl orange	UV/TiO_2 on glass	Lopez et al., 2010
Methylene blue	UV/TiO_2 (Merck) on volcanic ash	Esparza et al., 2010
Rhodamine B	UV/TiO_2 bilayer	Zhuang et al., 2010
Pesticides & herbicides		
Organophosphate & Phosphonoglycine	UV/TiO_2 immobilized on silica gel	Echavia et al., 2009
Azimsulfuron	UV/TiO_2 coated on glass rings	Pelentridou et al., 2009
Swep residues	Simulated sunlight/TiO_2 (Evonik Degussa P25)	Fabbri et al., 2009
Pharmaceuticals & cosmetics	Electrocoagulation & UV/TiO_2/H_2O_2	Boroski et al., 2009
	UV/TiO_2 (Aeroxide P25)	Rizzo et al., 2009 Radjenovic et al., 2009 Choina et al., 2010
	TiO_2/Fe_3O_4 & TiO_2/SiO_2/Fe_3O_4	Alvarez et al., 2010
Benzylparaben	UV/TiO_2 (Evonik Degussa P25)	Lin et al., 2011
Drugs		
Oxolinic acid	UV/TiO_2 (Evonik Degussa P25)	Giraldo et al., 2010
Atenolol & propranolol	UV/Commercial TiO_2	Hapeshi et al., 2010
	Solar/TiO_2 (six commercial samples)/H_2O_2	Ioannou et al., 2011
Ciprofloxacin, ofloxacin, norfloxacin &	UV/TiO_2 (Evonik Degussa P25)	An et al., 2010

Table 2.3.1. (continued).

Enrofloxacin		
	Simulated solar/TiO_2 P25	Li et al., 2012
Lamivudine	UV/TiO_2 (Evonik Degussa P25)	An et al. 2011
Oxytetracycline	UV/TiO_2 (Evonik Degussa P25)	Pereira et al., 2011
Others		
N,N-diethyl-m-toluamide (Insect repellent)	UV/TiO_2 (Evonik Degussa P25)	Medana et al., 2011 Adams et al., 2009
β-naphthol	UV/TiO_2-SiO_2	Qourzal et al., 2009
15 emerging contaminants	Solar UV/TiO_2 coated on glass spheres	Miranda-Garcia et al., 2010
Grey water	UV/TiO_2 (Aeroxide P25)	Sanchez et al., 2010
Microcystins (Cyanotoxin)	UV/TiO_2 film	Antoniou et al., 2008 Sharma et al., 2012
	UV/Doped TiO_2	Graham et al., 2010
	UV/ Nitrogen doped TiO_2	Triantis et al., 2012
Lipid vesicles & E. coli cells	UV/TiO_2 (Evonik Degussa P25)	Darlymple et al., 2011
Bacterial colony	UV/TiO_2 on titanium beads	Amarjargal et al., 2012
Paper mill wastewater	UV/TiO_2-coated bio-film	Li et al., 2011
	Solar/TiO_2	Ghaly et al., 2011
Endocrine disrupting compounds	UV/TiO_2 (Evonik Degussa P25)	Zhang W. et al., 2012
Municipal waste water	Solar/sol-gel TiO_2 & Evonik Degussa P25	Miranda-Garcia et al., 2011
Chlorophenols	UV/TiO_2 (Evonik Degussa P25) doped with Zr^{4+}	Venkatachalam et al., 2006
	Visible light/ TiO_2 nanoparticles	Cheng et al. , 2007

2.3.2 Air depuration

From literature, it is noticeable that the number of scientific publications dedicated to photocatalytic air treatment is significantly lower than the number of the ones related to photocatalytic water treatment.

Yet, this comparison is reversed when considering the number of relevant patents (Paz, 2010).

This indicates a growing interest in the implementation of photocatalysis for air treatment purposes, which surpasses that of water treatment.

As for indoor air treatment, which is basically any air-containing environment that is at least partially disconnected from outside environment, in a manner that the physical conditions prevailing are different, in terms of gas composition, temperature, pressure and so on.

In the majority of the cases, the levels of pollutants in the confined places are above the ambient concentrations outside.

Indoor environment term is relevant not only to buildings, but also to underground garages, vehicles, aircrafts, storehouses and similar. The indoor air environment is, at least to some extent, controllable. The control can be obtained by a variety of means, some of which can be very simple, such as open a window, whereas others can be quite sophisticated. The variety of chemicals which can be emitted indoors is enormous. Investigations of gaseous contaminants in buildings, have shown that the concentrations of individual species are in the order of 0.1 parts per million by volume (ppmv), and that the total concentration of VOCs is between 0.5 and 2.0ppmv (Obee, 1995). Among the contaminants can be found formaldehyde, acetaldehyde, aromatic compounds, hydrocarbons, NOx and CO. Photocatalysis seems to be well-suited for the purification of indoor air, in particular if compared with purification of water. To this, one may add the possibility of using photocatalysis for both VOCs mineralization and bacterial disinfection, upon addition of metallic nanoparticles. At any case, the photocatalytic market is still dominated by products utilizing super - hydrophilicity and by self-cleaning surfaces (some of which claim to have air purification properties). Indoor air treatment is carried out usually by using apparatuses through which air is circulated. Such systems contain a blower or an air-pump, a particulates filter or an electrostatic precipitator, a light source and a photocatalyst such as presented in Figure 2.3.2.

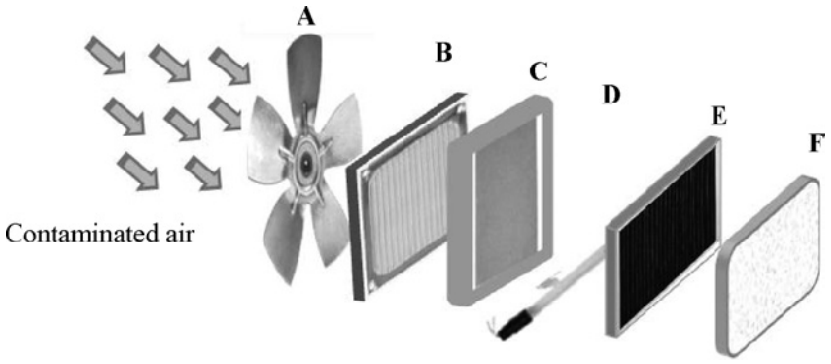

Figure 2.3.2. A schematic view of a photocatalytic indoor air treatment device. Changes may vary from product to product. (A) fan, (B) particulates (HEPA) filter, (C) photocatalyst, (D) light source, (E) activated carbon filter (optional) and (F) ionizer generator (optional).

It is common that the photocatalyst is fixed on a substrate, either in a three dimensional porous structure or a honeycomb-type construction to reduce pressure drop.

The photocatalytic air treatment reactors can be classified according to their geometry or according to the way by which the photocatalyst is introduced into the reactor. In terms of geometry the most common are tubular, annular and flat plate types of reactors. In terms of the photocatalyst type and arrangement of the photocatalyst within the reactors one finds a large variety of types. Can be found powder layer reactors and fluidized bed reactors (usually in a tubular geometry) were among the

first to be used. Coated wall-parallel flow reactors and honeycomb/foam monolithic reactors are probably the most abundant products nowadays. One may also find packed bed reactors, plasma driven reactors and permeable layer reactors. Another way for indoor air treatment uses photocatalytic surfaces such as painted walls or transparently coated windows. In that case, operation relies on natural convection, or on circulation of air by air-conditioning systems. The light source in this case can be either the regular light source of the indoor space or low intensity diffused solar light entering the indoor space.

As regards instead outdoor air treatment the main task is to use large area construction objects as platforms for air decontamination. For instance, those platforms can be walls, roofs, roads, pavements, bridges and buildings. Photocatalysis can be specifically adequate for outdoor treatment of NO_x, emitted at large by vehicles, as the nitric acid formed during the photocatalytic oxidation can be washed away by rain. The photocatalyst can be applied in various forms including in situ made concrete objects and over-coated thin layers. Quite often, these types of coatings are referred as "self-cleaning coatings", since photocatalytic coatings on construction materials act also to prevent the adsorption of soot or dust that tend to stick to grimy surfaces.

Outdoor air treatment differs from indoor air treatment by the type of contaminants consisting in principally less VOCs and more NOx, CO and SOx, by the use of solar light as the dominant irradiation source, by the fact that the primary task of the photocatalytic platforms is to serve for construction (unlike indoor-air treatment devices that are especially constructed and designed for air cleaning) and not less important, by their visibility to the general public. An example of application of titania in concrete is schematized in the following Figure 2.3.2.a.

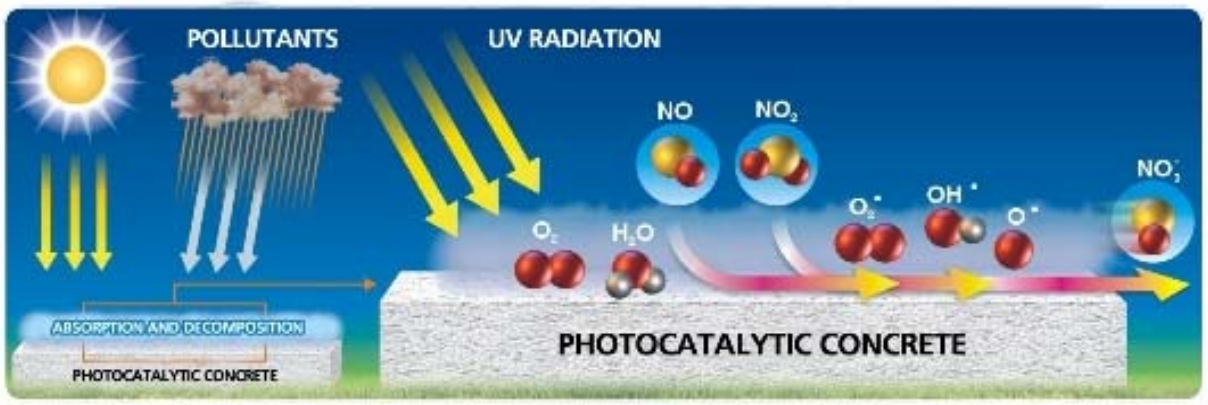

Figure 2.3.2.a. Schematization of the mechanism of action of the photocatalytic concrete [Ministry of transportation, Ontario].

Table 2.3.2. summarizes the main experiments conducted in air treatment by means of heterogeneous photocatalysis with titania.

Table 2.3.2. Literature case studies regarding air treatment using TiO_2 mediated photocatalysis.

Contaminant	Photocatalytic system	Reference
Ethanol	UV/TiO_2 (Evonik Degussa P25) doped with Fe,Pd and Cu	Araña et al. , 2004
Toluene	UV/TiO_2 (Millenium Chemicals S5-300B)	Demeestere et al. , 2008
	UV/TiO_2 pellets	Bouzaza et al. , 2002
Toluene and trichloroethylene	UV/TiO_2 (Evonik Degussa P25) doped with Pt and Ag	Young et al. , 2008
	UV/TiO_2 gel (Evonik Degussa P25)	Keshmiri et al. , 2006
Trichloroethylene	UV/TiO_2 (Evonik Degussa P25)	Mohseni, 2005
Toluene, n-hexane and n-butyl acetate	UV/TiO_2 (Kronos VLP7000)	Moulis et al. , 2013
VOCS	UV/TiO_2 (Millenium Chemicals PC500)	Deveau et al. , 2007
	UV/TiO_2-coated fibers glass mesh (Matrix Photocatalytic)	Pichat et al. , 2000
	UV/TiO_2-SiO_2 pellets	Zou et al. , 2006
"Bacteria"	UV/TiO_2 (Evonik Degussa P25)	Huang et al. , 2009

3. STATE OF THE ART IN THE THESIS FIELD: SOIL REMEDIATION

The soil remediation by means of photocatalytic process using TiO_2 is a quite new object of interest and it is less discussed in literature compared with the air and water depuration explained before. In literature, many publications on ferric oxides mediated photocatalysis in a soil matrix are found.

The photodegradation of bisphenol-A on the surface of iron oxides has been studied showing that the process depended strongly on pH value and light source (UV light > visible light). The degradation was greatly promoted by the addition of organic acids and alumina (Li et al., 2006; Li et al., 2007). The addition of transition metal cations, including Cu^{2+}, Ni^{2+} and Mn^{2+}, could accelerate 2-mercaptobenzothiazole photodegradation in the γ-Fe_2O_3/oxalate suspension under UV-A light irradiation (Wang et al., 2008).

The degradation of PAHs and organochlorine pesticide on soil surface in the presence of Fe_2O_3 using UV light source was investigated (Zhang et al., 2011) also in combination with TiO_2 (Zhang et al., 2006; Zhao et al., 2004). It was observed that, generally, humic substances inhibit the photocatalytic degradation, while the degradation rate increases with the soil pH value.

In any case, the photocatalysis mediated by TiO_2 is a technology in ongoing development as shown by quite recent papers. The case studies can be summarized in the following Table 3.1.

Table 3.1. Literature case studies regarding soil remediation using TiO_2 mediated photocatalysis.

Contaminant	Photocatalytic system	Reference	Contamination	Contamination amount
Pesticide				
Diuron	Sunlight/TiO_2 (Evonik Degussa P25)	Higarashi et al., 2002 (a)	induced	0.1 mg/g soil
Pesticide swep and surfactancts	UV/ TiO_2 (Evonik Degussa P25)	Fabbri et al., 2009 (b)	induced	0.13 mg/g soil
Aromatic compounds (benzene, chlorobenzene, naphtol…)	Simulated sunlight/ TiO_2 (Evonik Degussa P25)	Fabbri et al., 2008 (c)	**real**	0.3 mg/g soil
PAH	UV/TiO_2 nanoparticles	Zhang L. et al., 2008 (d)	induced	0.04 mg/g soil
	UV/TiO_2	Karaca et al., 2013 (e)	induced	0.04 mg/g soil
	UV/TiO_2	Karaca [a] et al., 2014 (f)	induced	0.04 mg/g soil

Table 3.1. (continued).

	UV/TiO_2/DEA	Karaca [b] et al., 2014 (g)	induced	0.04 mg/g soil
(anthracene)	UV/TiO_2	Karam et al., 2014 (h)	induced	0.04 mg/g soil
(pyrene)	UV/TiO_2 nanoparticles	Zhang L. et al., 2010 (i)	induced	0.04 mg/g soil
	UV/TiO_2 nanoparticles	Dong et al. , 2010 [b] (j)	induced	0.04 mg/g soil
(pyrene, phenathrene)	UV/TiO_2 nanoparticles	Dong et al., 2010 [a] (k)	induced	0.04 mg/g soil
	UV/TiO_2	Yang et al., 2014 (l)	induced	0.3 mg/g soil
(phenanthrene)	Visible light/ TiO_2 nanoparticles	Hanzhong et al., 2012 (m)	induced	0.1 mg/ g soil
Oil	Sunlight/TiO_2 slurry	Hamerski et al., 1999 (n)	induced	0.7 mg/g soil
PCB	UV/TiO_2/surfactants	Zhu et al., 2012 (o)	induced	0.03 mg/g soil
Bacteria	Visible light/ TiO_2-Pt	Chen et al., 2012 (p)	induced	0.02mg/g soil
Phytotoxic substances	UV/TiO_2	Qiu et al., 2013 (q)	induced	0.1 mg/g soil
Chlorophenols	UV/TiO_2/surfactant	Davezza et al., 2013 (r)	induced	0.03mg/g soil
Sulfonylurea herbicide residues	UV/TiO_2/ZnO UV/VIS light	Fenoll et al., 2013 (s)	induced	0.2 mg/g soil
Herbicides (ureas)	UV/TiO_2/ZnO	Fenoll et al., 2014 (t)	induced	0.1 mg/g soil
Dioxin	UV/TiO_2	Binh et al., 2014(u)	induced	0.03 mg/g soil
Cr (VI)	UV/TiO_2	Lopez-Vasquez et al., 2013 (v)	induced	0.11mg/g soil
	UV/TiO_2	Barrera-Diaz et al., 2012 (w)	induced	0.1mg/g soil

The most important thing to underline in the soil remediation context is that in most of the case studies the soil samples are artificially contaminated just to see the potential efficiency of the photocatalytic process in real case studies.

The only case in Table 3.1 related to a real contaminated soil is the one reported in the article by Fabbri et al. of 2008, dealing with a site contaminated by aromatic compounds.

This is consistent to the fact that this is an ongoing developing technology, therefore before being applied it must be tested. This concept is remarked in all the papers in the literature.

But, at the same time it is a drawback, due of the existence of a lack of knowledge.

In particular because of in real contaminated sites mixture of pollutants are present and not only a single specie, it is therefore more difficult to verify, or less, the possible effectiveness of the process, because each component reacts in a different way.

Another problem can be presented by the fact that different soils can behave in a different way, so that a deep examination of the influence of the different compounds present in the soil could be useful in order to optimize the photocatalytic process.

In accordance to the reference with IDs (c), (d), (e), (f), (g), (h), (i), (j), (k) ,(l), (m), (p), (q) and (r), the degradation of aromatic compounds, including polycyclic aromatic hydrocarbons and chlorophenols is reported. The TiO_2/UV light is in general considered an efficient method for the significant reduction of hydrocarbons (up to 95%) in addition to soil cleaning in the presence of surfactants. The influence of different parameters has been investigated such as:

- Wavelength (a, d);
- pH (d);
- Soil particle size (i);
- Humic acids concentrations (i);
- TiO_2 amount, crystallinity and morphology (f, k, p);
- Presence of H_2O_2 (j);
- Light intensity (j);
- Presence of additional ions as reagents (e, m);
- Presence of surfactants (c, g, l, o, p, r);
- Temperature (f, h);

Also, the photocatalytic degradation of pesticides and herbicides (carbamates, ureas, dioxins) was studied (b, q, s, t, u) observing significant enhancing of the degradation efficiency if TiO_2 is mixed with ZnO (s, t); the in-situ photocatalytic reduction of Cr(VI) in contaminated soil was studied (v, w).

An important aspect to remark is that, in many cases (a, b, c, g, h, l, o, t, u), the UV/TiO_2 mediated photocatalysis regards soils contaminated with persistent hydrocarbons pollution. More precisely, this methodology is implemented after other ones that are cheaper or, anyway, it is applied in a old contaminated soils which contamination was higher in the beginning.

4. INSTRUMENTS AND METHODS

4.1 TYPICAL PHOTOCATALYTIC EXPERIMENT

In a typical photocatalytic experiment 5g of polluted soil, different amounts of TiO_2 (P25 by Evonik Evonik Degussa) mixed with 5 mL of deionized water were used (Figure 4.1).

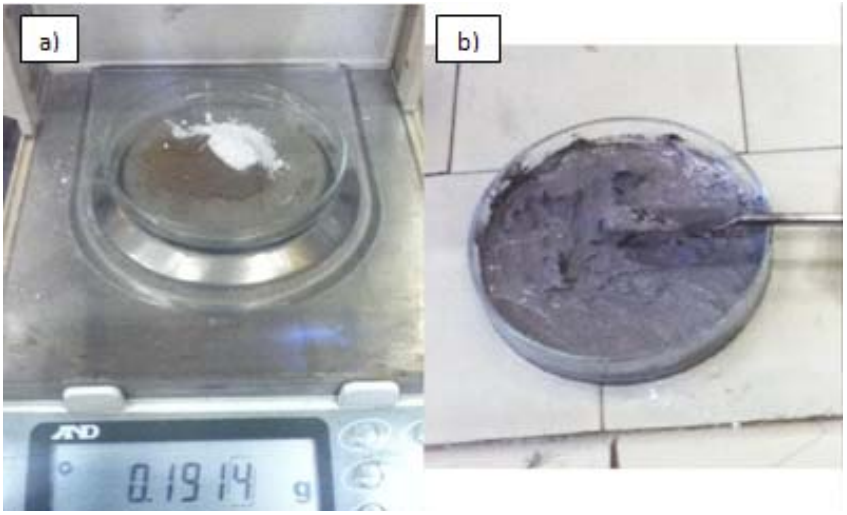

Figure 4.1. Photocatalysis preparation: a) weighting, b) mixing.

This mixture was then irradiated with UV lights under the device shown in Figure 4.1.1.

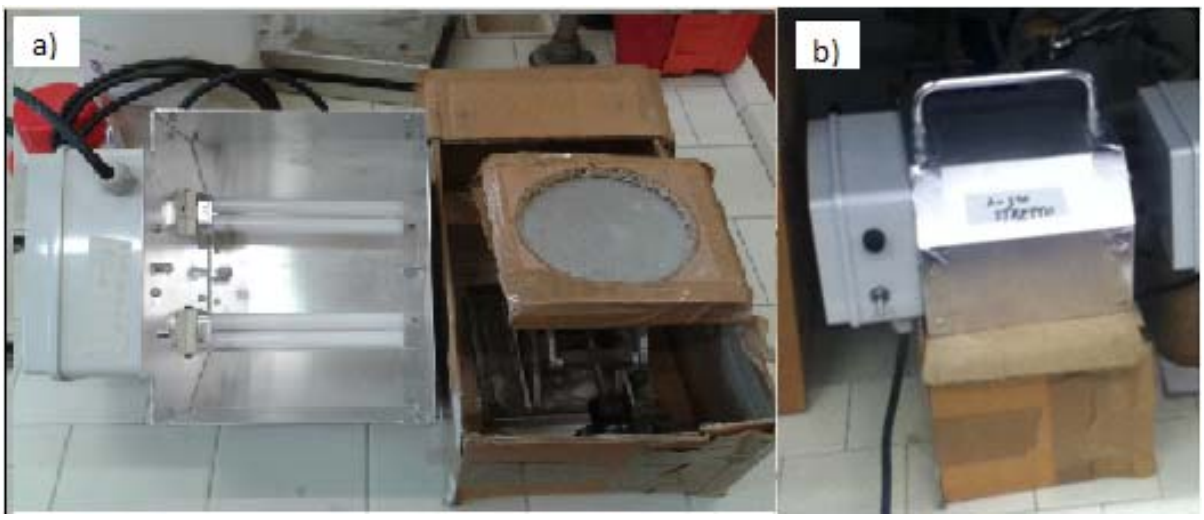

Figure 4.1.1. Device utilized to irradiate the samples: a) open, b) closed.

The UV lamps were put at a distance of 300 mm above the sample.

The UV lights characteristics are summarized as below (Figure 4.1.2).

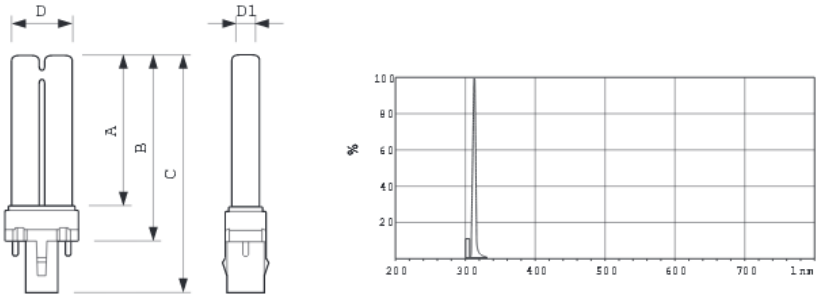

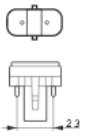

PL-S 9W/01/2P 1CT

Product	A (Max)	B (Max)	C (Max)	D (Max)	D1 (Max)
PL-S 9W/01/2P	129	144.5	167	28	13

Figure 4.1.2. UV lamps technical features.

All the experiments have been carried out either using UV lamps and without, in order to compare each result with the corresponding reference (blank). During the irradiation, it was observed that the water evaporated (typically every 8 hours), thus additional water (10 mL) was mixed whenever the sample dried.

At the end of the experiment, both samples (blank and sample) were subjected to an extraction (Figure 4.1.3) which is a separation method of substances (the hydrocarbons) from soil matrix. It was carried out by using hexane (100mL) and stirring the mixture for 24 hours at room temperature.

It is to note that in the official method for the analysis of hydrocarbons > C_{12} in soil reported in ISPRA Manual 75/2011, the extraction is carried out with acetone/n-heptane for 1 hour under stirring followed by a GC – MS determination.

After the extraction, the mixture was filtered (Whatman filter n° 597) obtaining a solution and a solid. The solid was dried and analyzed, if necessary, while the solution was taken to dryness with a Rotavapor. 10mL of acetone were added in order to prepare the solution to analyze by GC – MS.

Figure 4.1.3. a) extraction, b) filtration, c) drying.

4.2 ROTAVAPOR

The main components of a rotary evaporator are:

- an evaporation flask containing the solution to be evaporated;
- a thermostatic bath, in which plunges the evaporation flask to keep the solution to a suitable and desired temperature;
- a motorized mechanism, able to put in rotation the evaporation flask;
- a vacuum system, to substantially reduce the pressure within the evaporator system;
- an inclined condenser that provides to knock down the vapors which develops;
- a condensate-collecting flask at the bottom of the condenser, which catch the distilling solvent after it re-condenses.

The flasks, the capacitor and connecting elements between these are made of glass, and the entire system mounted must guarantee a perfect vacuum seal.

The device used for the research was a Rotavapor BÜCHI Waterbath B-480 (Figure 4.2).

Figure 4.2. BÜCHI Rotavapor Waterbath B-480.

4.3 GC-MS: GAS CHROMATOGRAPHY – MASS SPECTROMETRY (Skoog, Holler, & Crouch, 2009)

To the dried sample obtained from the Rotavapor, 10 mL of pure acetone were added which sweeps up the remained hydrocarbons in the flask. Then, with a micro syringe were taken 0.4 µL of the solution and injected in a Gas chromatography–mass spectrometry (GC-MS) device (Figure 4.3). This latter is an analytical method that combines the features of gas-liquid chromatography and mass spectrometry to identify different substances within a test sample.

Initially the sample underwent to the gas chromatography (GC), in which it is breakdown in the constituting molecules, according to their chemical properties in the mixture and their relative affinity for the stationary phase of the column. This occurs while the sample travels around the length of the column. The molecules obtained are retained by the column and then elute comes off from the it at different times, called the retention time. This allows the mass spectrometer (MS) downstream to capture, ionize, accelerate, deflect, and detect the ionized molecules separately.

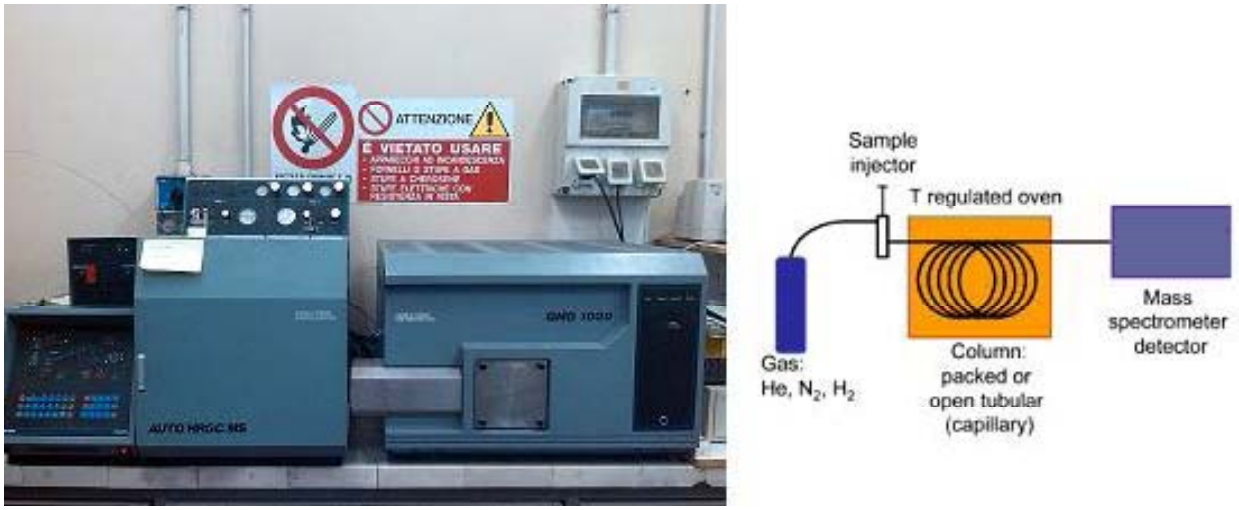

Figure 4.3. Carlo Erba GC-MS and general operational scheme.

The GC-MS analysis was carried out using a Carlo Erba Instruments AUTO / HRGC / MS 1000 MS, as a gas chromatograph coupled to a mass spectrometer detector Carlo Erba Instruments MS QMD 1000. The interpretation of the chromatogram was performed with the provided program management of the device, equipped with the NIST and Wiley libraries.

The typical GC – MD settings were:

- Range of T° = [80°C – 280°C] with first minute maintaining 80°C and then increasing the temperature with a rate of 10°C /min;
- Splitless;
- Column: DB5-HS Agilent J&W (5% diphenyl-, 95% dimethilesiloxane);
- Carrier: He (1cc/min);
- Detector 500;
- Mass detected: from 50 to 350;

4.4 SEM: SCANNING ELECTRON MICROSCOPE (Skoog, Holler, & Crouch, 2009)

The scanning electron microscope (SEM) is a type of electronic microscope which uses a focused electron beam to analyze a small squared area of a sample by moving along subsequent parallel lines. Some electrons are reflected, the so called scattered, and some others penetrate the surface of the sample and are absorbed by the atoms producing electrically excited ions; these ions can return at their fundamental state through secondary electrons emissions (fluorescence). These emissions can be detected and analyzed in order to obtain information on the typology and composition of the sample. In particular the measurement of secondary electrons allows to study the morphology of the sample while the measurement of backscattered electrons in addition to producing an image of the sample gives information on its composition because their emission is related to the atomic number

of the elements present. For this study an Environmental SEM model XL-30 (Philips) (Figure 4.4) was used, which differs from SEM because the chamber where the sample is placed can work at low void pressure instead of high void pressure as in SEM and it's closer to the column of electrons beam. Also, the sample metallization is not required.

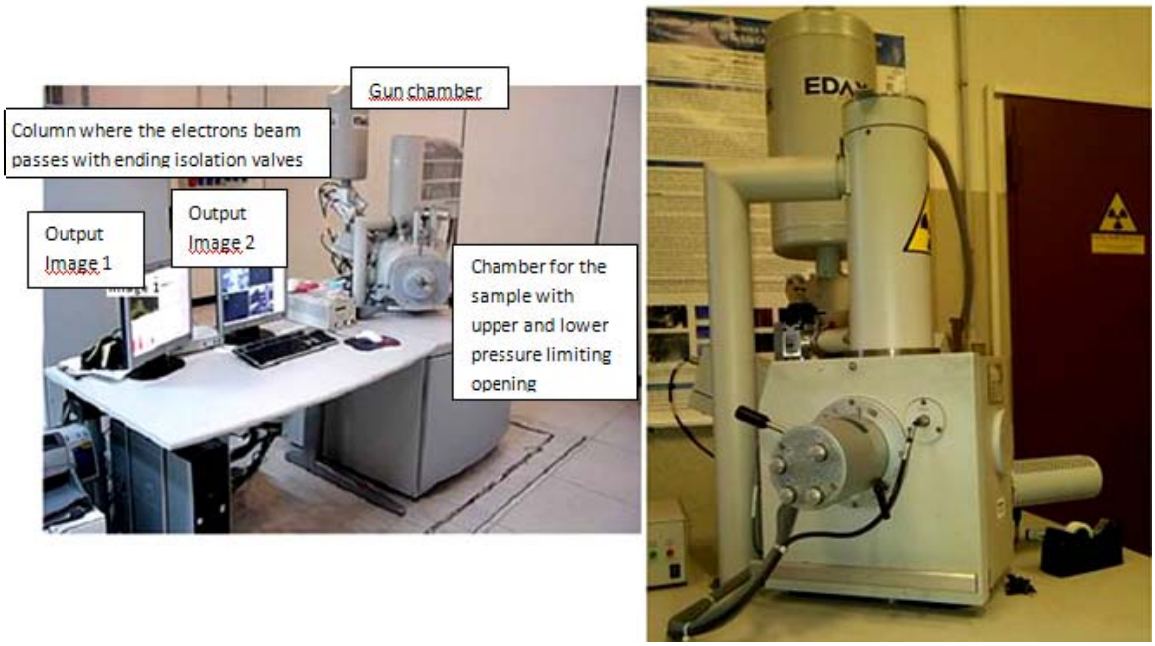

Figure 4.4. Environmental SEM model XL-30 (Philips).

4.5 TEM: TRANSMISSION ELECTRON MICROSCOPE

The transmission electron microscope (TEM) operates on the same basic principles as the light microscope but it uses electrons instead of light. What you can see with a light microscope is limited by the wavelength of light. TEMs use electrons as "light source" and their much lower wavelength makes it possible to get a resolution a thousand times better than with a light microscope.

It is possible to see objects to the order of a few angstrom (10^{-10} m).

A "light source" at the top of the microscope emits the electrons that travel through vacuum in the column of the microscope. Instead of glass lenses focusing the light in the light microscope, the TEM uses electromagnetic lenses to focus the electrons into a very thin beam. The electron beam then travels through the specimen you want to study. Depending on the density of the material present, some of the electrons are scattered and disappear from the beam. At the bottom of the microscope the unscattered electrons hit a fluorescent screen, which gives rise to a "shadow image"

of the specimen with its different parts displayed in varied darkness according to their density. The image can be studied directly by the operator or photographed with a camera.

A schematization of the instrument is reported below (Figure 4.5).

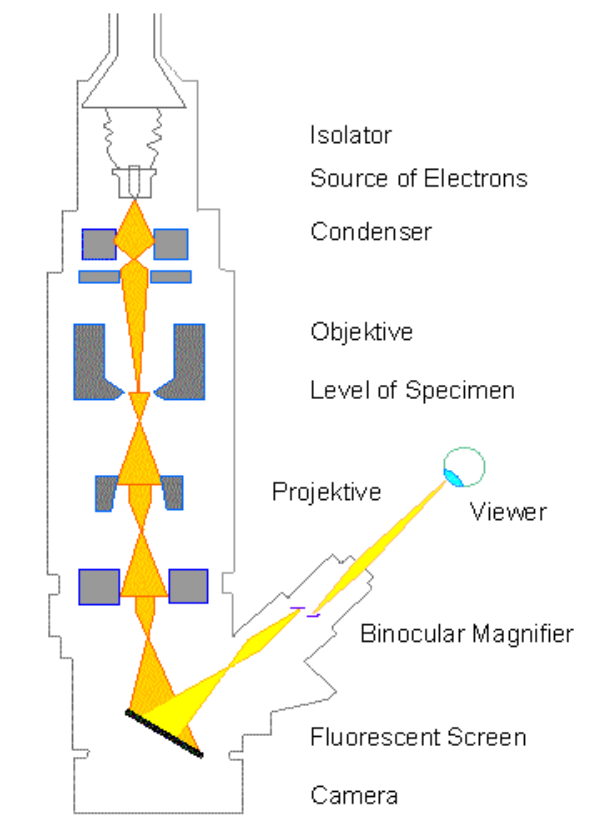

Figure 4.5. TEM operational scheme.

4.6 FT-IR: FOURIER TRANSFORM INFRARED SPECTROMETER (Silverstein, Webster, Kiemle,2005)

The FT-IR spectroscopy is a vibration absorption spectroscopy (Figure 4.6). It works according to the fact that when a molecule is struck by an IR beam of appropriate wavelength, induces a variation in the level of vibration energy by lengthening or shortening the chemical bond (stretching), or by changing the bond angle (bending). This absorption is characteristic of each functional group, which allows to use this phenomenon for qualitative analysis, according to the following equation:

$$n = \frac{1}{2\pi} * \sqrt{\frac{f}{\mu}}$$

where:

- n = vibrational frequency (cm^{-1});
- c = velocity of light (cm/s);
- f = force constant of bond (dyne/cm)
- μ = reduced mass of the system X-Y = (Mx*My) / (Mx + My)

Gruppo	n (cm^{-1}) stretching
O-H	3650-2500
N-H	3550-3050
C-H	3040-2840
C ≡ C	2260-2100
C=O	1850-1630
C=C	1690-1590
C-O	1300-1060
C-C	1200-800

Figure 4.6. Characteristic bands of the main functional group.

In this study a FT-IR PerkinElmer Spectrum100 (Figure 4.6.2) was used and for the interpretation and analysis of the spectra the OMNIC program was adopted.

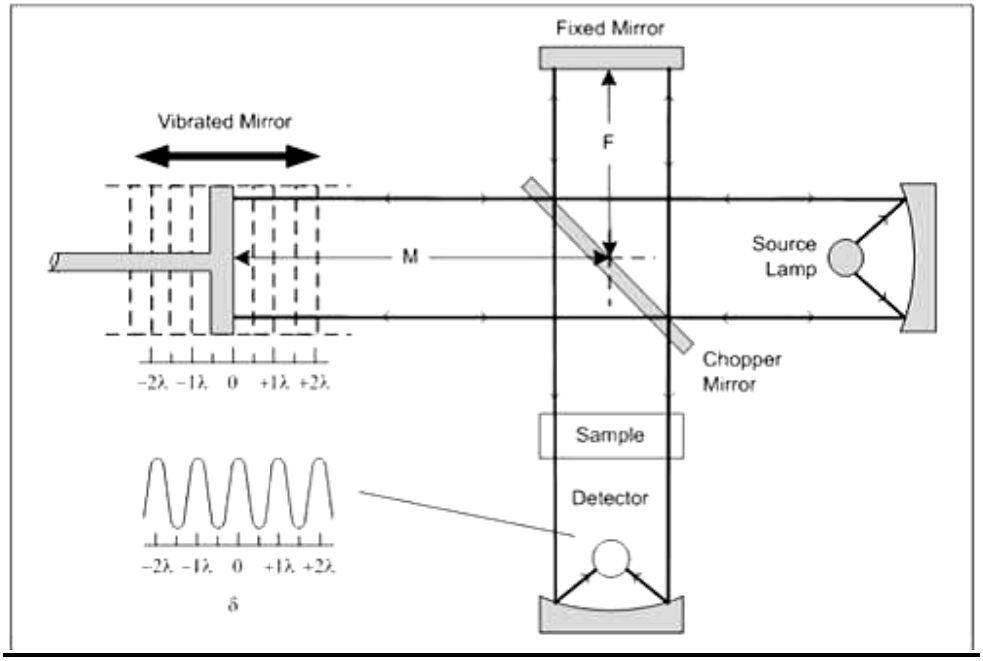

Figure 4.6.1. Schematization of a FT-IR device.

Figure 4.6.2. FT-IR PerkinElmer Spectrum100.

4.7 TEMPERATURE SENSORS

The capillary tube temperature sensor, (thermocouple) is a probe which monitors the temperature of a sample. It consists of two dissimilar conductors that contact each other at one or more spots. It produces a voltage when the temperature of one of the spots differs from the reference temperature at other parts of the circuit.

The little capillary, that contains the two conductors, (Fig. 4.7 (a)) in contact with the sample transmits the temperature value to a receiving control unit (Fig. 4.7(b)) that instantaneously monitors the read value to a computer screen to which it is connected (Fig. 4.7 (c)).

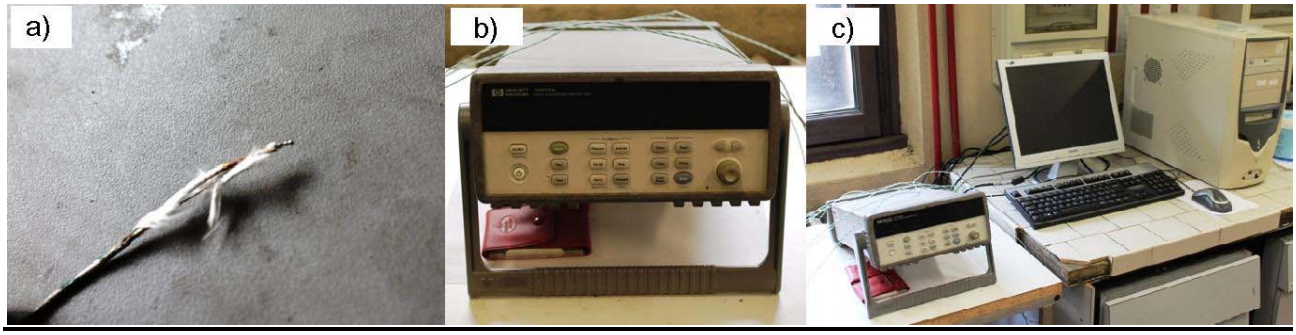

Figure 4.7 a) thermometric probe , b) receiving control unit, c) the whole apparatus.

By the receiving control unit it is possible to adjust the frequency of sampling.

The receiving control unit utilized in this study was a HP 34970A Data Acquisition / Data Logger Switch Unit.

4.8 XRD

The X-ray diffraction (XRD) is a non-destructive technique used for the qualitative and quantitative analysis of crystalline materials in solid state. Using this analytical technique it is possible record the X-rays diffracted by crystalline materials. Each material produces a diffraction spectrum that forms a fingerprint making possible the identification of an unknown material for comparison with a library of spectra of known substances. Basically, the X-ray diffraction is obtained as a reflection of a beam of X-rays from a family of atomic planes parallel and equidistant, following Bragg's law.

$$2d \text{ sen } \theta = n\lambda$$

$$d = \lambda / 2\text{sen } \theta$$

where :

- d is the spacing between diffracting planes;
- θ is the incident angle;
- n is any integer;
- λ is the wavelength of the beam.

When a beam of monochromatic X-rays with a wavelength (wavelength of the radiation that is produced by an X-ray tube) is incident on a lattice plane with an angle θ there is a diffraction if the path of the rays reflected by successive planes (with a distance d) and a multiple of the wavelength. The study of the intensity of diffraction at various angles (setting by the device) allows to identify the symmetry of the crystal and the size of its unit cell.

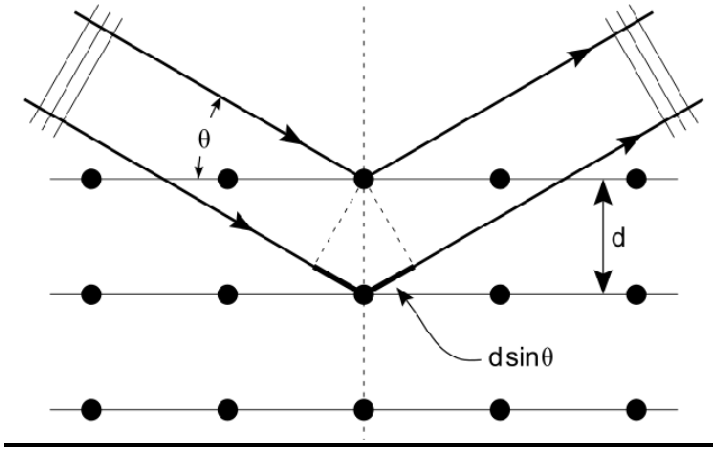

Figure 4.8. Scheme of X-ray diffraction.

5. MATERIALS

5.1 TITANIA CHARACTERIZATION

The photocatalyst used for this study is the TiO_2 P25 developed by the company Evonik Degussa. The powder was studied in the previous work (Burigo, 2014) with a transmission electron microscopy (TEM) and with XRD. The output images given by TEM are reported in Figure 5.1. The nominal size of the nanoparticles is about 21 nm and agrees with the characteristics included in the product card present in Evonik database. The specific surface area is about $50\pm15 m^2/g$ (Evonik).

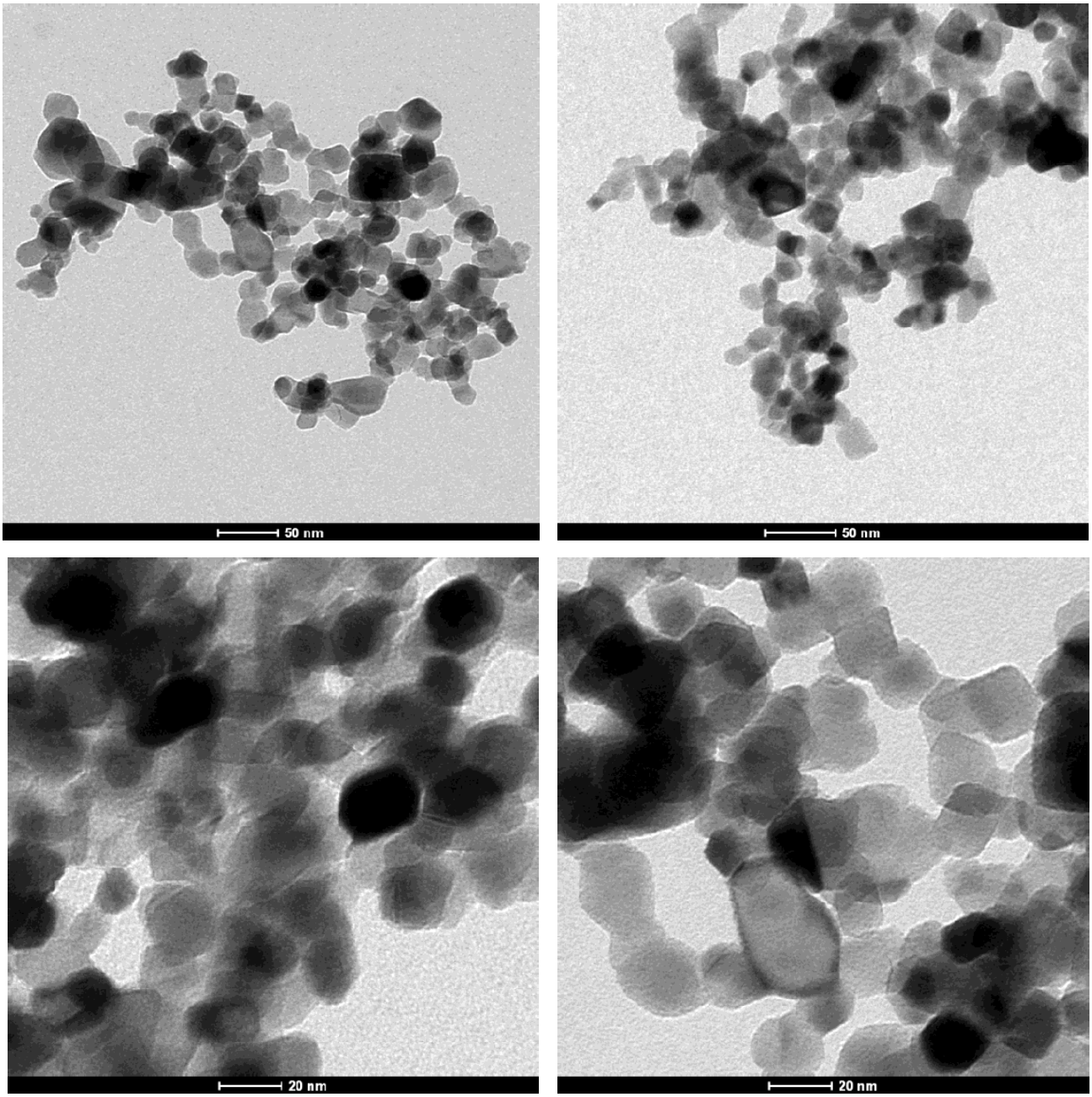

Figure 5.1. TEM images of TiO_2 P25.

The composition of TiO_2 and the ratio between anatase and rutile was evaluated with XRD.

In Figure 5.1.1 and in Table 5.1 the diffractogram and the main peaks are reported.

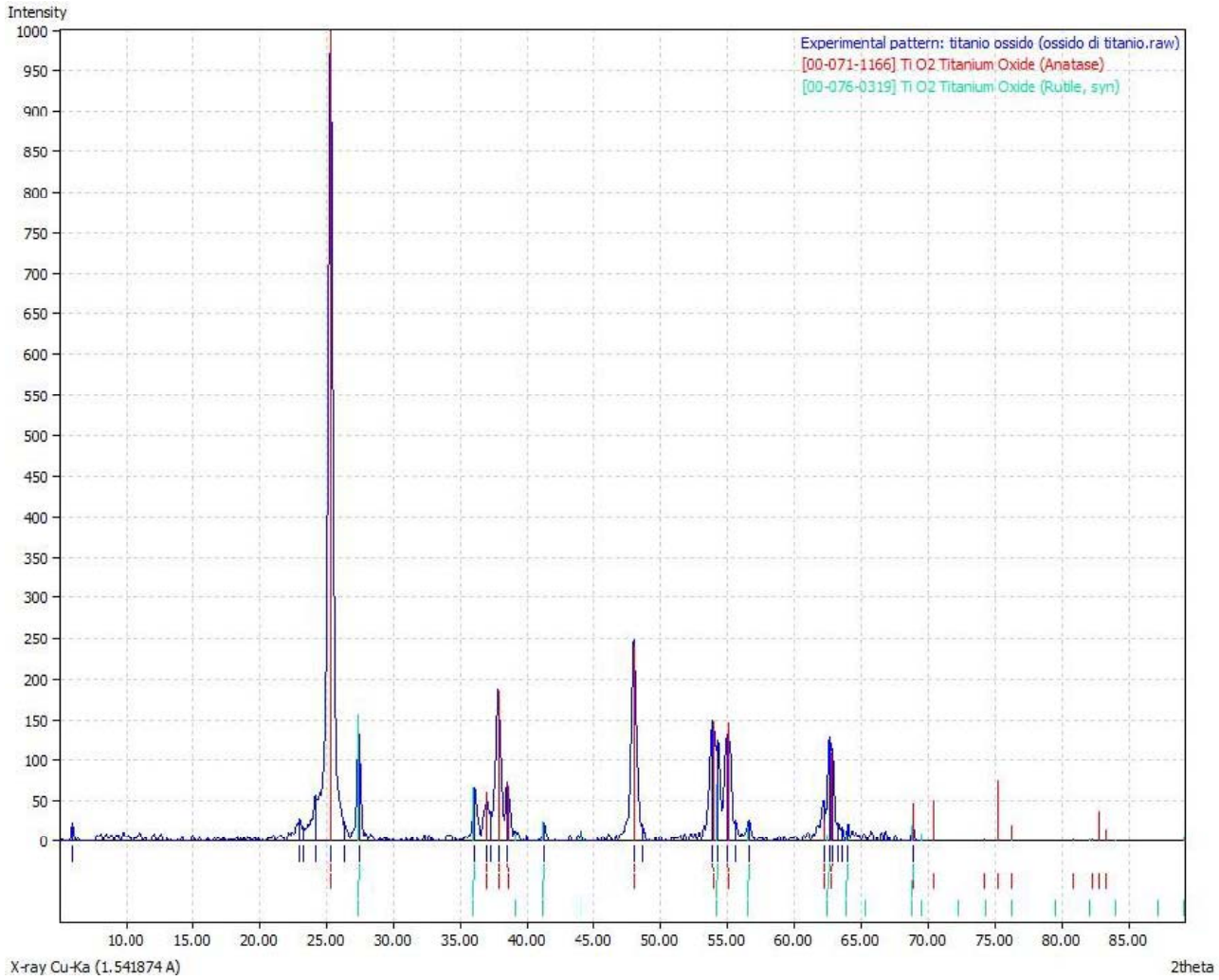

Figure 5.1.1. X-ray diffractometer (XRD) pattern of TiO_2 Evonik Degussa P25: the blue line is the difractogram of the TiO_2 P25 powder, red line regarding anatase phase and green line rutile phase.

Table 5.1. XRD peaks of TiO_2.

2theta	intensity
25.3	995.43
27.45	153.73
36.04	78.45
37.8	192.52
38.5	85.27
48.03	276.48
53.98	160.29

The blue line is the difractogram of the TiO_2 P25 powder, the red one is related to the anatase phase and the green line rutile phase.

The peaks at 25.30 and 27.45 are related to the main crystallographic plane and respectively the former to anatase and the latter to rutile. Comparing the intensity values the content of rutile was about 15.8%, in agreement with Evonik product card.

The amorphous phase was difficult to quantify but seems to be a small amount.

5.2 SOIL CHARACTERIZATION

The soil given by the client, RE.AL.Service Spa, was contaminated with an unknown mixture of hydrocarbons.

Various analysis were made in the previous study in order to investigate and analyze the mixture of pollutants present in the sample and the nature of soil:

- FT-IR
- Extractions with different solvents and subsequent GC-MS analysis
- SEM
- XRD

The spectrum given by the FT-IR analysis of the soil sample is reported in Figure 5.2. The characteristics infrared bands for hydrocarbons are between 2800 and 3000 cm-1.

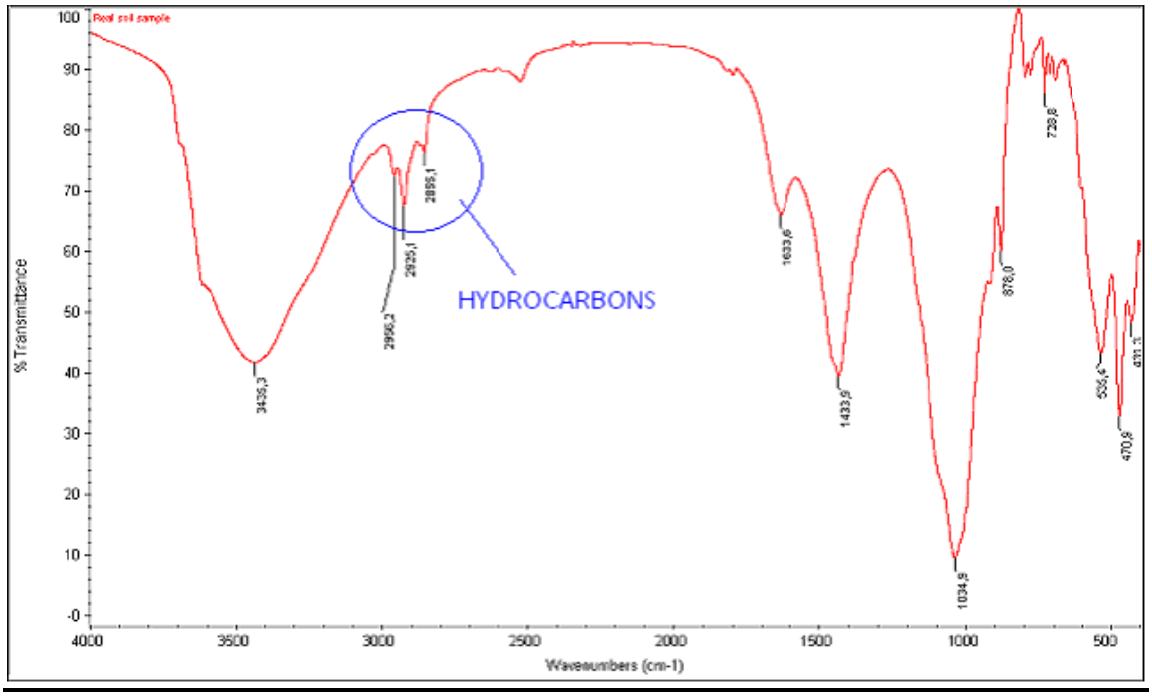

Figure 5.2. FT-IR spectra of Re.al. sample.

A series of 3 extractions was made with 3 different solvents of different polarity. Firstly was used hexane, secondly dichloromethane and thirdly acetone. It was used 100g of sample in 200ml of solvent. The objective of the extractions was to try to extract all the hydrocarbons from the polluted sample for the subsequent identification of each kind of compound and the analysis of the clean soil matrix. In Figure 5.2.1 is reported the IR spectrum of the liquid resulting from the extraction in hexane. The spectrum indicates the presence of only aliphatic hydrocarbons.

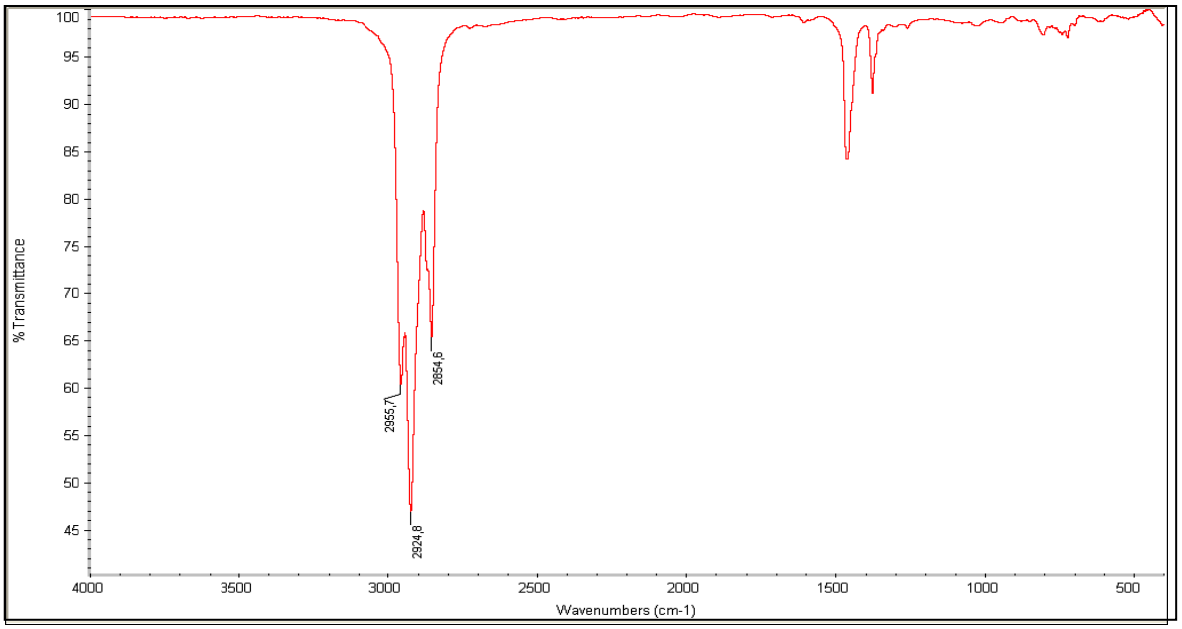

Figure 5.2.1. FT-IR of liquid resulting from the extraction in hexane.

The extracted liquid was then dried with a Rotavapor and analyzed with GC-MS. Below, in Figure 5.2.2, the result of the GC-MS analysis regarding the extraction with hexane is reported.

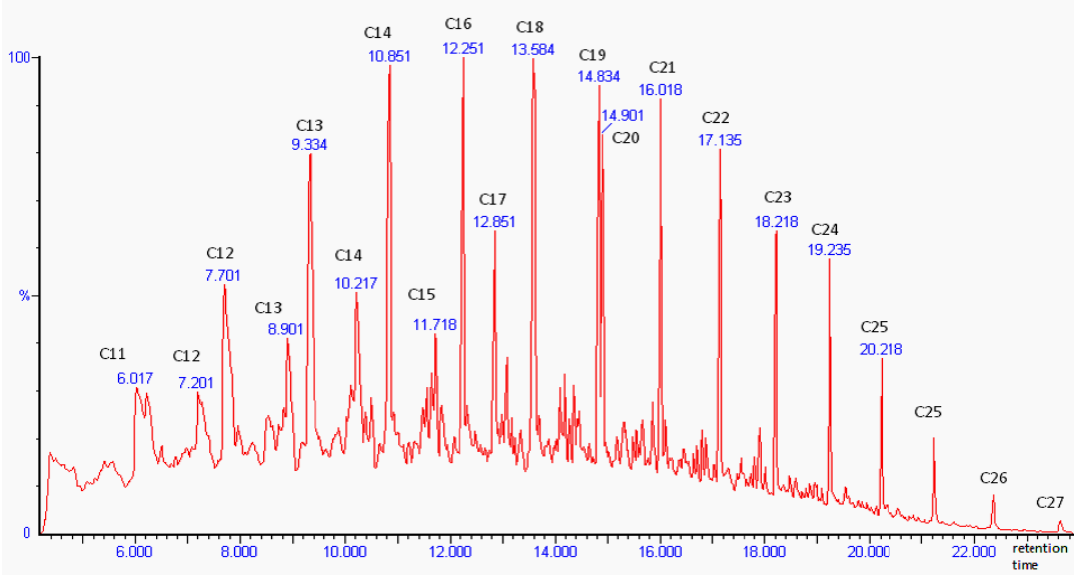

Figure 5.2.2. Chromatograph of the Re.al. polluted soil after the extraction in hexane.

For each peak the mass fragmentation was analyzed in order to identify to which pollutant it was related. Below are reported the mass spectra of each peak.

Peak at 6.017: Aliphatic hydrocarbon C_{11}

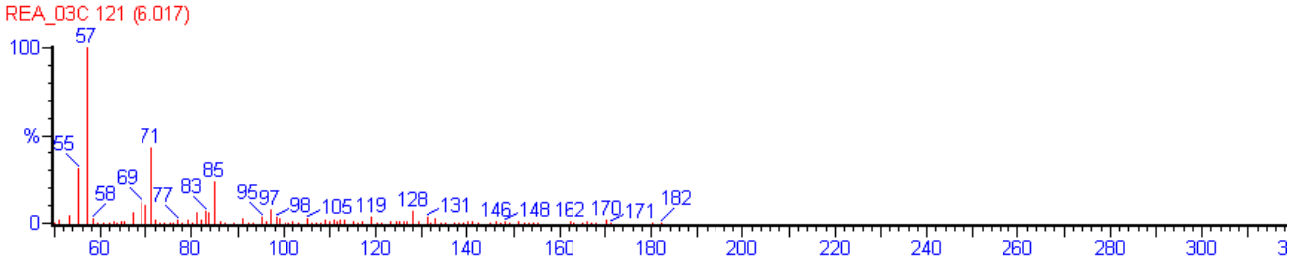

Peak at 7.201: Aliphatic hydrocarbon iso-C_{12}

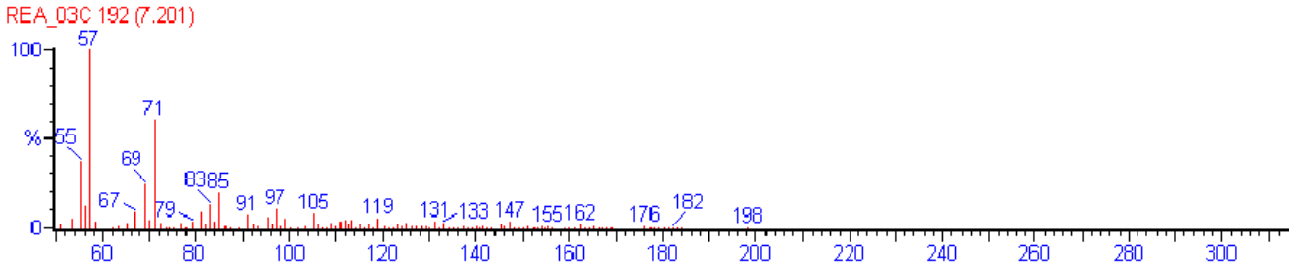

Peak at 7.701: Aliphatic hydrocarbon C_{12}

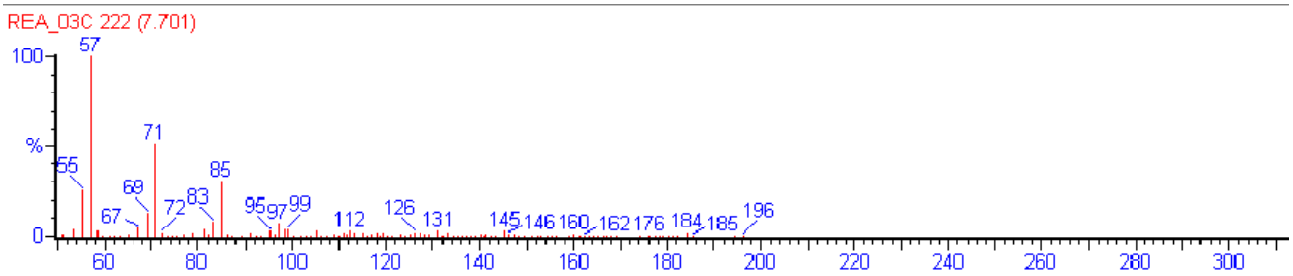

Peak at 8.901: Aliphatic hydrocarbon iso-C_{13}

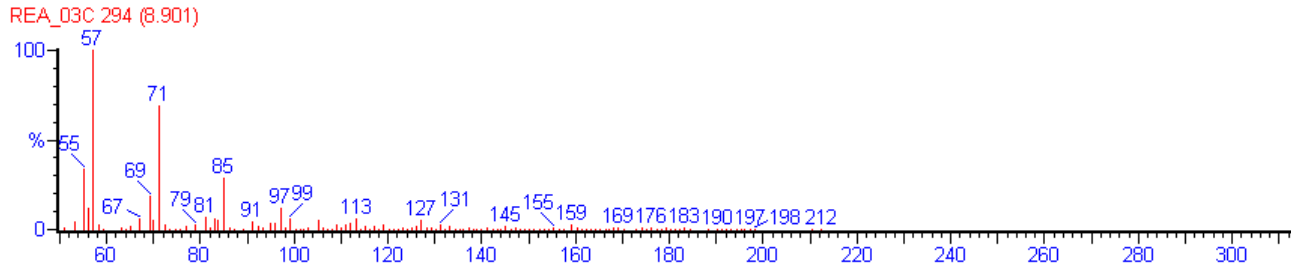

Peak at 9.334: Aliphatic hydrocarbon C_{13}

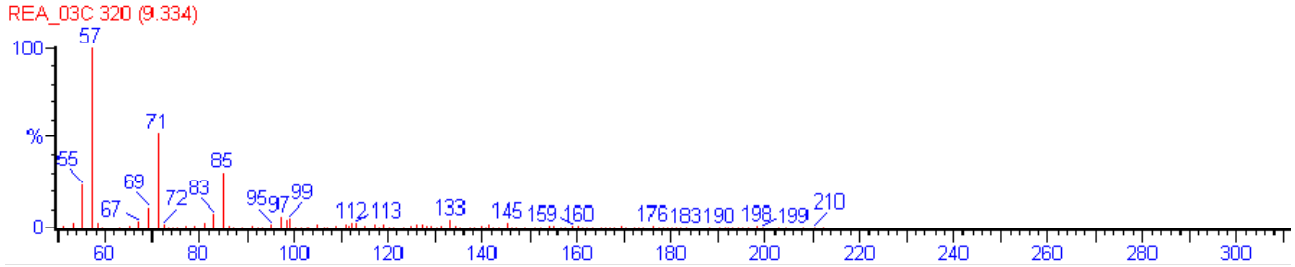

Peak at 10.217: Aliphatic hydrocarbon iso-C_{14}

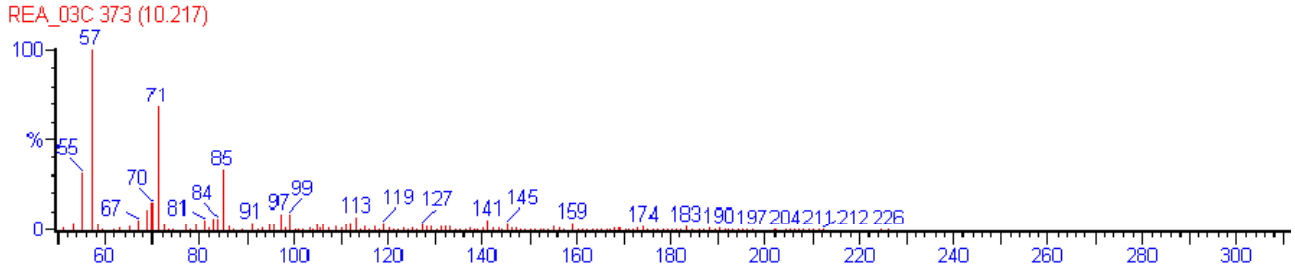

Peak at 10.851: Aliphatic hydrocarbon C_{14}

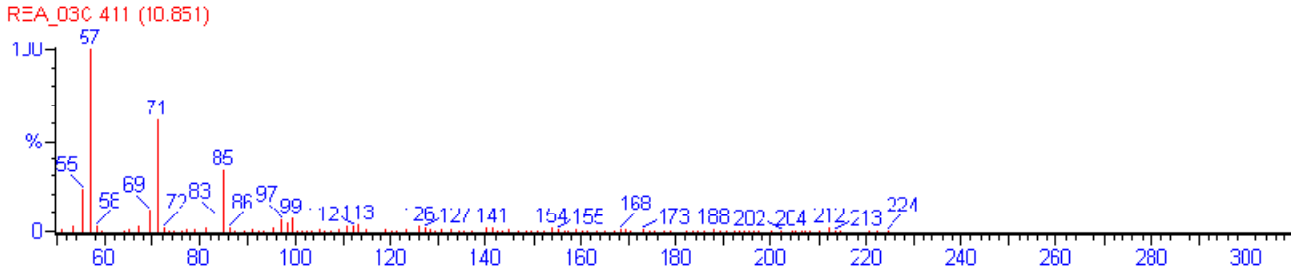

Peak at 11.718: Aliphatic hydrocarbon C_{15}

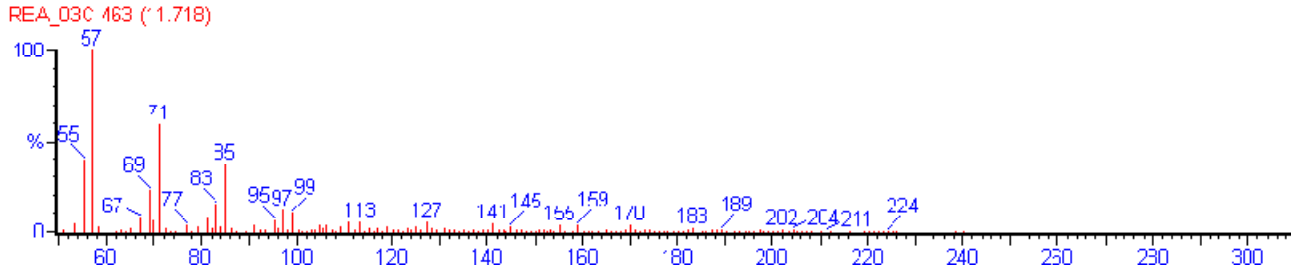

Peak at 12.251: Aliphatic hydrocarbon C_{16}

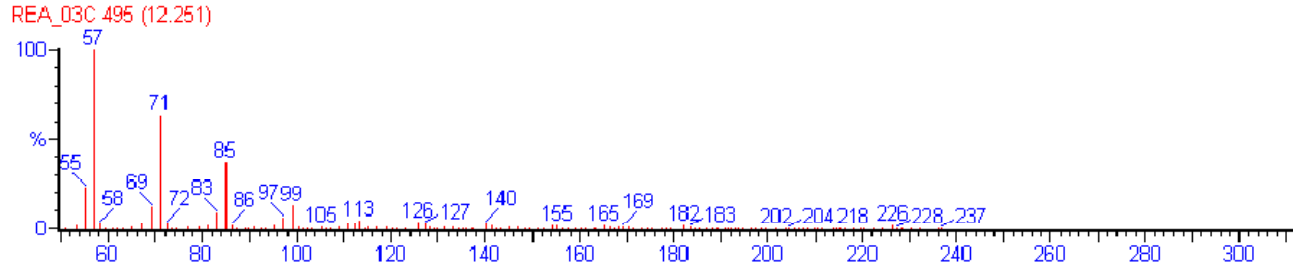

Peak at 12.851: Aliphatic hydrocarbon C_{17}

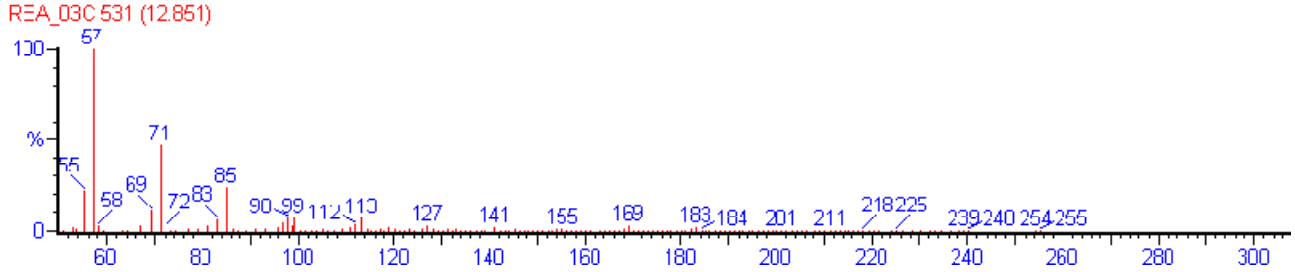

Peak at 13.584: Aliphatic hydrocarbon C_{18}

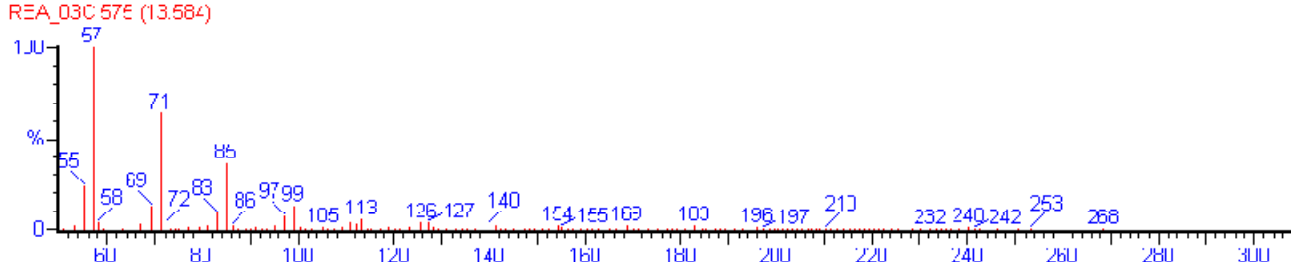

Peak at 14.184: Aliphatic hydrocarbon iso-C_{19}

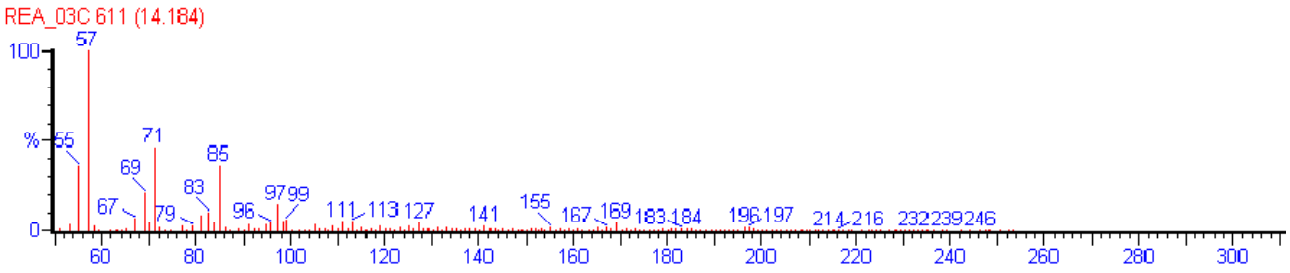

Peak at 14.834: Aliphatic hydrocarbon C_{19}

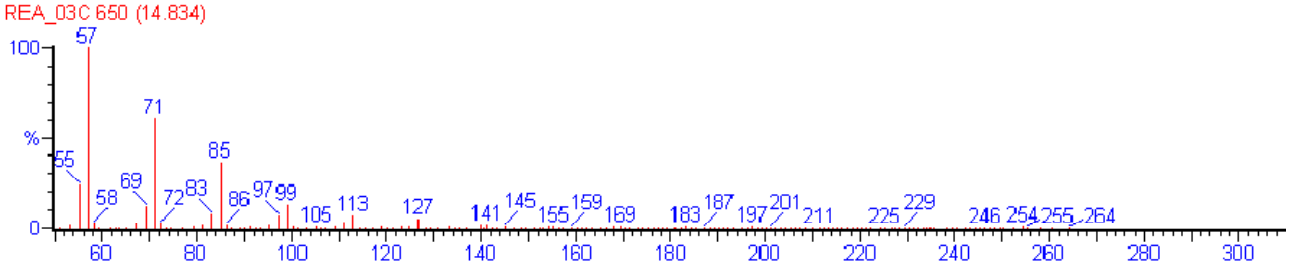

Peak at 14.901: Aliphatic hydrocarbon C_{20}

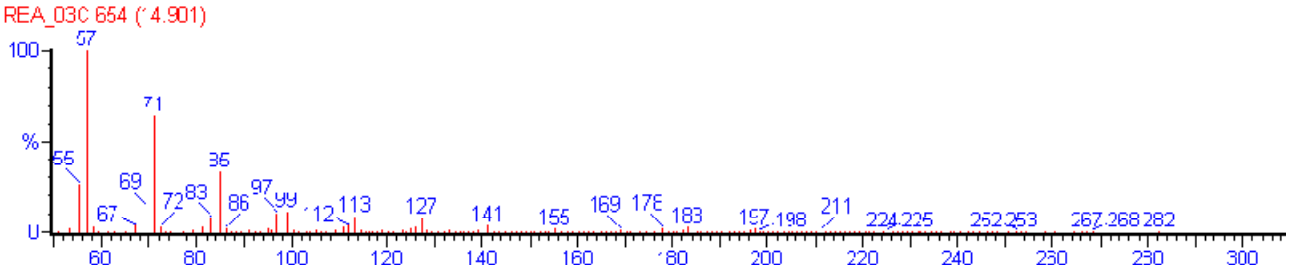

Peak at 16.018: Aliphatic hydrocarbon C_{21}

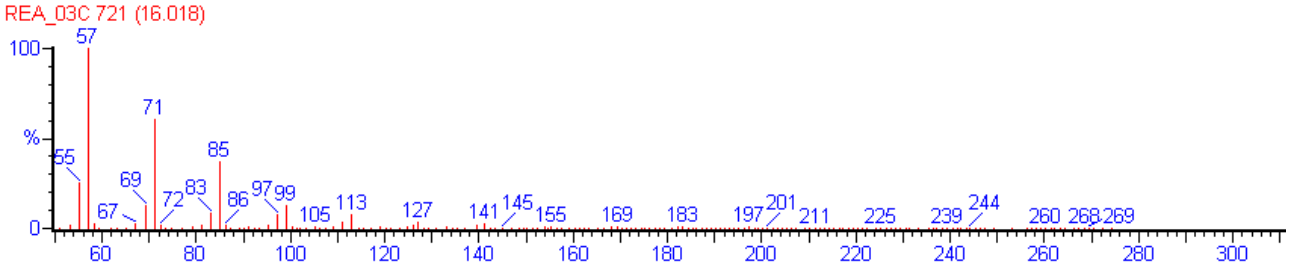

Peak at 17.135: Aliphatic hydrocarbon C_{22}

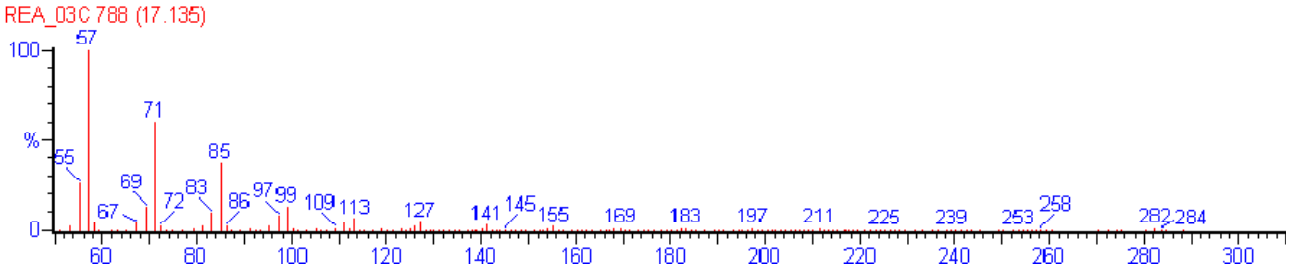

Peak at 18.218: Aliphatic hydrocarbon C_{23}

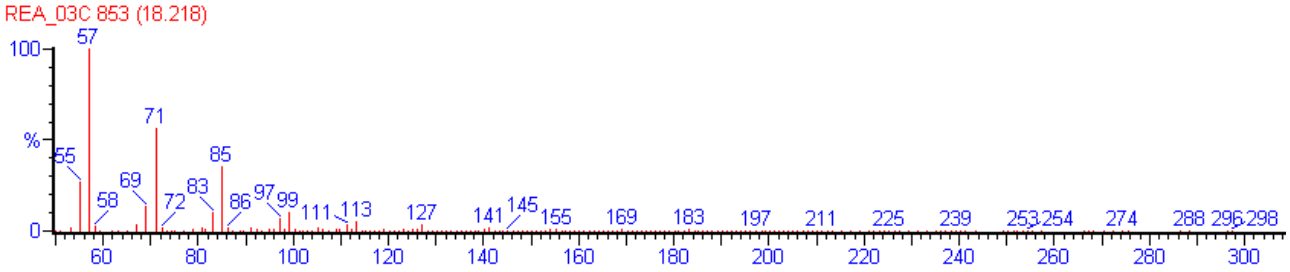

Peak at 19.235: Aliphatic hydrocarbon C_{24}

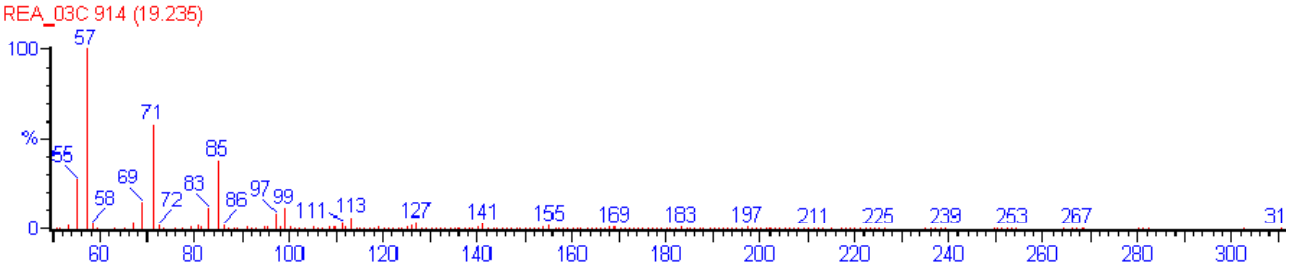

Peak at 20.218: Aliphatic hydrocarbon iso-C_{25}

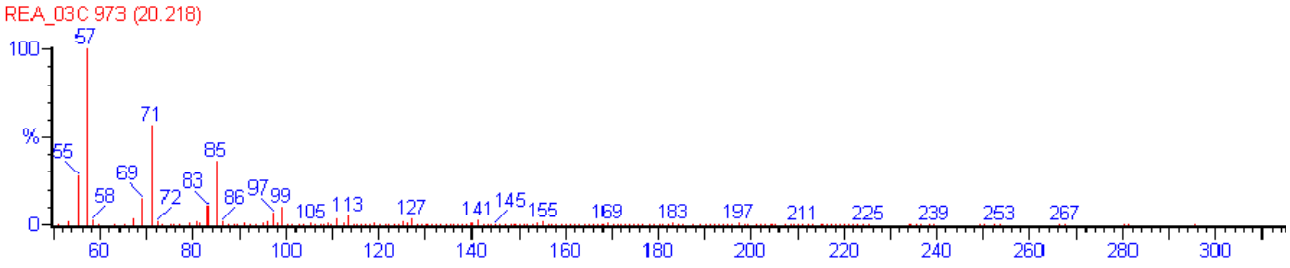

Peak at 21.235: Aliphatic hydrocarbon C_{25}

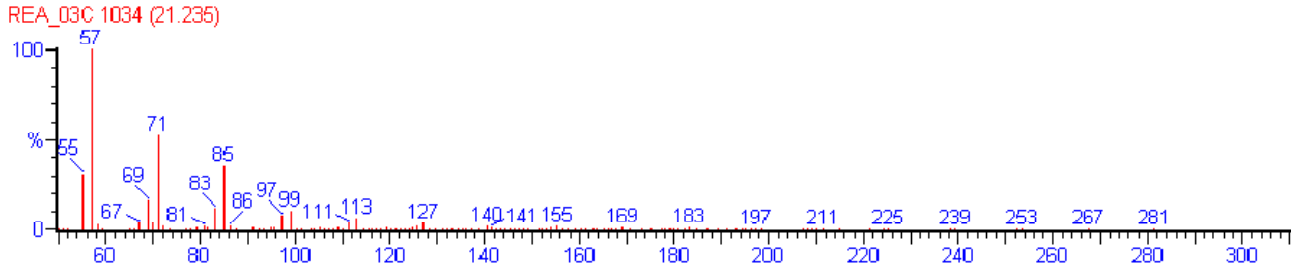

Peak at 22.352: Aliphatic hydrocarbon C_{26}

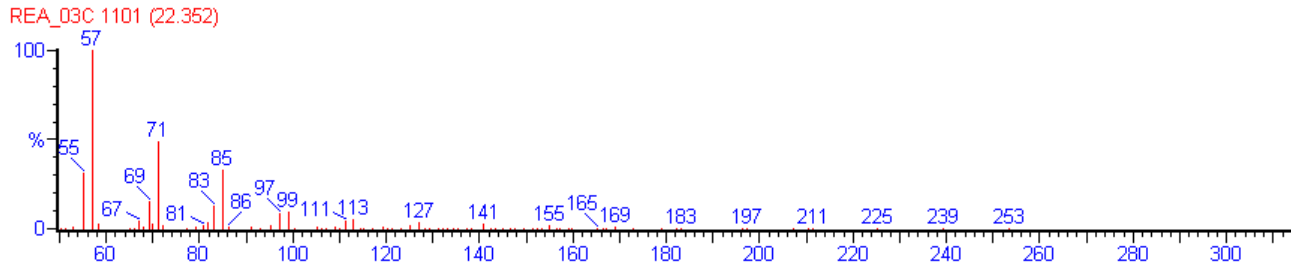

The pollutants are all long-chain aliphatic hydrocarbons from C_{11} to C_{26}. No aromatic compounds are present.

It is possible to note that for lighter compounds (retention time < 10 minutes, from C_{11} to C_{14}) both the normal and corresponding isomers are present: in general iso-isomers are more volatile giving rise to the firsts peak of the couples. For instance, the peak at time 7.201 corresponds to the iso-isomer of dodecane (C_{12}) and the peak at 7.701 to the normal dodecane. For higher molecular weight hydrocarbons the masses reported for the base peaks in the spectra correspond, reasonably, to the loss of a fragment $-C_2H_4$ or $-C_2H_5$ followed by progressive loss of $-CH_2$.

Starting from ions at m/z 113 (corresponding to C_8) loss of hydrogen is observed with the formation of ions at m/z 111 from which fragments-CH_2 are progressively lost.

The soils obtained after the extractions Figure 5.2.5, Figure 5.2.6, Table 5.1.2) and the original Re.al. sample (Figure 5.2.3, Figure 5.2.4, Table 5.1.1) were then analyzed with ESEM (Environmental Scanning Electron Microscope) in order to verify, with a comparison between them, the efficiency of the extractions and to show the morphology of the samples.

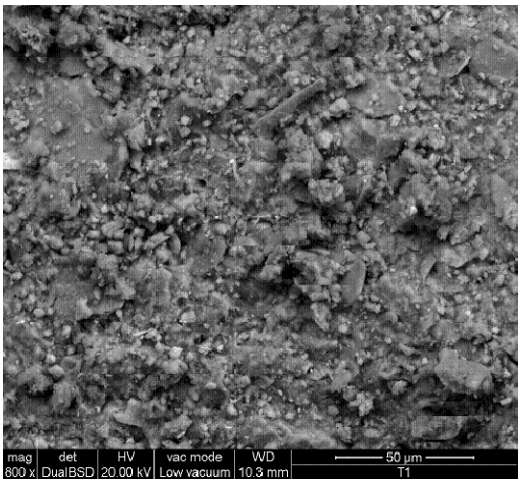

Figure 5.2.3. ESEM of Re.al. polluted soil (RE.AL soil sample): morphology.

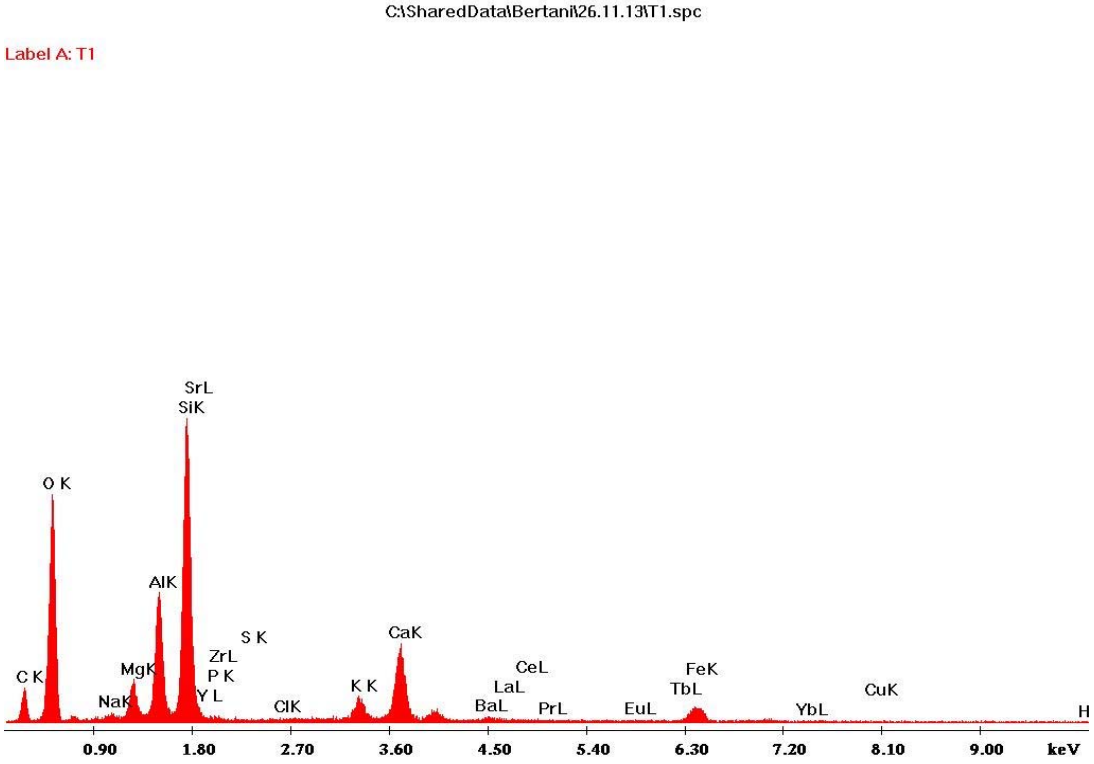

Figure 5.2.4. Spectra of elements in Re.al. soil sample by ESEM.

Table 5.1.1. Quantification of elements in Re.al. soil sample by SEM.

Elem	Wt %	At %
C K	15,87	25,47
O K	40,02	48,22
NaK	0,39	0,33
MgK	2,36	1,87
AlK	7,06	5,04
SiK	17,86	12,26
SrL	0,95	0,21
P K	0,16	0,10
ZrL	0,00	0,00
ClK	0,00	0,00
K K	1,95	0,96
CaK	6,86	3,30
BaL	1,33	0,19
FeK	4,15	1,43
CuK	0,37	0,11
HgL	0,66	0,06
Total	100,00	

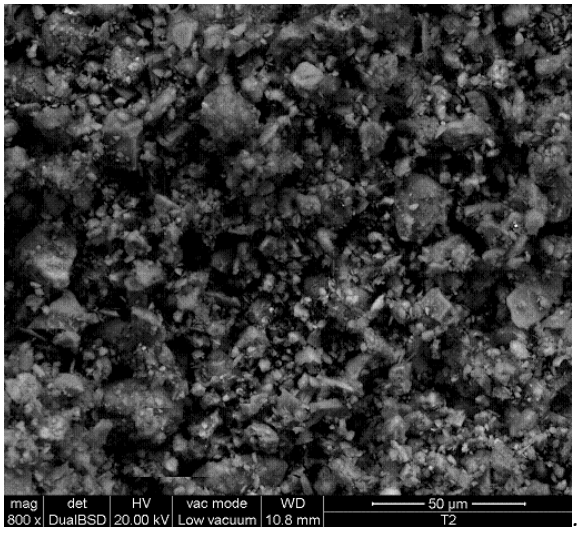

Figure 5.1.5. ESEM of soil sample after 3 extractions: morphology.

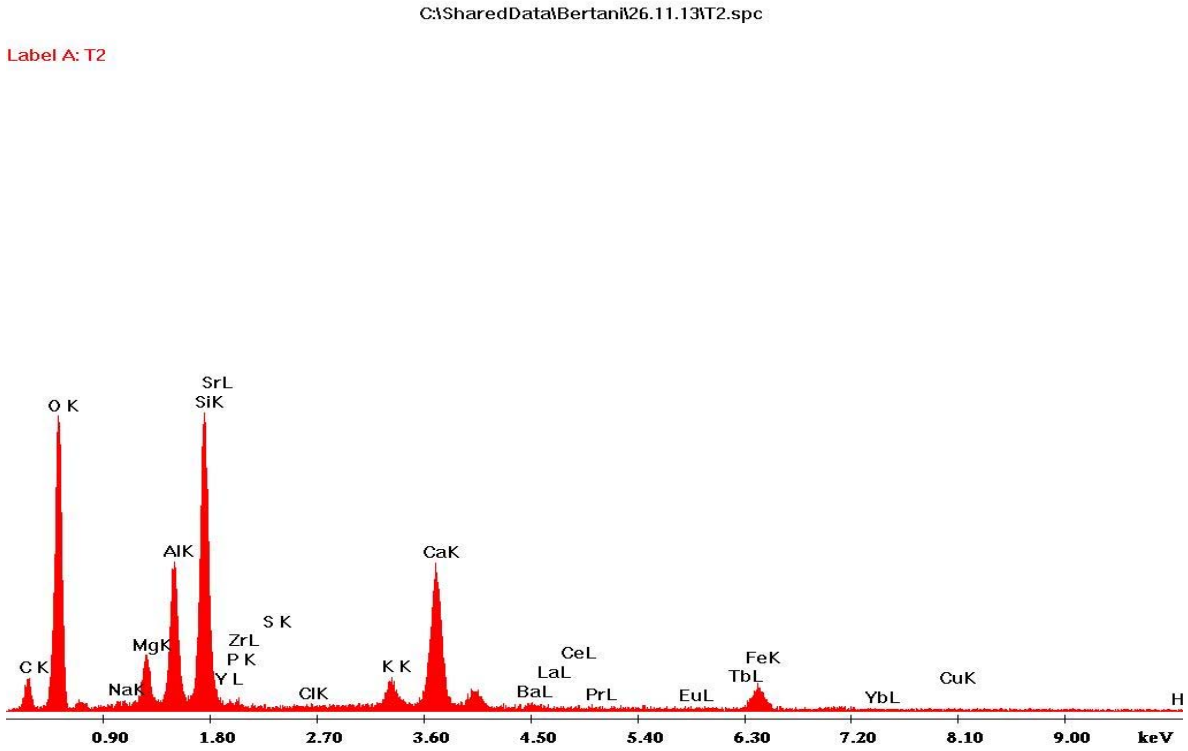

Figure 5.1.6. Spectra of elements of soil sample after 3 extractions by ESEM.

Table 5.1.2. Quantification by SEM of the elements in soil sample after 3 extractions.

Elem	Wt %	At %
C K	11,35	19.31
O K	41,86	53.45
NaK	0,52	0.47
MgK	2,93	2.47
AlK	6,61	5
SiK	13,74	9.99
SrL	1,25	0.29
P K	0,21	0.13
ZrL	0,14	0.03
ClK	0,03	0.02
K K	1,84	0.96
CaK	10,22	5.21
BaL	1,26	0.19
FeK	4,44	1.62
CuK	0,53	0.17
HgL	3,06	0.31
Total	100,00	100

The ESEM analysis has confirmed that the extraction was successful because the percentage of carbon is decreased from 15,87% to 11,35%. The remaining percentage is due to carbon compounds that occur naturally in soils like humic acids and $CaCO_3$.

The remained soil was studied also with XRD device. The result is reported in Figure 5.1.7 and the main bands with the respective intensity in Table 5.1.3.

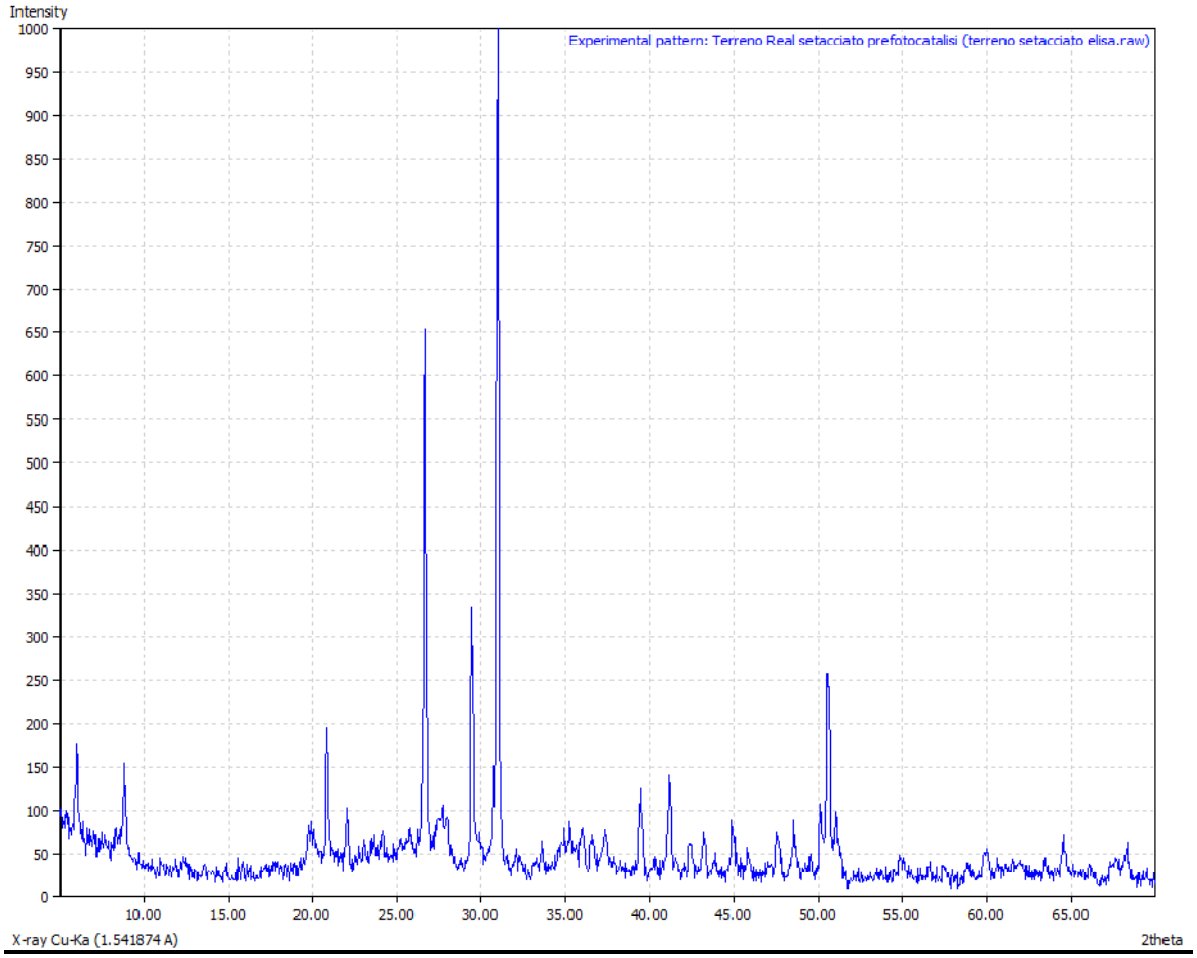

Figure 5.1.7. X-ray diffractometer (XRD) pattern of Re.al. soil sample.

Table 5.1.3. XRD peaks of Re.al. soil sample after 3 extractions.

2theta	intensity
6	164
8.85	154.55
19.89	86.94
20.85	195.99
22	101.88
26.65	651.45
29.44	328.77
30.94	996.96
39.45	124.96
41.14	141.07
50.48	254.25
50.57	252.68

It was noticeable that the soil sample was a mixture and by comparing the bands with the library it was possible to underline the main bands present, characteristics of oxides, phosphates, silicates and carbonate. In Figure 5.1.8 is reported as example the analogy of some silicates with the bands of the soil sample (blue line) and in Figure 5.1.9 the analogy of some carbonate (Zhang Y.X. et al., 2014).

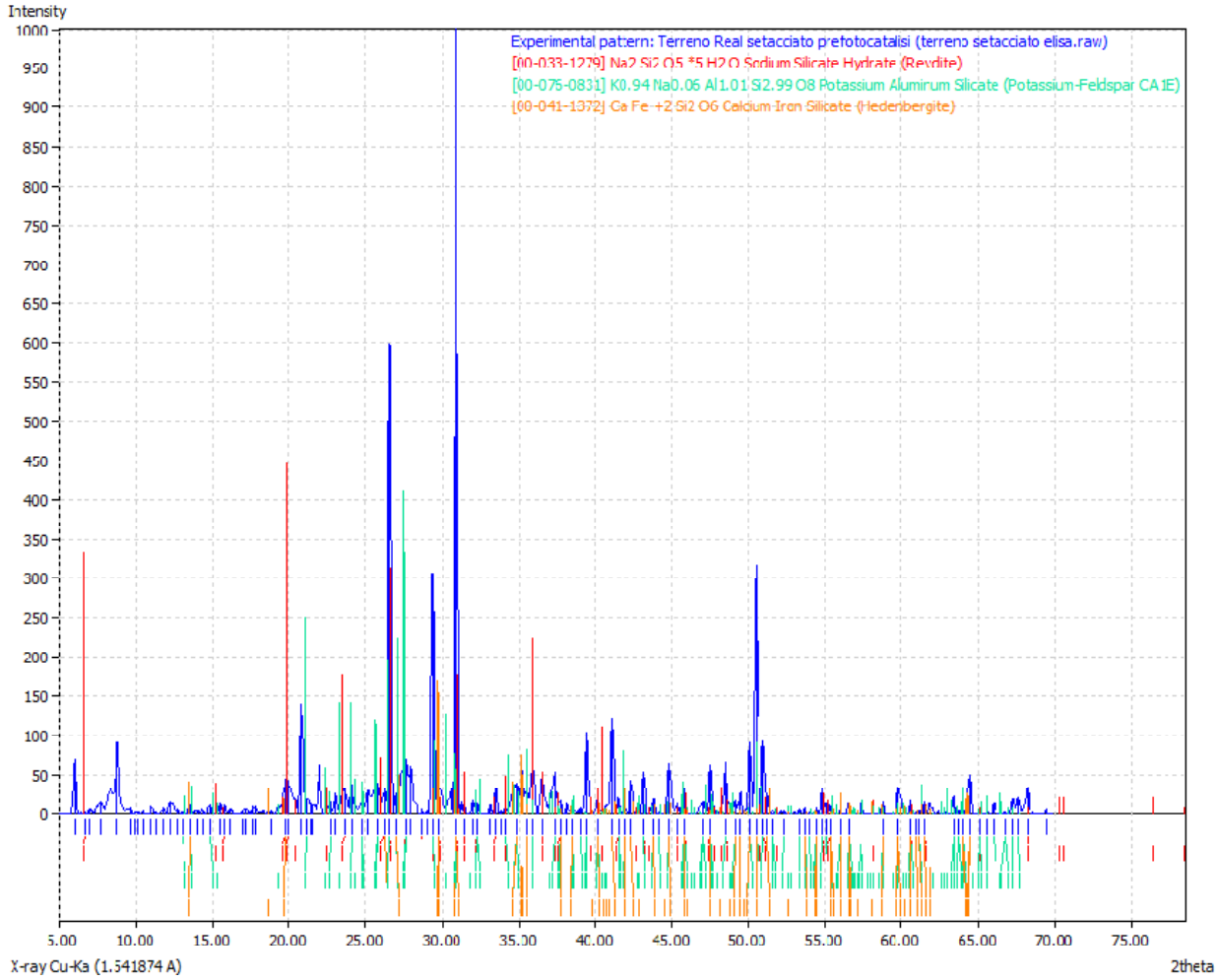

Figure 5.1.8. X-Ray diffractometer (XRD) pattern of Re.al. soil and the overlay of different silicates graphs.

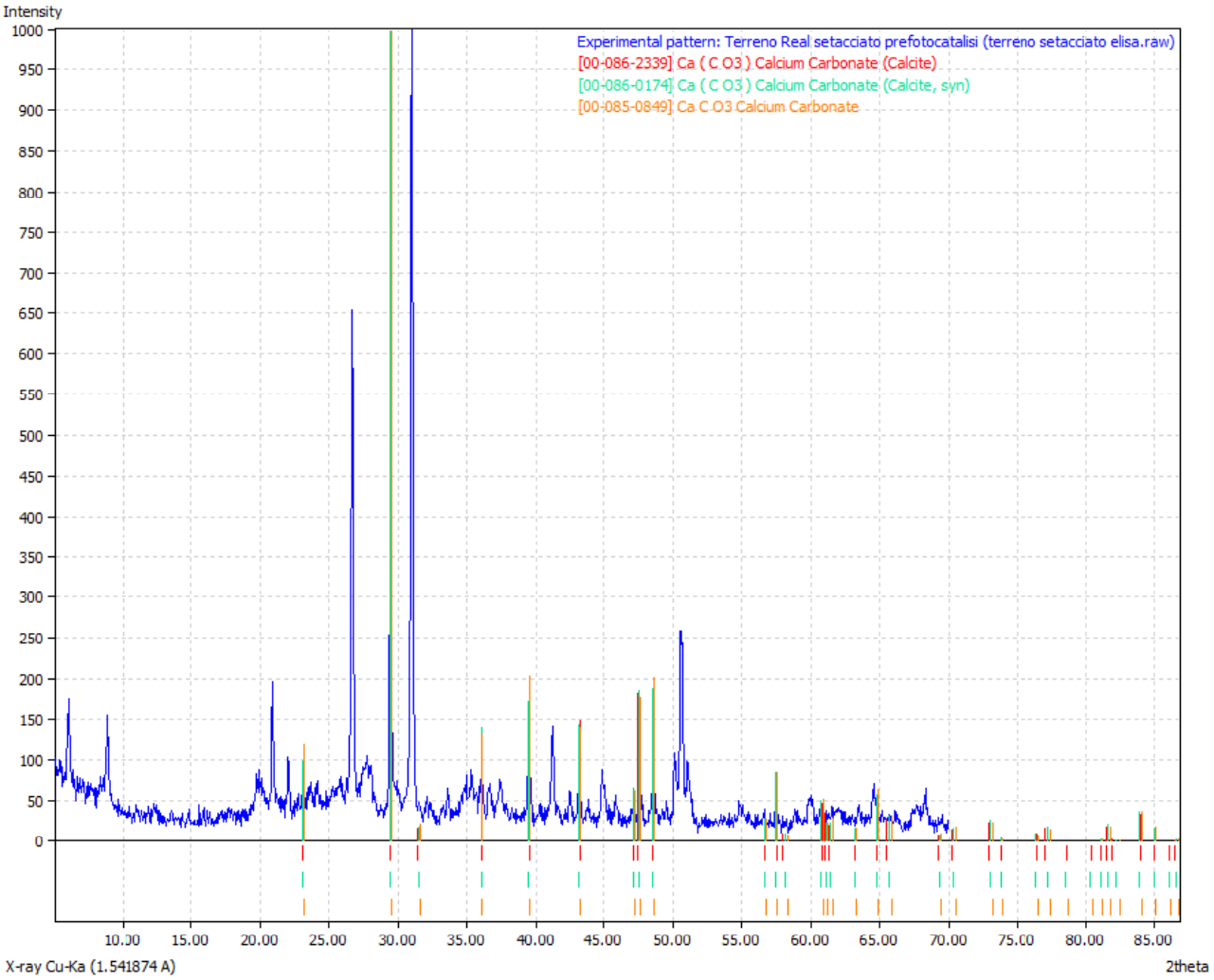

Figure 5.1.9. X-Ray diffractometer (XRD) pattern of Re.al. soil and the overlay of different carbonates graphs.

6. THE PHOTOCATALYTIC EXPERIMENTS: RESULTS

Different experimental parameters have been evaluated: the experiments are described in this section.

6.1 EVALUATION OF THE INFLUENCE OF THE REACTION TIME

EXP. 1: 5g soil; 5mL deionized water; 10% TiO_2 w/w ; 24h; no light (Blank).

In a Petri dish 5g of contaminated soil and 0.5g of TiO_2 were mixed together with 5mL of deionized water.

The mixture was left in the dark for 24 hours. Then, 100 mL of hexane were added to the sample and it was stirred for other 24 hours for the hydrocarbons extraction.

The sample was subsequently filtered with a Whatman filter 597 and the filtrate was taken to dryness by means of a Rotavapor.

10 mL of pure acetone were then added to the flask and then 0.4 µL were injected in a GC – MS for the analysis.

EXP. 2: 5g soil; 5mL deionized water; 10% TiO_2 w/w ; 24h; UV light.

The mixture of soil, titania and deionized water was irradiated under the UV lamps for 24 hours.

After about 4hours from the beginning, 10 mL of deionized water have been added being the sample dried. The addition of 10 mL of water was repeated other two times during the irradiation.

After 24 hours the extraction was performed with 100mL of hexane. Thus, the sample was filtered, taken to dryness and analyzed with GC – MS.

The GC – MS chromatograms for EXP.1 and EXP.2 are reported in the following Figure 6.1.1.

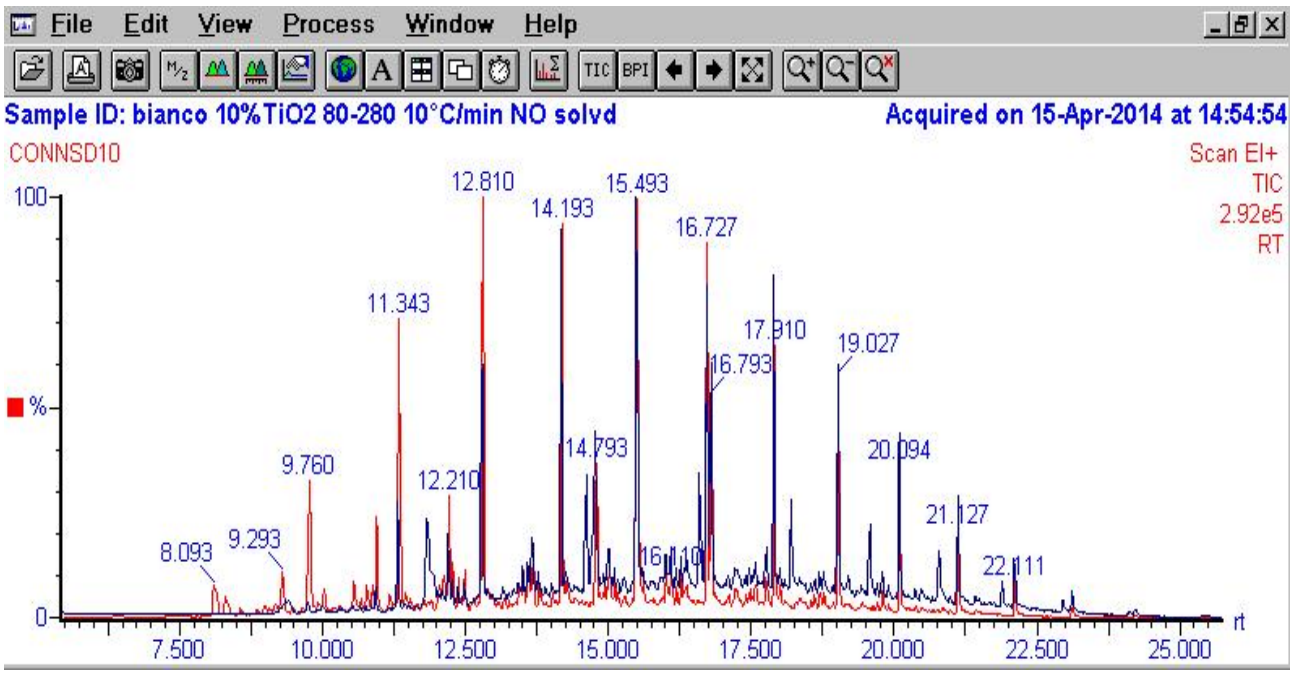

Figure 6.1.1. Superimposition of the GC- MS chromatograms related respectively to EXP.1 (red) and EXP.2 (blue).

The quantitation of the process efficiency reported in Table 6.1.1., has been performed calculating the ratios between the integral of each peak with the C_{20} one, which wasn't resulted to be degraded.

Table 6.1.1. Degradation degree % calculated for the hydrocarbons present in the EXP.1 and EXP.2.

Specie	Retention time [min]	EXP.1 (Blank) [integral i-th/reference integral]	EXP.2 [integral i-th/reference integral]	Degradation %
C12	8,093	0,133	/	100
C13	9,293	0,149	/	100
C14	10,943	0,195	0,0520071	73,35
C15	11,343	0,614	0,21396026	65,13
C16	12,210	0,715	0,489841563	31,49
C18	13,677	0,128	0,127660482	0,49
C19	14,193	0,647	0,578586986	10,64
C20	15,493	1	1	0

EXP. 3: 5g soil; 5mL deionized water; 10% TiO_2 w/w ; 48h; no light (Blank).

EXP. 4: 5g soil; 5mL deionized water; 10% TiO_2 w/w ; 48h; UV light.

The procedure followed for EXP.3 and EXP.4 was the same of EXP.1 and EXP.2 respectively with the only difference that in EXP.3 the sample was put in dark conditions for 48 hours, while the sample in EXP.4 was irradiated for the same amount of hours.

The GC – MS chromatograms for EXP.3 and EXP.4 are reported in the following Figure 6.1.2.

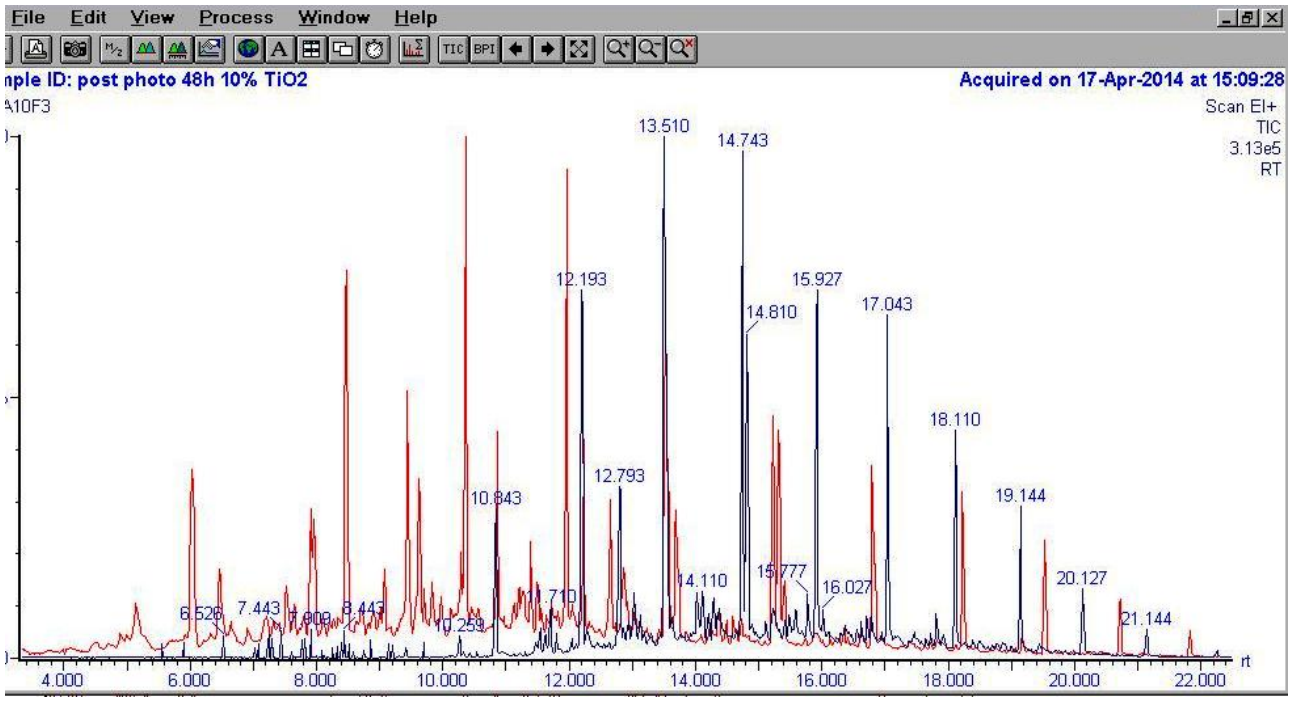

Figure 6.1.2. Superimposition of the GC- MS chromatograms related respectively to EXP.3 (red) and EXP.4 (blue).

The related evaluation of the process efficiency is reported in Table 6.1.2.

Table 6.1.2. Degradation degree % calculated for the hydrocarbons present in the EXP.3 and EXP.4.

Specie	Retention Time [min]	EXP.3 (Blank) [integral i-th/reference integral]	EXP.4 [integral i-th/reference integral]	Degradation %
C10	5,142	0,3217	/	100
C11	6,026	0,6696	/	100
C12	6,459	0,2982	/	100
C13	8,476	0,8968	0,021196486	100
C14	10,360	1,0000	0,027234695	97,28
C15	11,393	0,1678	0,069918694	58,32
C16	12,226	0,2921	0,172031067	41,11
C18	13,526	0,9197	0,8923	2,98
C19	14,337	0,0893	0,082101217	8,04
C20	15,227	0,4725	0,432271892	8,52
C21	16,077	1	1	0

The results (Table 6.1.1. and 6.2.2) indicate that a non significant improve of the degradation efficiency is achieved by performing the photo degradation for longer time than 24 hours.

6.2 EVALUATION OF THE INFLUENCE OF TiO_2 AMOUNT

After the optimization of the time of irradiation of the sample to the UV lights, it was decided to optimize the % w/w of TiO_2 in the sample preparation.

EXP. 5: 5g soil; 5mL deionized water; 5% TiO_2 w/w ; 24h; no light (Blank).

EXP. 6: 5g soil; 5mL deionized water; 5% TiO_2 w/w ; 24h; UV light.

The procedure followed for EXP.5 and EXP.6 was the same of the previous experiments.
The GC – MS chromatograms for EXP.5 and EXP.6 are reported in the following Figure 6.2.1.

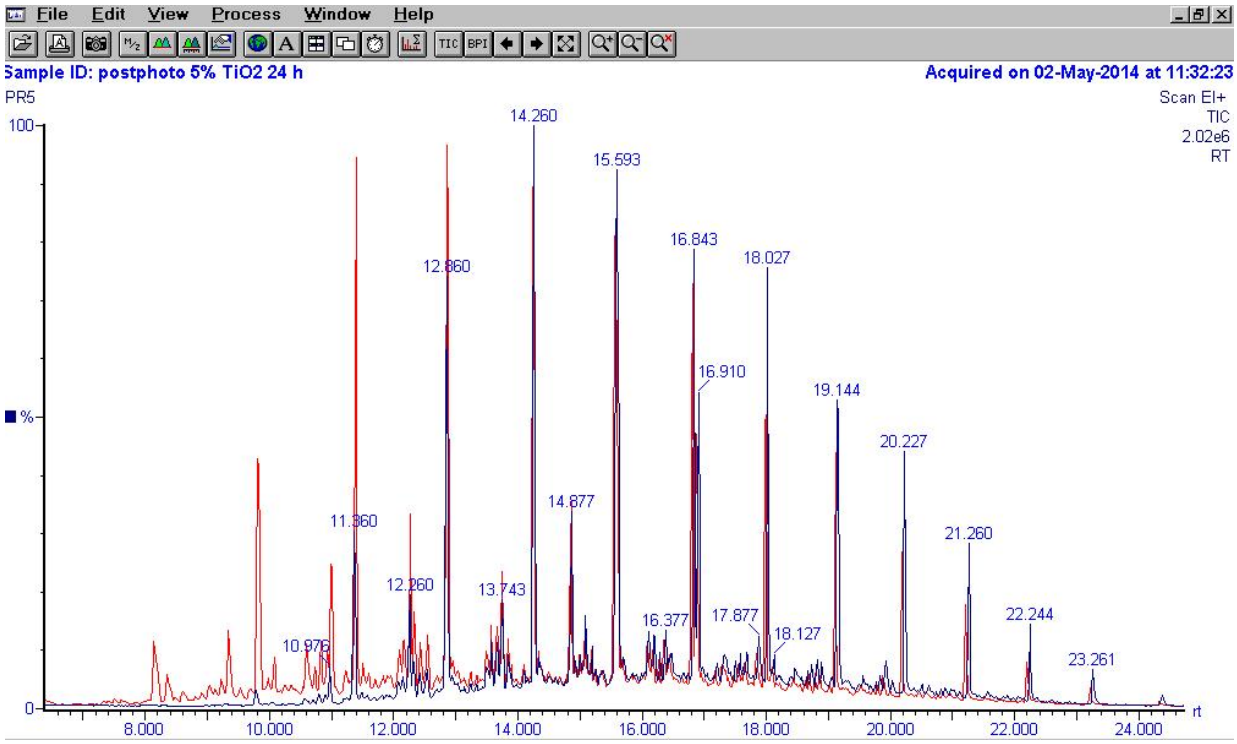

Figure 6.2.1. Superimposition of the GC- MS chromatograms related respectively to EXP.5 (red) and EXP.6 (blue).

The related evaluation of the process efficiency is reported in Table 6.2.1.

Table 6.2.1. Degradation degree % calculated for the hydrocarbons present in the EXP.5 and EXP.6.

Specie	Retention time [min]	EXP.5 (Blank) [integral i-th/reference integral]	EXP.6 [integral i-th/reference integral]	Degradation %
C12	8,143	0,254437	/	100
C13	9,343	0,230648	/	100
C14	10,993	0,301592	0,093366	69,04
C15	11,393	1,03963	0,412955	60,27
C16	12,276	0,383314	0,235148	38,65
C17	12,860	1,146583	0,860765	24,92
C18	13,743	0,193038	0,170354	11,75
C19	14,260	1	1	0
C20	15,560	1,350074	1,338983	0,82

EXP. 7: 5g soil; 5mL deionized water; 15% TiO_2 w/w ; 24h; no light (Blank).

EXP. 8: 5g soil; 5mL deionized water; 15% TiO_2 w/w ; 24h; UV light.

The GC – MS chromatograms for EXP.7 and EXP.8 are reported in the following Figure 6.2.2.

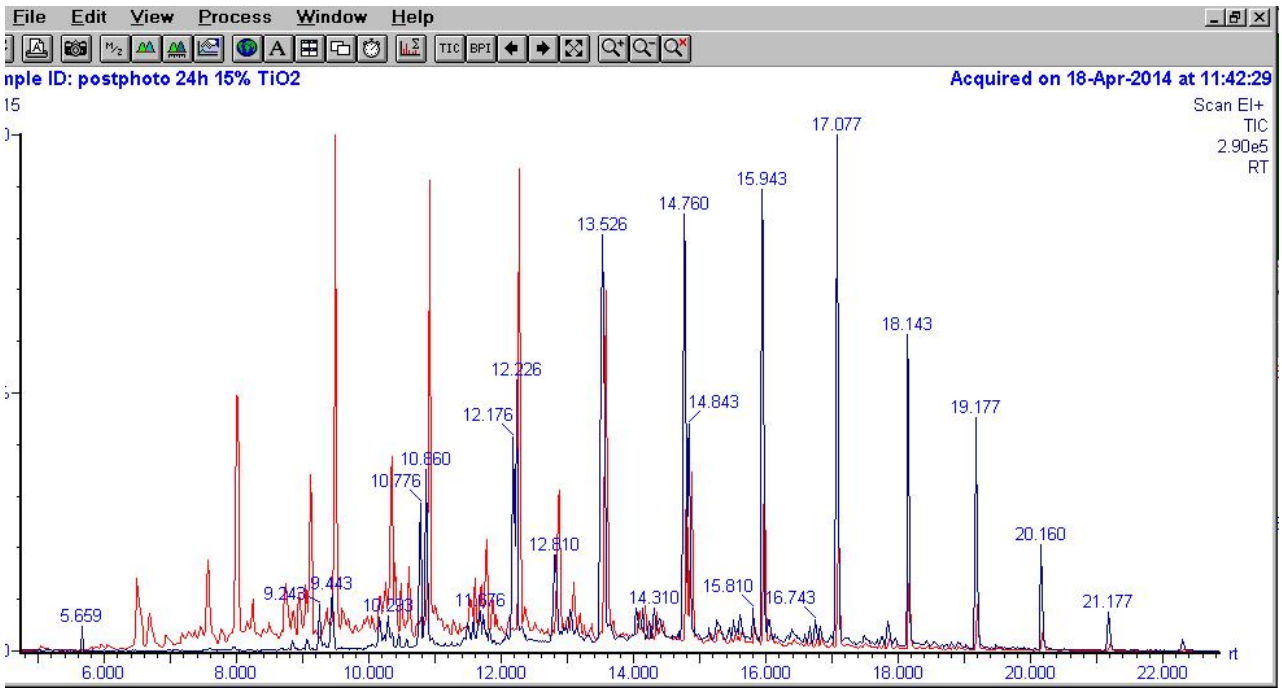

Figure 6.2.2. Superimposition of the GC- MS chromatograms related respectively to EXP.7 (red) and EXP.8 (blue).

The related evaluation of the process efficiency is reported in Table 6.2.2.

Table 6.2.2. Degradation degree % calculated for the hydrocarbons present in the EXP.7 and EXP.8.

Specie	Retention Time [min]	EXP.7 (Blank) [integral i-th/reference integral]	EXP.8 [integral i-th/reference integral]	Degradation %
C11	6,493	0,632954823	/	100
C12	7,559	0,650679198	/	100
C13	9,109	0,779945587	/	100
C14	10,343	0,947863736	0,075099	92,07
C15	11,776	0,473446884	0,107766	77,23
C16	12,276	1,847977193	0,442611	76,04
C17	12,876	0,928399226	0,378673	59,21
C18	14,177	0,136266535	0,065581	51,87
C19	14,793	1	1	0
C20	15,827	0,092005327	0,074818	18,68
C21	15,977	0,689217415	0,074818	89,14

Before fixing the 15% w/w of titania, it was wanted to verify again the process performance, so the experiments EXP.7 and EXP.8 were replicated in respectively EXP.9 and EXP.10.

EXP. 9: 5g soil; 5mL deionized water; 15% TiO_2 w/w ; 24h; no light (Blank).

EXP. 10: 5g soil; 5mL deionized water; 15% TiO_2 w/w ; 24h; UV light.

The results from the GC – MS are reported in the Figure 6.2.3 below.

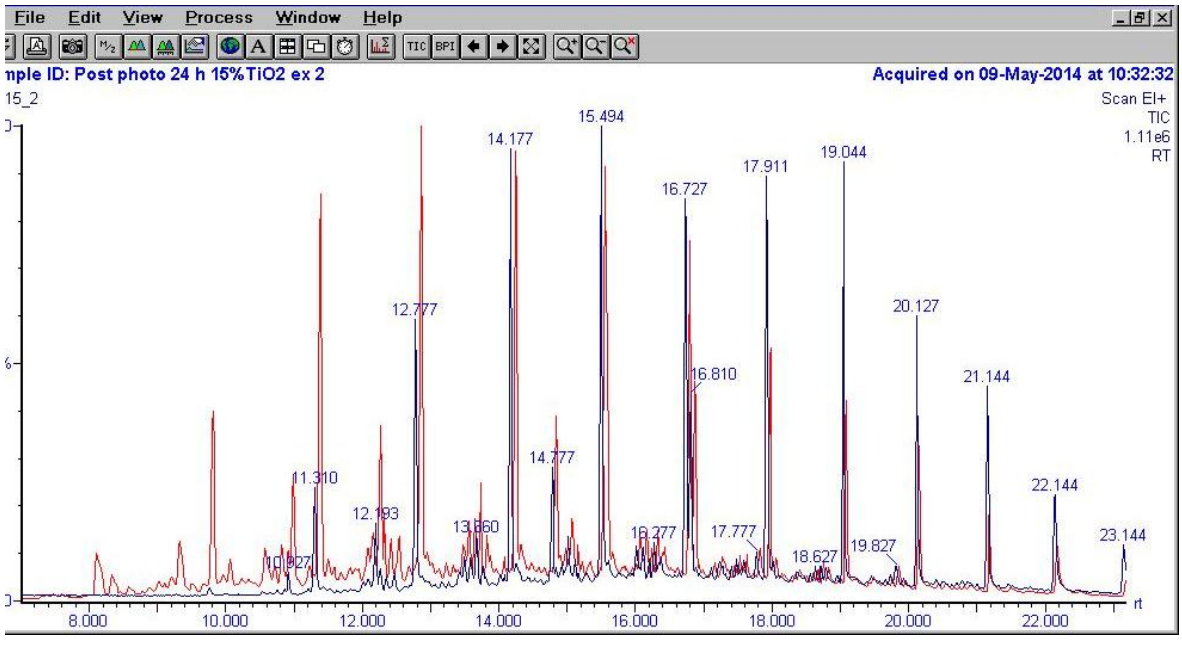

Figure 6.2.3. Superimposition of the GC- MS chromatograms related respectively to EXP.9 (red) and EXP.10 (blue).

The degradation efficiency calculations are reported in Table 6.2.3.

Table 6.2.3. Degradation degree % calculated for the hydrocarbons present in the EXP.9 and EXP.10.

Specie	Retention Time [min]	EXP.9 (Blank) [integral i-th/reference integral]	EXP.10 [integral i-th/reference integral]	Degradation %
C11	6.342	0.496387	/	100
C12	7.426	0.748069	/	100
C13	9.093	0.989808	/	100
C14	10.360	1.258011	0.219131	82.58
C15	11.826	0.710251	0.176653	75.12
C16	12.343	3.349823	1.15894	65.40
C17	12.943	1.538403	0.496876	67.70
C18	14.260	0.299325	0.096346	67.81
C19	14.893	1	1	0
C20	16.077	1.781188	0.07326	95.88
C21	16.160	0.18638	0.07326	60.69

In Figure 7.1.2. (paragraph 7), a more detailed analysis on the TiO_2 % w/w is reported, considering also the ones from EXP.1 and EXP.2 carried out with 10% w/w of TiO_2, showing that the highest degradation efficiency has been achieved with 15% w/w of TiO_2.

6.3 TEMPERATURE

In order to evaluate the influence of the heating released by the UV lamps irradiation on the degradation of hydrocarbons in the mixture the following two experiments (EXP.11 and EXP.12) have been carried out to exclude an evaporation process. Furthermore, a preliminary indication of the thermal balance of the photocatalytic process can be obtained.

EXP.11: 10g soil; 10mL deionized water; 8h; UV light.

EXP. 12: 10g soil; 10mL deionized water; 15% TiO_2 w/w ; 8h; UV light.

Particularly, in these experiments the temperature profile for each one was measured thanks to a temperature sensor (paragraph 4.7) which recorded automatically the temperature value every 30 seconds.

Also in EXP.11 and EXP.12 the samples were fed with 10mL of deionized water after 4h due to the water evaporation.

In Figure 6.3.1 and 6.3.2. are respectively reported the temperature profile of EXP.11 and EXP.12.

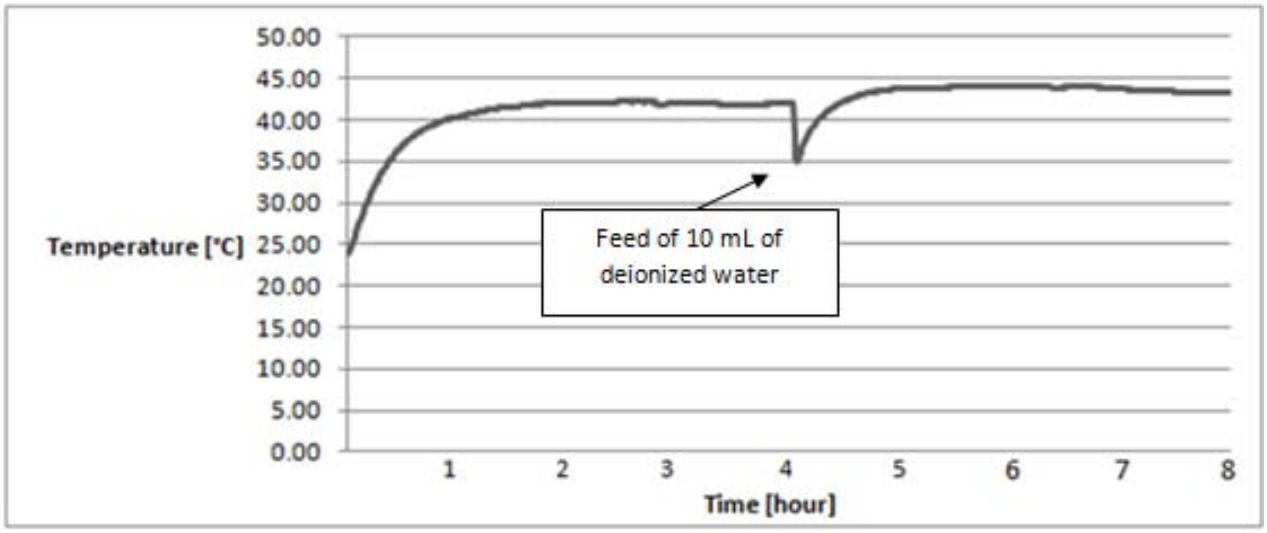

Figure 6.3.1. Temperature profile related to the EXP.11.

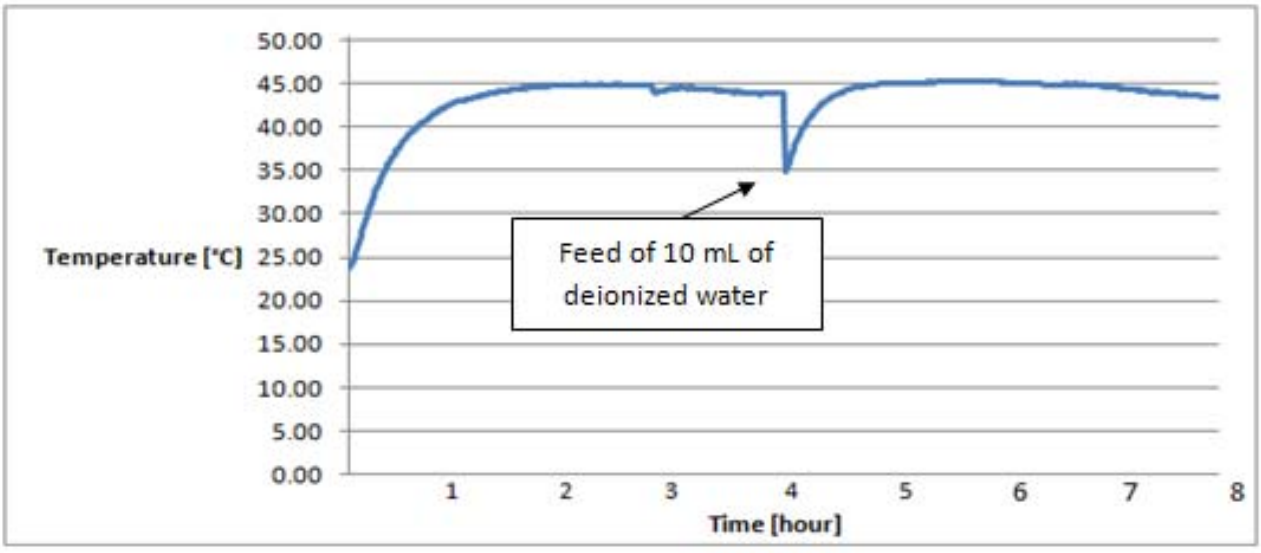

Figure 6.3.2. Temperature profile related to the EXP.12.

6.4 EVALUATION OF THE INFLUENCE OF H_2O_2 AMOUNT

To evaluate the effect of the H_2O_2 in the process efficiency were carried out the following experiments:

EXP.13: 5g soil; 5mL H_2O; 15% TiO2 w/w; 24h; no light (Blank).

EXP.14: 5g soil; 5mL H_2O; 15% TiO2 w/w; 24h; UV light.

The procedure followed for the EXP.13 and EXP 14. Was the same as the one for the experiments in the paragraph 6.2.

The degradation efficiency calculated, according to the output data from GC – MS, is reported in the following Figure 6.4.1.

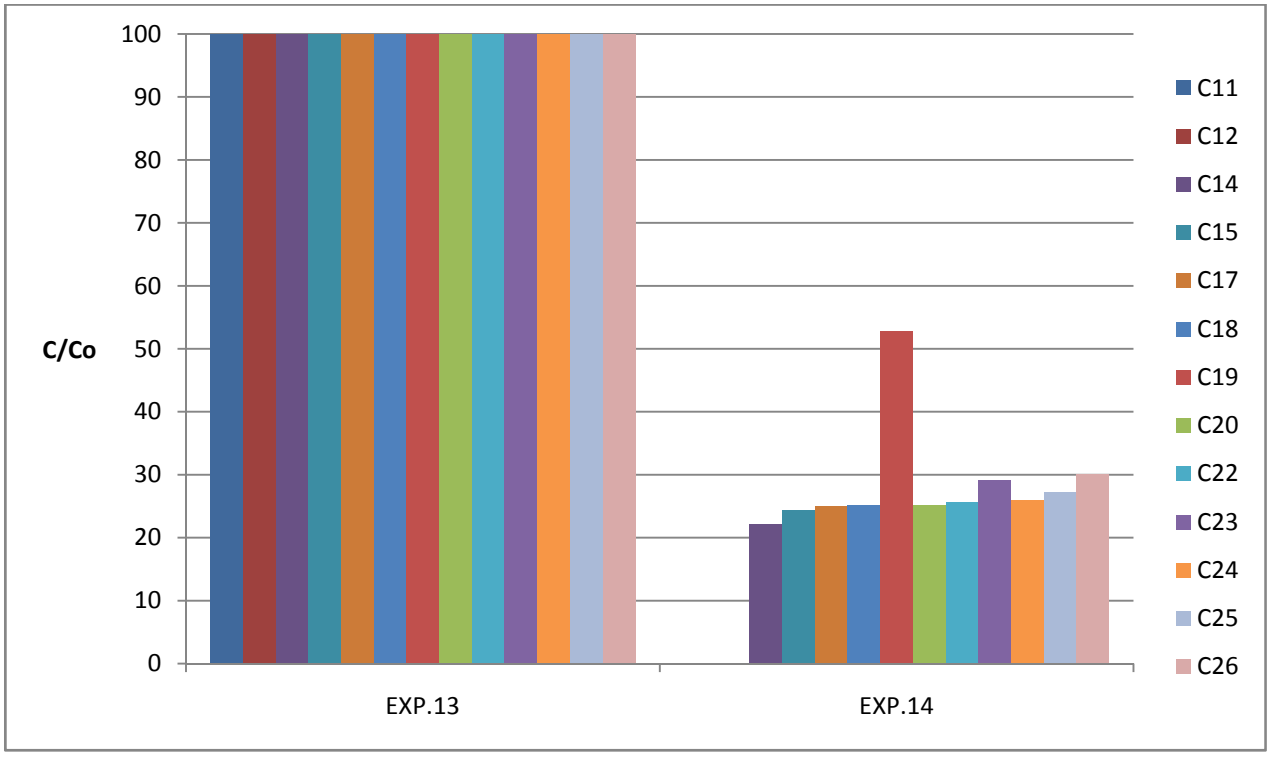

Figure 6.4.1. Hydrocarbons degradation at the end of the test for EXP.13-14.

EXP.15: 5g soil; 5mL H_2O_2 $2*10^{-2}$ M (in 5mL); 15% TiO2 w/w; 24h; no light (Blank).

EXP.16: 5g soil; 5mL H_2O_2 $2*10^{-2}$ M (in 5mL); 15% TiO2 w/w; 24h; UV light.

The degradation efficiency calculated for these experiments is reported in Figure 6.4.2.

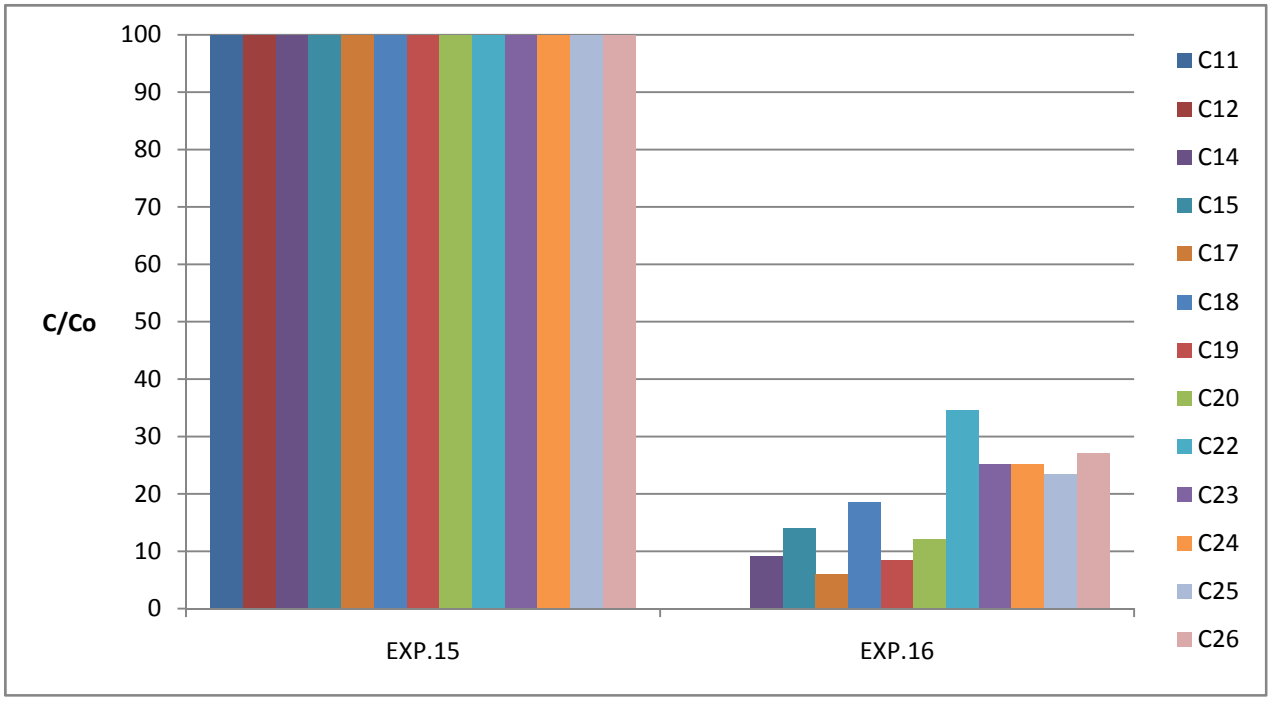

Figure 6.4.2. Hydrocarbons degradation at the end of the test for EXP.15-16.

EXP.17: 5g soil; 5mL H_2O_2 $5*10^{-2}$ M (in 5mL); 15% TiO2 w/w; 24h; no light (Blank).

EXP.18: 5g soil; 5mL H_2O_2 $5*10^{-2}$ M (in 5mL); 15% TiO2 w/w; 24h; UV light.

The degradation efficiency calculated for these experiments is reported in Figure 6.4.3.

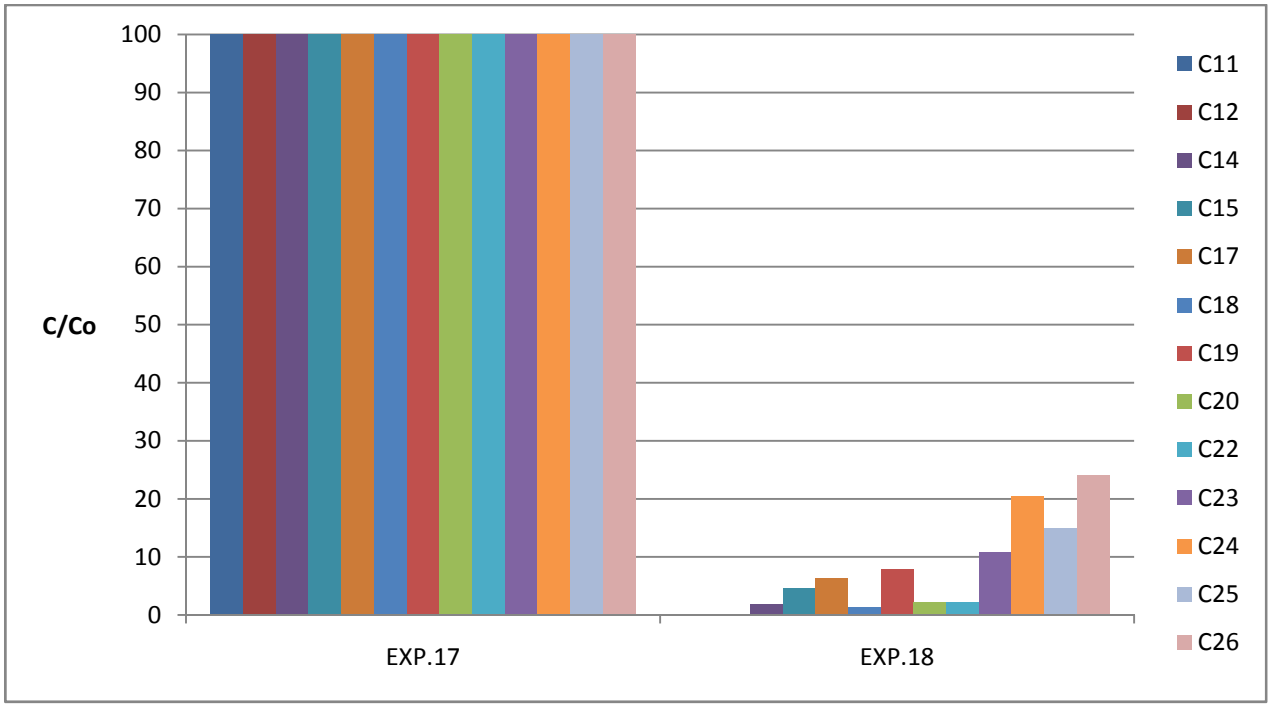

Figure 6.4.3. Hydrocarbons degradation at the end of the test for EXP.17-18.

EXP.19: 5g soil; 5mL H_2O_2 10^{-1} M (in 5mL); 15% TiO2 w/w; 24h; no light (Blank).

EXP.20: 5g soil; 5mL H_2O_2 10^{-1} M (in 5mL); 15% TiO2 w/w; 24h; UV light.

The degradation efficiency calculated for these latter experiments is reported in Figure 6.4.4.

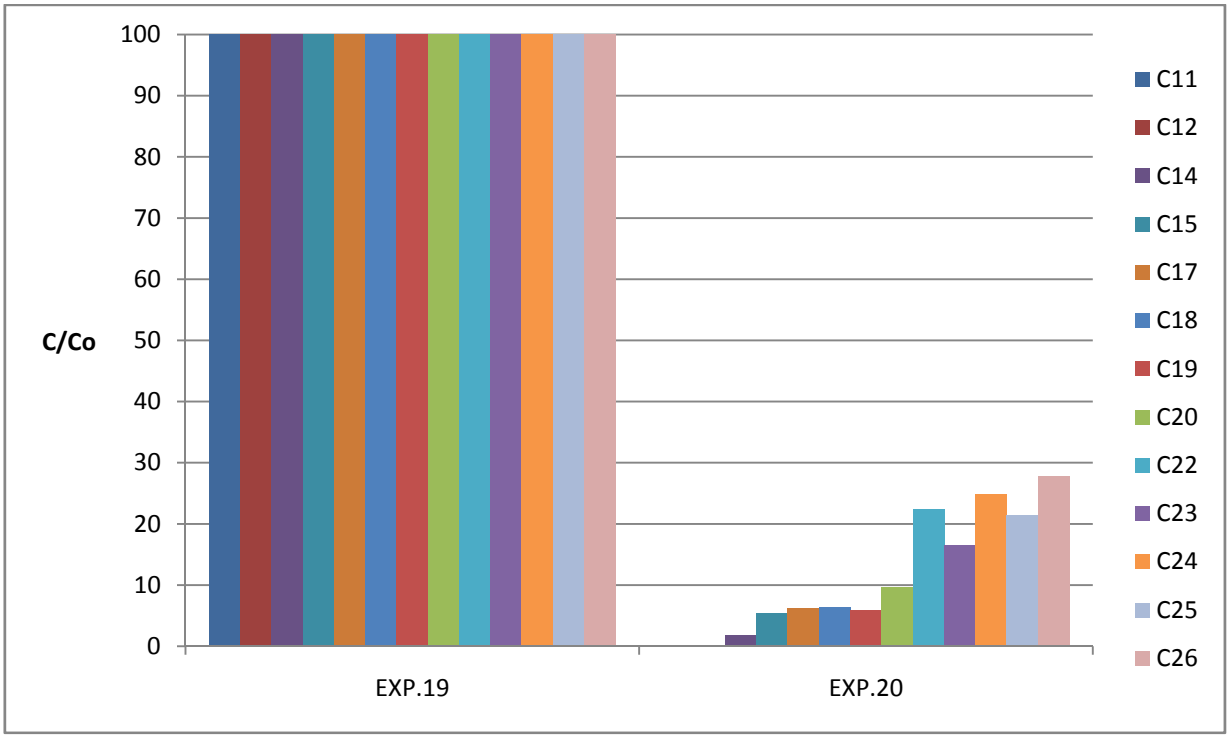

Figure 6.4.4. Hydrocarbons degradation at the end of the test for EXP.19-20.

EXP.21: 5g soil; 5mL H_2O_2 1 M (in 5mL); 15% TiO2 w/w; 24h; no light (Blank).

EXP.22: 5g soil; 5mL H_2O_2 1 M (in 5mL); 15% TiO2 w/w; 24h; UV light.

The degradation efficiency calculated for these latter experiments is reported in Figure 6.4.5.

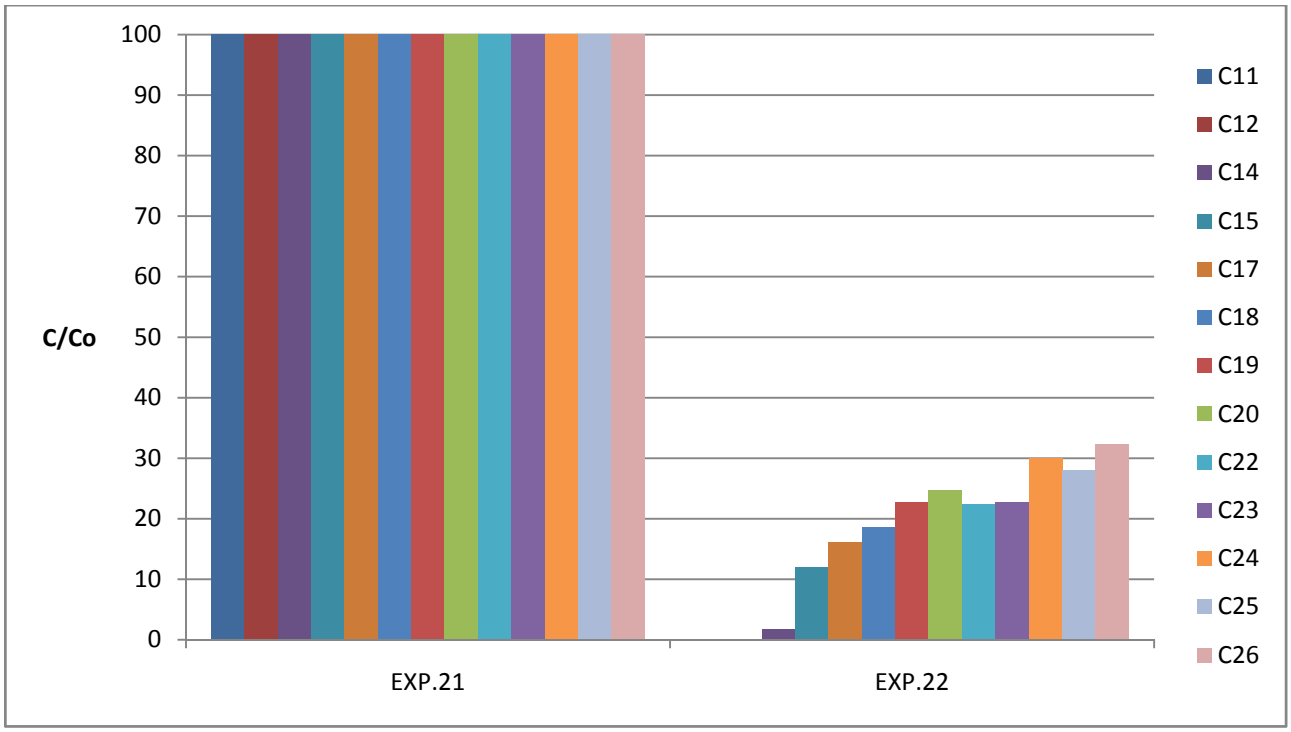

Figure 6.4.5. Hydrocarbons degradation at the end of the test for EXP.21-22.

EXP.23: 5g soil; 5mL H_2O_2 (8.8 M) ; 15% TiO2 w/w; 24h; no light (Blank).

EXP.24: 5g soil; 5mL H_2O_2 (8.8 M); 15% TiO2 w/w; 24h; UV light.

The degradation efficiency calculated for these latter experiments is reported in Figure 6.4.6.

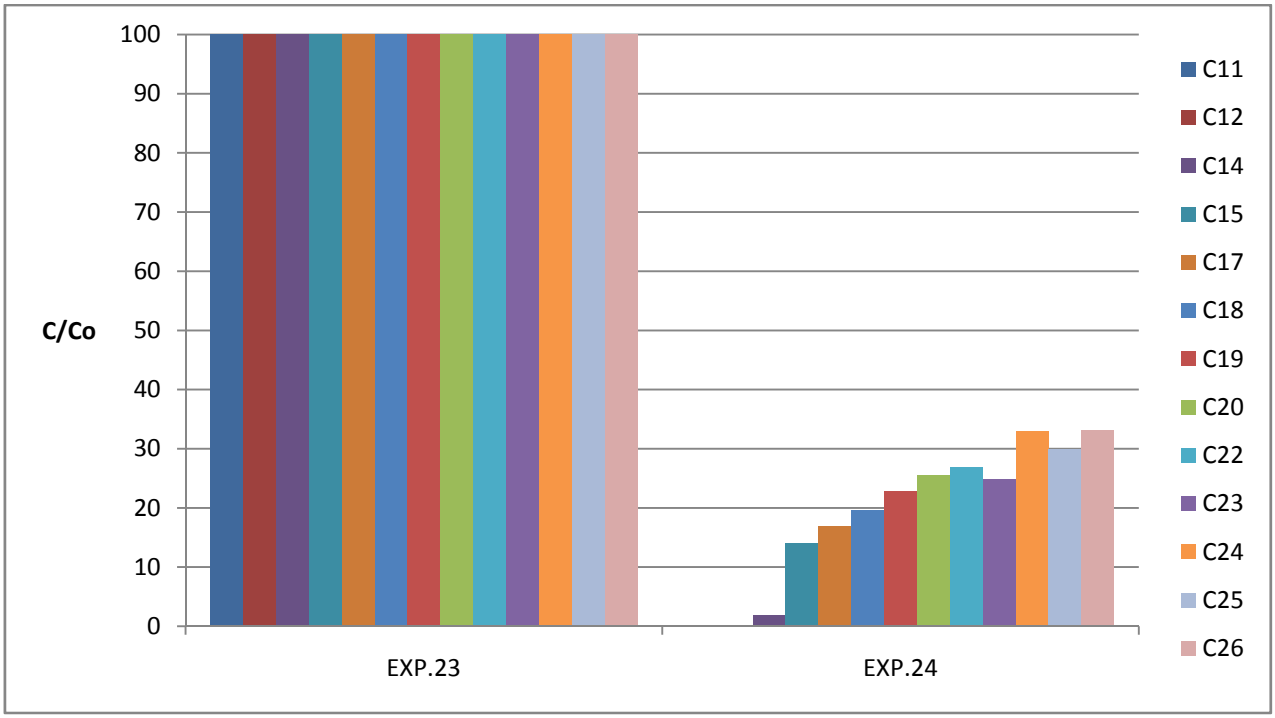

Figure 6.4.6. Hydrocarbons degradation at the end of the test for EXP.23-24.

From the reported results in this paragraph, it is possible to observe that the highest degradation efficiency is reached using $[H_2O_2] = 5*10^{-2}$ M. Therefore, this latter concentration was used to carry out all the subsequent experiments. A more detailed analysis on the H_2O_2 evaluation is presented in paragraph 7.1.4.

6.5 EVALUATION OF pH INFLUENCE

After the hydrogen peroxide, the pH condition were evaluated.
To measure the contaminated soil pH, a sample of 10g was taken and it was mixed for 30 minutes with deionized water, according to the standard ASTM procedure D 4972-01.
The pH of the slurry was measured either with litmus paper and pH meter.
The results obtained were: 6.6 – 6.9 (litmus paper 1), 6.5 – 7 (litmus paper 2), 7.31 (pH meter 1), 7.47 (pH meter 2). For all the measurements performed in the different experiments, a pH meter has been used. Therefore, 5 different samples (plus their related blank) at 5 different pH conditions were prepared.

EXP.25: 5g soil; 5mL H_2SO_4 $1.04*10^{-3}$ M (= $1.02*10^{-2}$ g H_2SO_4 in 100 mL deionized H_2O); pH = 3.43; 15% TiO2 w/w; 24h; no light (Blank) .

EXP.26: 5g soil; 5mL H_2SO_4 $1.04*10^{-3}$ M (= $1.02*10^{-2}$ g H_2SO_4 in 100 mL deionized H_2O); pH = 3.36; 15% TiO2 w/w; 24h; UV light.

After the usual procedure the samples in both the experiments were analyzed with the GC – MS. From the calculations of the degradation efficiencies, Figure 6.5 has been obtained.

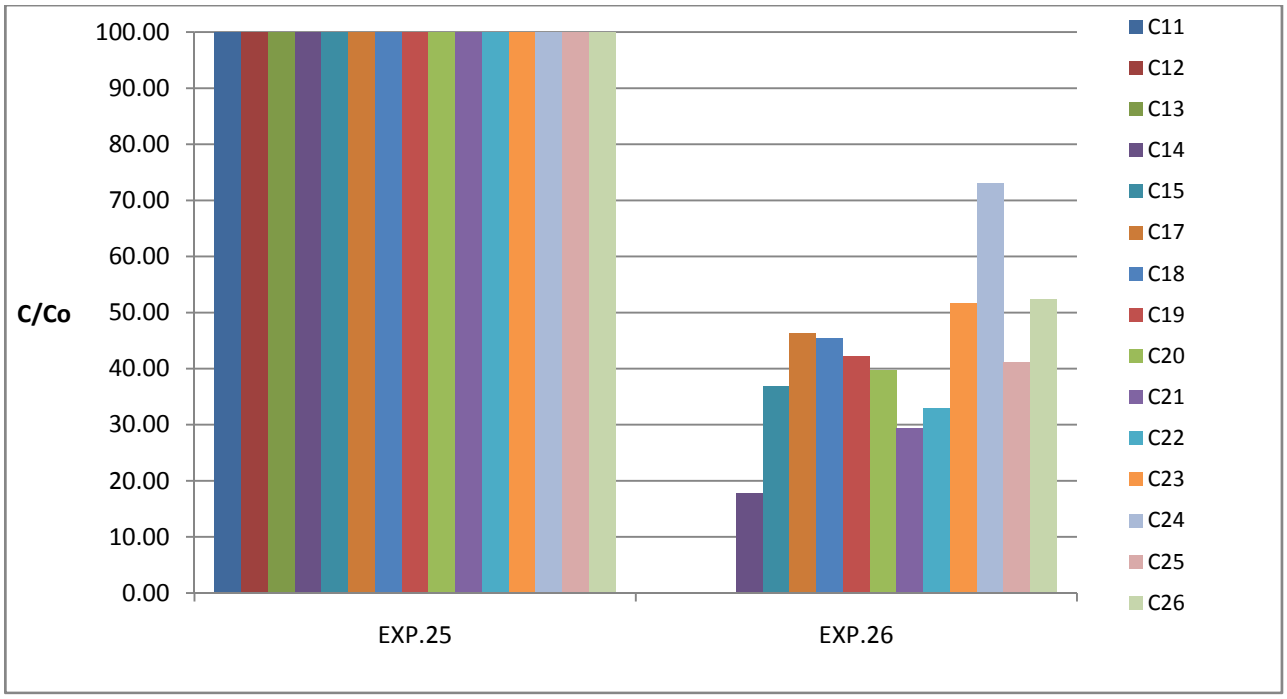

Figure 6.5. Hydrocarbons degradation at the end of the test for EXP.25-26.

EXP.27: 5g soil; 5mL H_2SO_4 $1.04*10^{-4}$ M (= $1.02*10^{-2}$ g H_2SO_4 in 1L deionized H_2O); pH = 5.11; 15% TiO2 w/w; 24h; no light (Blank) .

EXP.28: 5g soil; 5mL H_2SO_4 $1.04*10^{-4}$ M (= $1.02*10^{-2}$ g H_2SO_4 in 1L deionized H_2O); pH = 5.27; 15% TiO2 w/w; 24h; UV light.

The degradation efficiency of the hydrocarbons calculated for these latter experiments is reported in Figure 6.5.1.

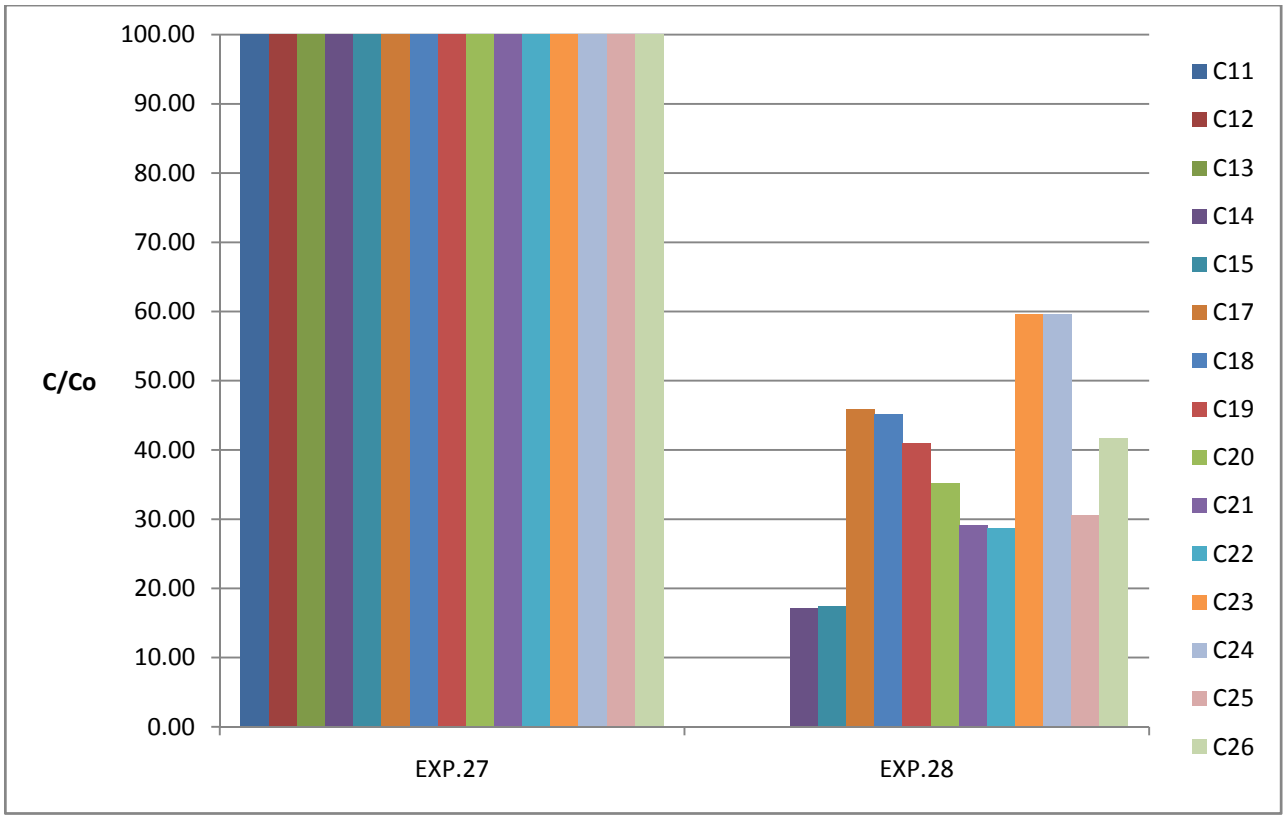

Figure 6.5.1. Hydrocarbons degradation at the end of the test for EXP.27-28.

EXP.29: 5g soil; 5mL deionized H_2O; pH = 7.29; 15% TiO2 w/w; 24h; no light (Blank) .

EXP.30: 5g soil; 5mL deionized H_2O; pH = 7.16; 15% TiO2 w/w; 24h; UV light.

From the calculations of the degradation efficiencies of EXP.29 and EXP.30, Figure 6.5.2. below has been obtained.

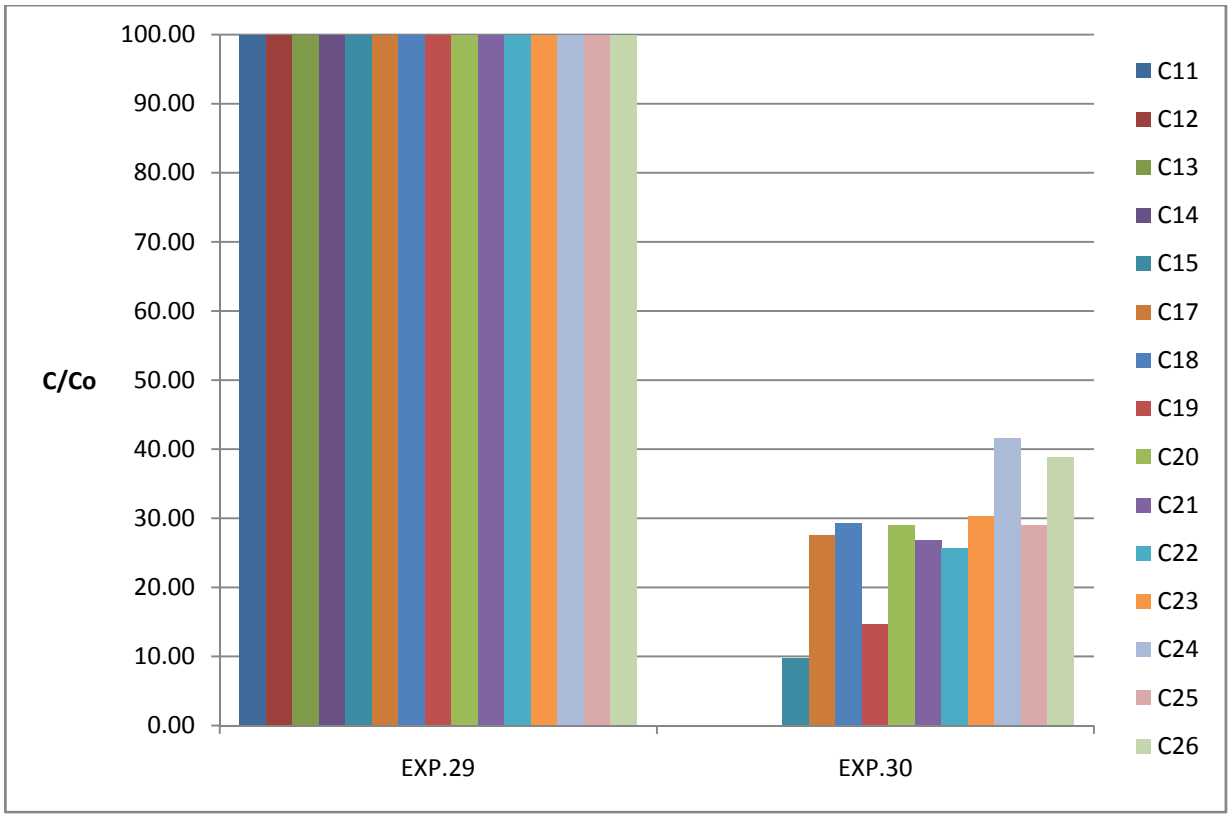

Figure 6.5.2. Hydrocarbons degradation at the end of the test for EXP.29-30.

EXP.31: 5g soil; 5mL NaOH $1*10^{-5}$ M (= $4.*10^{-4}$ g NaOH in 1L deionized H_2O); pH = 8.85; 15% TiO2 w/w; 24h; no light (Blank) .

EXP.32: 5g soil; 5 mL NaOH $1*10^{-5}$ M (= $4.*10^{-4}$ g NaOH in 1L deionized H_2O); pH = 9.21; 15% TiO2 w/w; 24h; UV light.

The degradation efficiency of the hydrocarbons calculated for these latter experiments is reported in Figure 6.5.3.

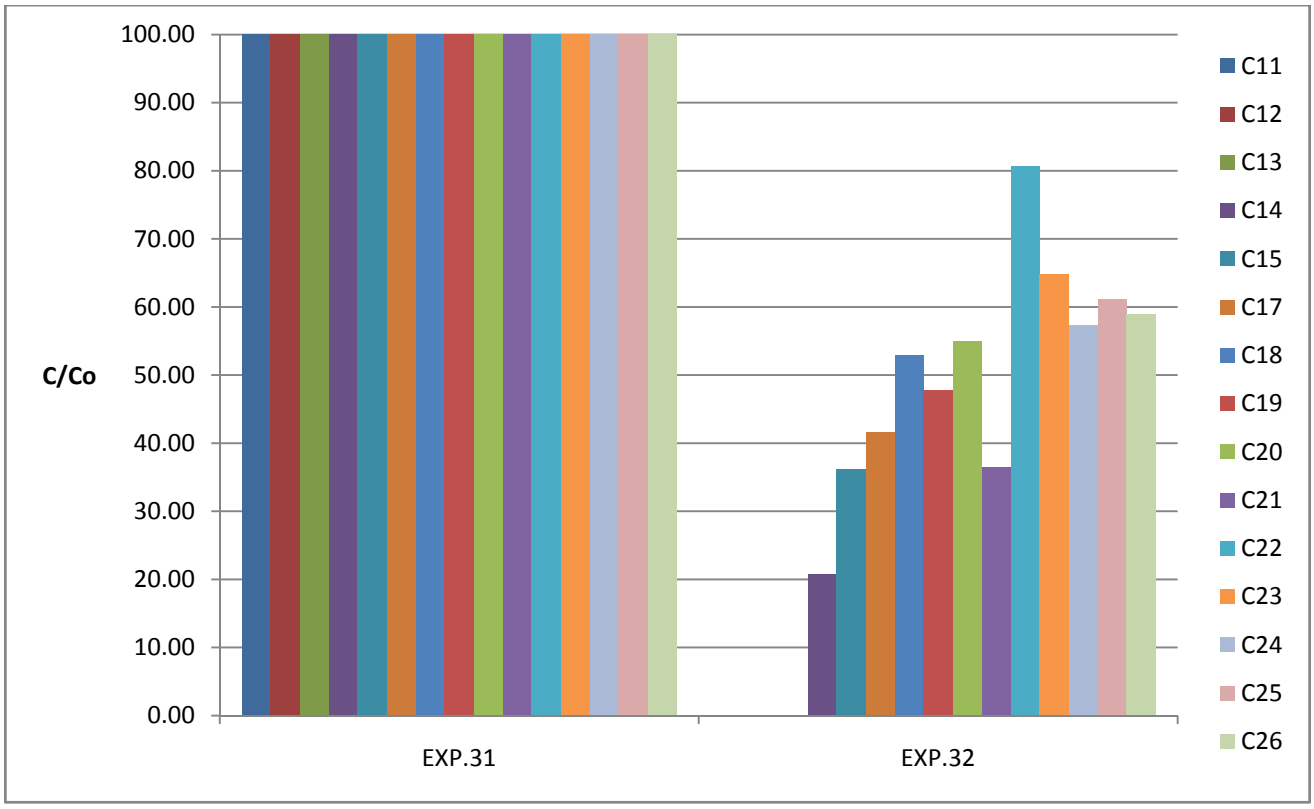

Figure 6.5.3. Hydrocarbons degradation at the end of the test for EXP.31-32.

EXP.33: 5g soil; 5mL NaOH $1*10^{-4}$ M (= $4.*10^{-4}$ g NaOH in 100 mL deionized H_2O); pH = 10.73; 15% TiO2 w/w; 24h; no light (Blank) .

EXP.34: 5g soil; 5 mL NaOH $1*10^{-4}$ M (= $4.*10^{-4}$ g NaOH in 100 mL deionized H_2O); pH = 10.87; 15% TiO2 w/w; 24h; UV light.

From the calculations of the degradation efficiencies of EXP.33 and EXP.34, Figure 6.5.4. has been obtained.

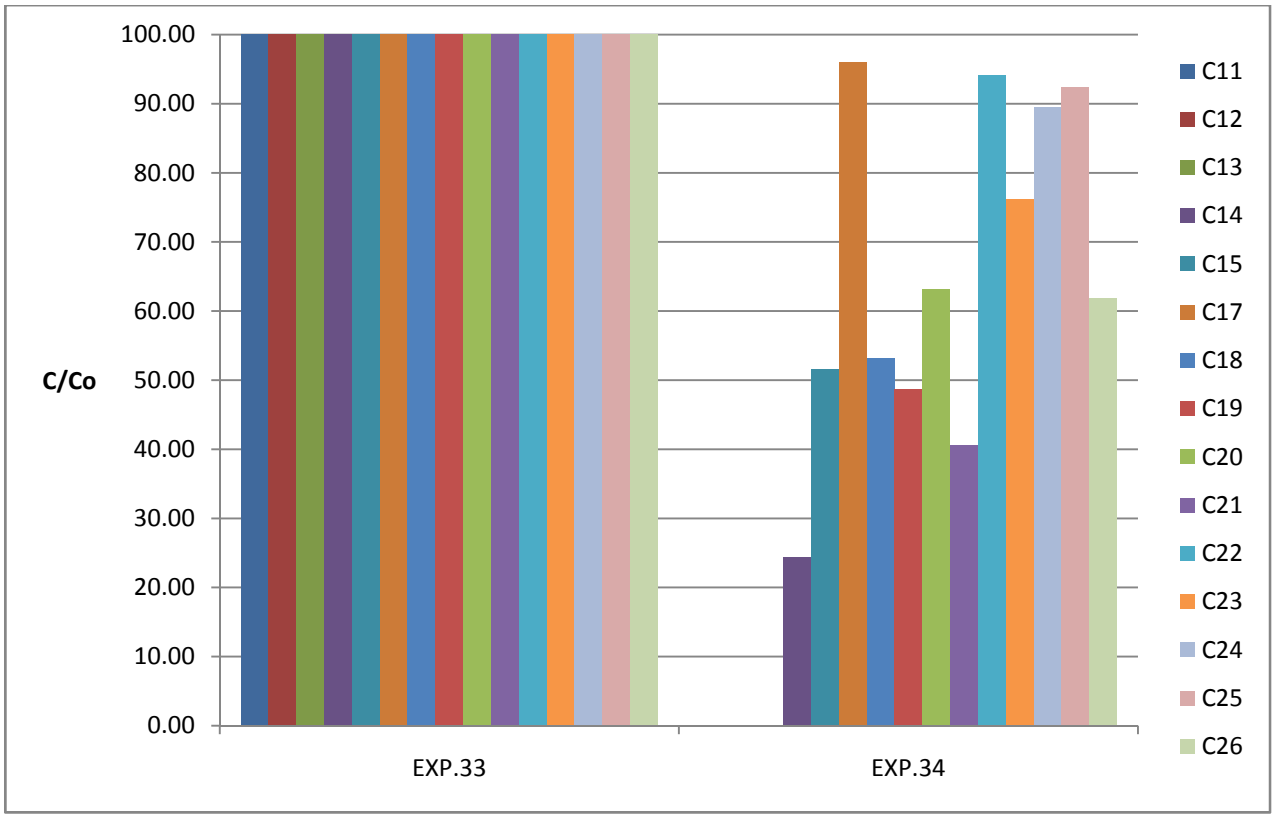

Figure 6.5.4. Hydrocarbons degradation at the end of the test for EXP.33-34.

According to the result obtained from the experiment in this paragraph, it has been decided to proceed the experimental evaluation of the process parameters without adjusting the soil pH.
A more precise discussion about the pH evaluation is reported in paragraph 7.1.5.

6.6 EVALUATION OF THE EFFICIENCY OF DIFFERENT SOLVENTS FOR EXTRACTION

The photocatalytic process could produce polar and non polar products. Thus, the extraction process with hexane was compared with the extraction using acetone (EXP. 35) and isopropyl alcohol (EXP. 36).

EXP.35: 5g soil; 5mL H_2O_2 $5*10^{-2}$ M; 15% TiO2 w/w; 24h; no light .

EXP.36: 5g soil; 5mL H_2O_2 $5*10^{-2}$ M; 15% TiO2 w/w; 24h; no light .

The procedure to carry out and analyze EXP.35 and EXP.36 was the usual one, with the only difference that in the extraction step was used, instead of hexane, respectively isopropyl alcohol (100 mL) for EXP.35 and acetone (100mL) for EXP.36.

The chromatograms of EXP.35 and EXP.36 in output from GC – MS were finally compared with the one of EXP.7, in which the extraction was performed using hexane (100mL).

The results are reported respectively in Figure 6.6 (EXP 35) anf Figure 6.6.1 (EXP.36).

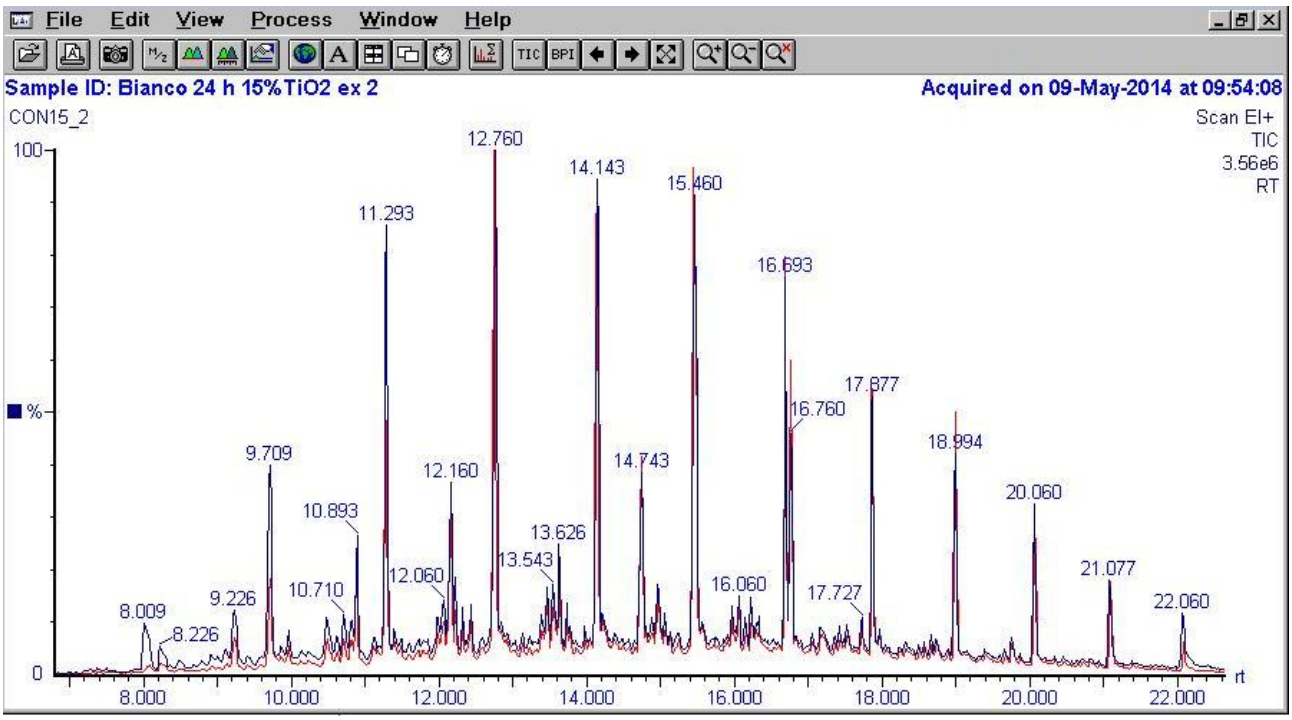

Figure 6.6. Superimposition of the GC- MS chromatograms related respectively to EXP.7 (red) and EXP.35 (blue).

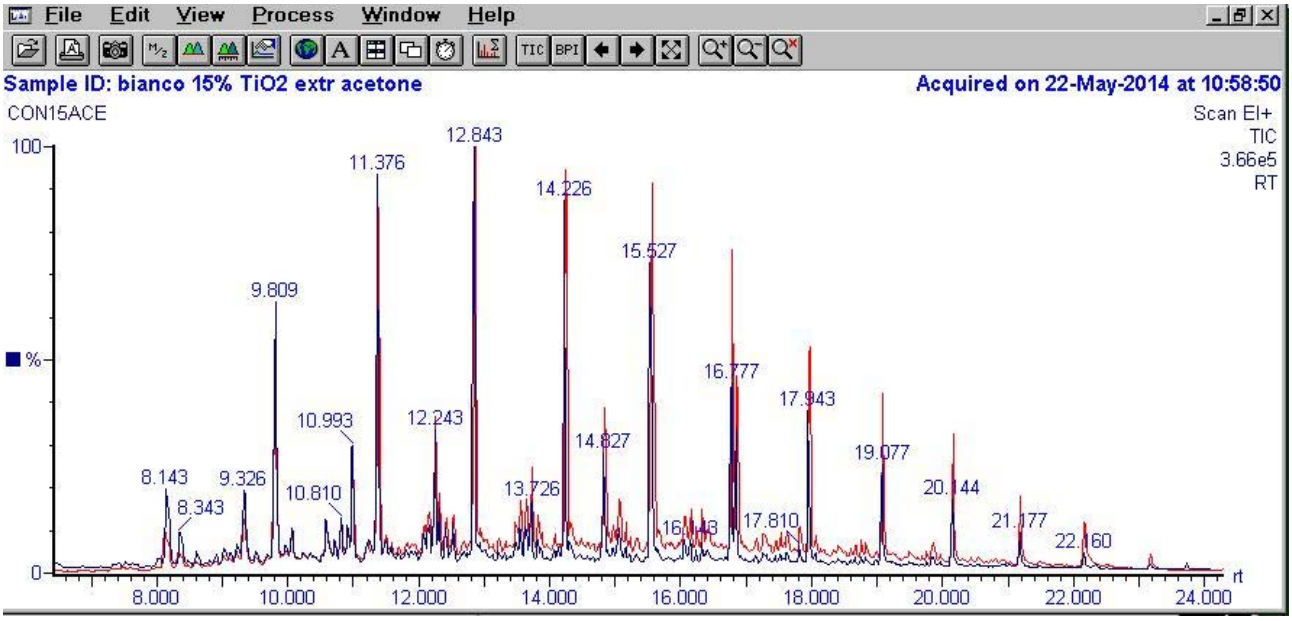

Figure 6.6.1. Superimposition of the GC- MS chromatograms related respectively to EXP.7 (red) and EXP.36 (blue).

It was observed that the chromatograms of isopropyl alcohol and acetone, reported respectively in Figure 6.6 and Figure 6.6.1, are superimposable with that for hexane extraction, indicating that no additional by products are found during the photo degradation. For this reason, all the experiments have been carried out with hexane as solvent in the extraction step.

6.7 OPTIMIZED PARAMETERS

A further experiment was carried out with all the optimized parameters found in the previous experiments.

EXP.37: 5g soil; 5mL H_2O_2 $5*10^{-2}$ M; 15% TiO2 w/w; 24h; no light (Blank).

EXP.38: 5g soil; 5mL H_2O_2 $5*10^{-2}$ M; 15% TiO2 w/w; 24h; UV light .

After the usual procedure, the EXP.37 and EXP.38 were analyzed with GC – MS giving the following results reported in Table 6.7.

Table 6.7. Degradation degree % calculated for the hydrocarbons present in the EXP.37 and EXP.38.

Peak	Retention Time [min]	EXP.37 [integral i-th/ reference integral]	EXP.38 [integral i-th/ reference integral]	Degradation %
tetrachloroethane	3.543	1	1	-
C13	8.078	0.127613966	0	100.00
C14	9.761	0.332062338	0.025243025	92.40
C15	11.328	0.431738818	0.054298595	87.42
C17	12.812	0.407265514	0.078848629	80.64
C18	14.196	0.286251224	0.088788707	68.98
C19	14.796	0.125006238	0.02854704	77.16
C20	15.513	0.336518956	0.141990544	57.81
C21	16.030	0.021386948	0.005570964	73.95
C22	16.747	0.143524708	0.121256682	15.52
C23	17.930	0.106577251	0.106082462	0.46
C24	19.047	0.079630222	0.072534988	8.91
C25	20.131	0.050984906	0.032607914	36.04
C26	22.160	0.316837001	0.021108279	93.34
C27	23.177	0.102652029	0.011068386	89.22

6.8 PHOTOCATALYTIC DEGRADATION IN THE PRESENCE OF HYDROPHYLIC SOLVENTS (THF AND DIOXANE)

In order to improve the homogeneity of the catalytic process, photodegradation reactions have been carried out in the presence of THF and dioxane, to achieve the hydrocarbons solubilization in the mixture H_2O/solvent.

EXP.39: 5g soil + 20 mL of THF (mix for 1h); 5mL H_2O; 5% TiO2 w/w; 24h; no light (Blank) .

EXP.40: 5g soil + 20 mL of THF (mix for 1h); 5mL H_2O; 5% TiO2 w/w; 24h; UV light .

EXP.41: 5g soil + 20 mL of dioxane (mix for 1h); 5mL H_2O; 15% TiO2 w/w; 24h; no light (Blank).

EXP.42: 5g soil + 20 mL of dioxane (mix for 1h); 5mL H_2O; 15% TiO2 w/w; 24h; UV light .

The samples were analyzed according to the usual procedure.

For the EXP.39 and EXP.41 (Blanks), no hydrocarbons degradation was observed.

The results obtained from EXP.40 were compared with EXP.6 due to the similar experimental conditions (Figure 6.8), while the results of EXP.42 were compared with the ones of EXP.8 for the same reason (Figure 6.8.1).

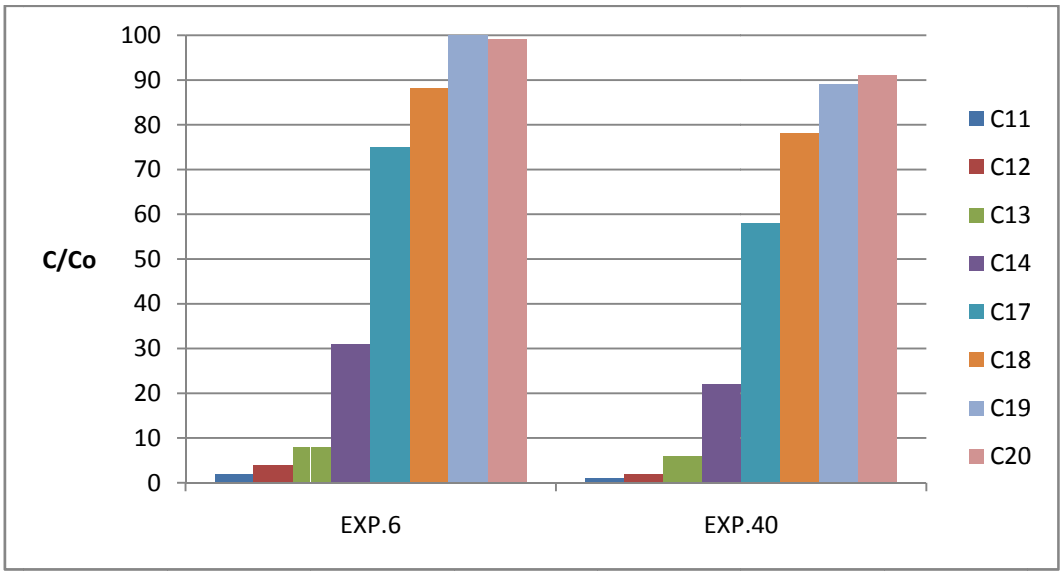

Figure 6.8. Hydrocarbons degradation at the end of the test for EXP.6 and EXP.40.

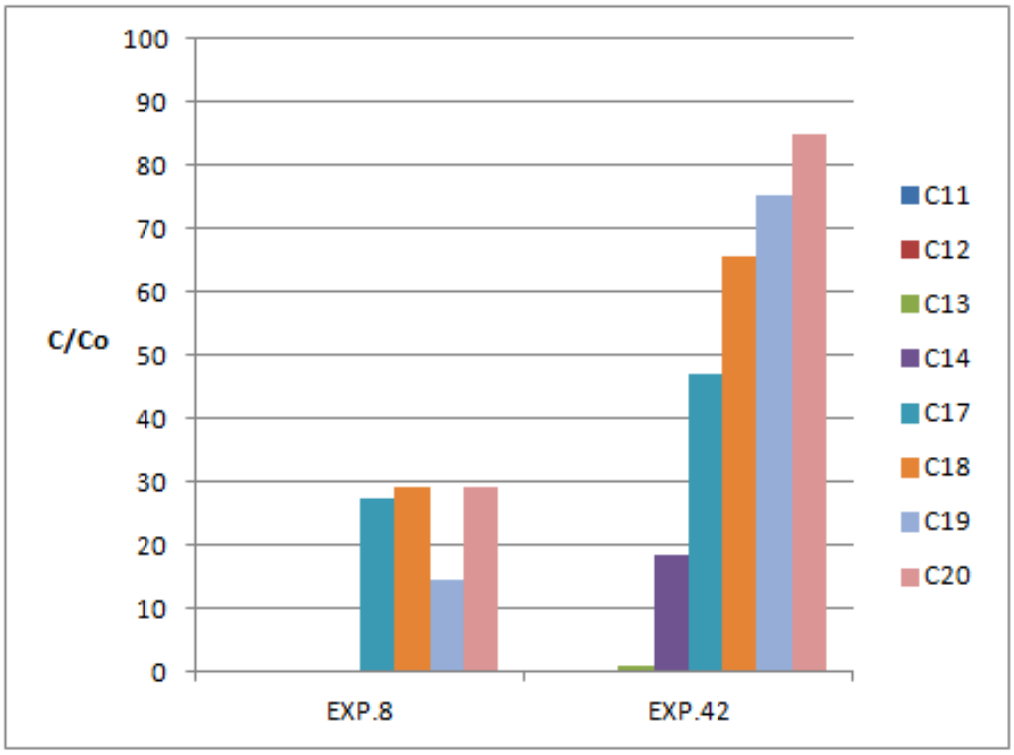

Figure 6.8.1. Hydrocarbons degradation at the end of the test for EXP.8 and EXP.42.

From Figure 6.8 it can be observed that the effect of THF enhance the degradation performance, while Figure 6.8.1. shows that dioxane is not effective in the hydrocarbons degradation process. Therefore, it seems that THF, rather than dioxane, is suitable to improve the process efficiency. Anyway, no one of the two can be concretely implemented due to their high cost and their negative environmental impact.

6.9 FURTHER QUANTITATIVE EVALUATIONS

a) An internal standard evaluation

In order to have a quantitative evaluation of the hydrocarbons degradation in the soil:
10µL of tetrachloroethane as internal standard were added to the 10mL of acetone solution to analyze (see paragraph 4.1).
A typical chromatogram is reported in Figure 6.9.

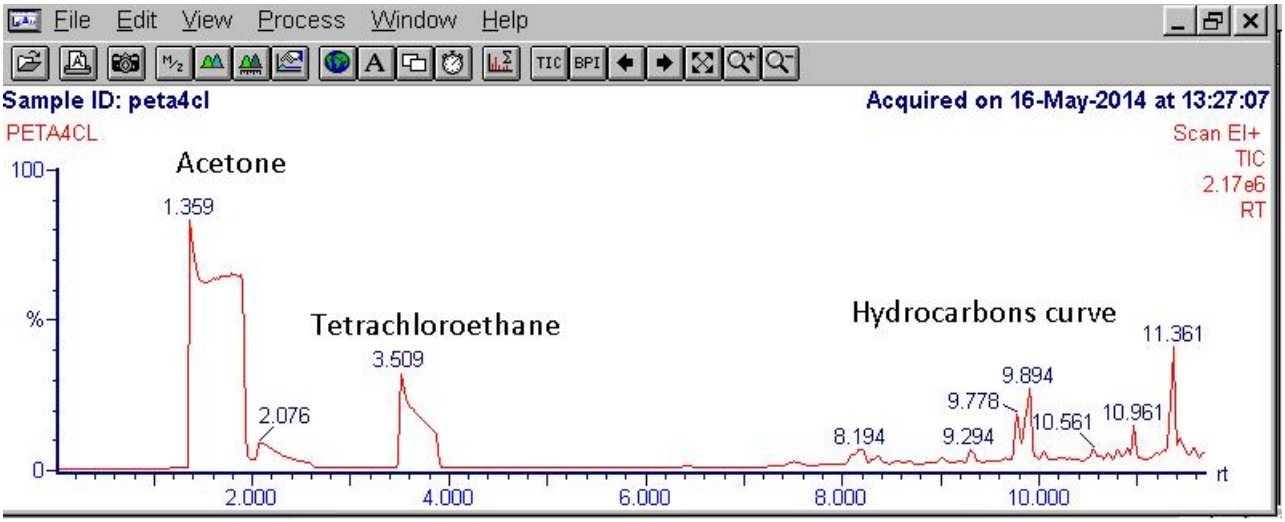

Figure 6.9. The tetrachloroethane peak in the GC – MS chromatogram.

It was decided to use this compound as internal standard due to its noticeable presence in the GC-MS analysis, consisting in a peak between the acetone one and the hydrocarbons curve (Figure 6.9). Other standards were tried (i.e. toluene, chlorobenzene and carbon tetrachloride) but the tetrachloroethane was better positioned in the GC-MS chromatograms. An experiment in order to observe the results obtained with the addition of internal standard was performed.

EXP.43: 5g soil; 5mL deionized H_2O; 15% TiO2 w/w; 24h; no light (Blank).

EXP.44: 5g soil ; 5mL deionized H_2O; 15% TiO2 w/w; 24h; UV light .

The chromatogram in output from GC – MS are reported in Figure 6.9.1.

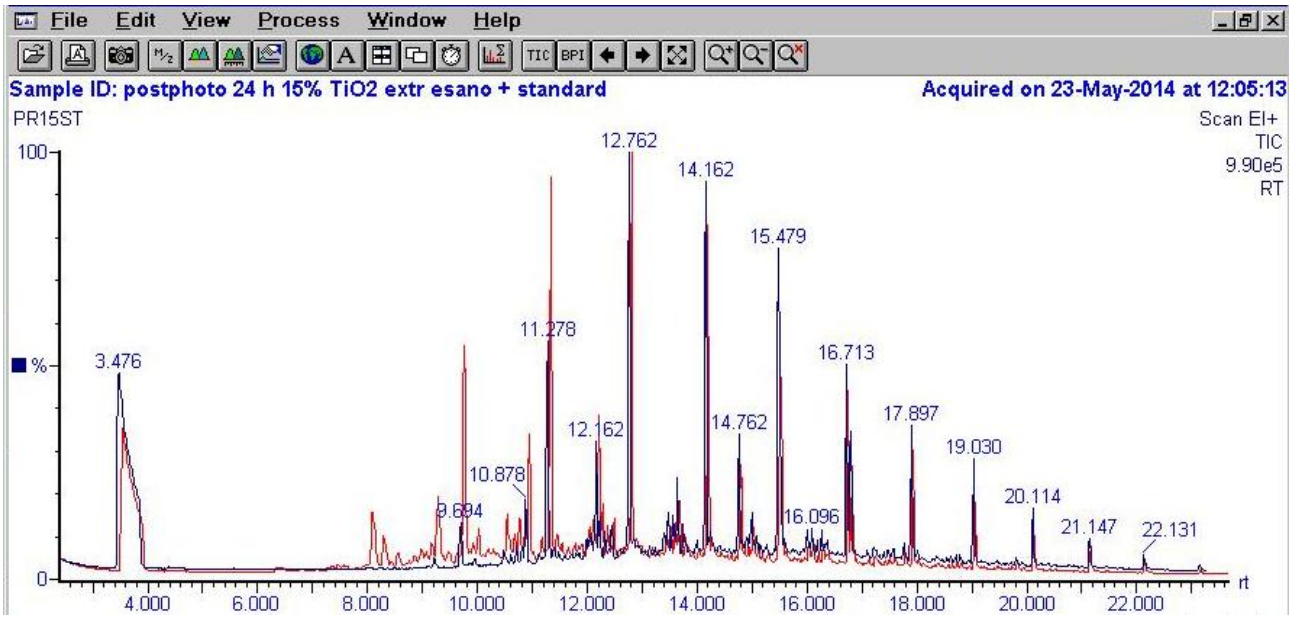

Figure 6.9.1. Chromatogram superimposition of EXP.43 (red) and EXP.44 (blue).

The degradation efficiency was comparable with the one obtained in the EXP.10.

b) Determination of the pollution amount

An extraction process was carried out in the starting polluted soil (EXP.45).

EXP.45: 5g soil; extraction with hexane (100 mL, 24h).

The sample was therefore analyzed with GC – MS using 10µL of internal standard.
Therefore, knowing the amount of moles of standard present, the quantification of the hydrocarbons species inside the sample was possible according to the following proportion:

$$Integral\ of\ the\ standard : 9.47 * 10^{-5} moles\ standard = Integral^{\ i-th} : x\ moles^{\ i-th}$$

Results of EXP.45 are reported in Table. 6.9.

c) Evaluation of the degradation efficiency

After EXP.45, it was performed another one:

EXP.46: 5g soil ; 5mL H_2O_2 $5*10^{-2}$ M; 15% TiO2 w/w; 24h; UV light.

EXP.46 has been carried out in the same conditions of EXP.45, but the sample was irradiated for 24 hours under the UV lights. In this way, after the analysis of EXP.46 and considering EXP.45 as reference, it was possible to quantify the degradation efficiency for each hydrocarbons specie. The results of EXP.45 and EXP.46 are summarized in the following Table 6.9, Table 6.9.1 and 6.9.2.

Table 6.9. Degradation degree % calculated for the hydrocarbons present in the EXP.45 and EXP.46.

Peak	Retention time [min]	EXP.45 [integral i-th/ Standard integral]	EXP.46 [integral i-th/ Standard integral]	Degradation %
tetrachloroethane	3.543	1	1	
C12	8.078	0.127613966	/	100
C13	9.278	0.128599146	/	100
C14	9.761	0.332062338	0.032380468	90.25
C15	10.945	0.130245987	0.035931244	72.41
C16	11.328	0.431738818	0.126538718	70.69
C17	12.812	0.407265514	0.05984235	85.31
C18	13.696	0.069571531	0.036713054	47.23
C19	14.196	0.286251224	0.169696761	40.72
C20	14.796	0.125006238	0.078794808	36.97
C21	16.747	0.143524708	0.096206466	23.04
C23	18.160	0.28353544	0.26246634	7.43
C24	19.177	0.175588121	0.153223442	12.74
C25	20.177	0.080582228	0.072356264	10.21

Table 6.9.1. Hydrocarbons moles calculation in the Re.al. soil and after 24 h of photocatalysis.

Specie	EXP.45 [moles]	EXP.46 [moles]	Degraded moles	C degraded moles
C12	1.2085E-05	0	1.2085E-05	0.000145021
C13	1.21783E-05	0	1.21783E-05	0.000158318
C14	3.14463E-05	3.06643E-06	2.83799E-05	0.000397318
C15	1.23343E-05	3.40269E-06	8.93161E-06	0.000133974
C16	4.08857E-05	1.19832E-05	2.89024E-05	0.000462439
C17	3.8568E-05	5.66707E-06	3.2901E-05	0.000559317
C18	6.58842E-06	3.47673E-06	3.1117E-06	5.60106E-05
C19	2.7108E-05	1.60703E-05	1.10377E-05	0.000209716
C20	1.18381E-05	7.46187E-06	4.37622E-06	8.75244E-05
C21	1.35918E-05	9.11075E-06	4.48104E-06	9.41018E-05
C23	2.68508E-05	2.48556E-05	1.99524E-06	1.90398E-05
C24	1.66282E-05	1.45103E-05	2.11794E-06	5.08304E-05
C25	7.63114E-06	6.85214E-06	7.78999E-07	1.9475E-05
TOTAL	**0.000257734**	**0.000106457**	**0.00015**	**0.0024**

Table 6.9.2. Hydrocarbons mass calculation in the Re.al. soil and after 24 h of photocatalysis.

Specie	EXP.45 [g]	EXP.46 [g]
C12	0.002054457	0
C13	0.002240814	0
C14	0.006226368	0.000607153
C15	0.002614871	0.00072137
C16	0.009240161	0.002708207
C17	0.009256331	0.001360097
C18	0.00167346	0.000883088
C19	0.007264942	0.004306836
C20	0.003338342	0.002104247
C21	0.00402317	0.002696783
C23	0.008699661	0.008053202
C24	0.00562033	0.004904468
C25	0.00268616	0.002411953
TOTAL	**0.064939065**	**0.030757404**

From the reported calculation about EXP.45, it possible to observe that the amount of hydrocarbons pollutants in 5g of Re.al. contaminated soil is 0.065 grams, so it represents about the 1.23% w/w.

The result of the comparison between EXP.45 and EXP.46 indicates that the total hydrocarbons amount after 24 hours of photocatalysis decreases for about 53% w/w.

Another quantification of the degradation efficiency was performed by analyzing the dried soils from EXP.3 (Blank) and EXP.4 with ESEM.

The analyses obtained are reported in Figure 6.9.2., Figure 6.9.3 and Figure 6.9.4. for EXP.3, while the analyses related to EXP.4 are reported in Figure 6.9.5., Figure 6.9.6., and Figure 6.9.7.

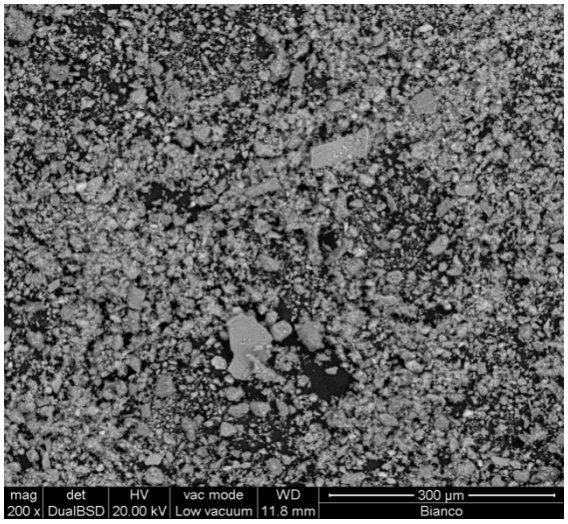

Figure 6.9.2. ESEM of the EXP.3: morphology.

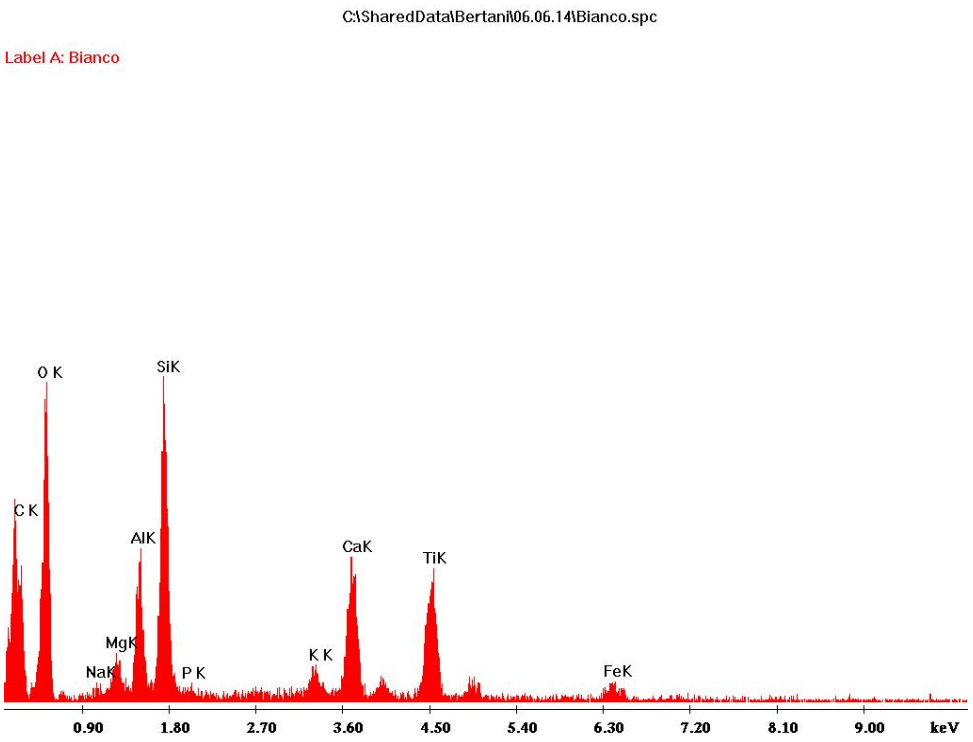

Figure 6.9.3. Spectra of elements of the EXP.3.

Elem	Wt %	At %
C K	24.55	36.48
O K	41.47	46.26
NaK	0.35	0.28
MgK	1.14	0.84
AlK	3.88	2.57
SiK	9.31	5.92
P K	0.15	0.09
K K	1.14	0.52
CaK	6.49	2.89
TiK	9.08	3.38
FeK	2.43	0.78
Total	100.00	100.00

Figure 6.9.4. ESEM characterization of the elements constituting EXP.3.

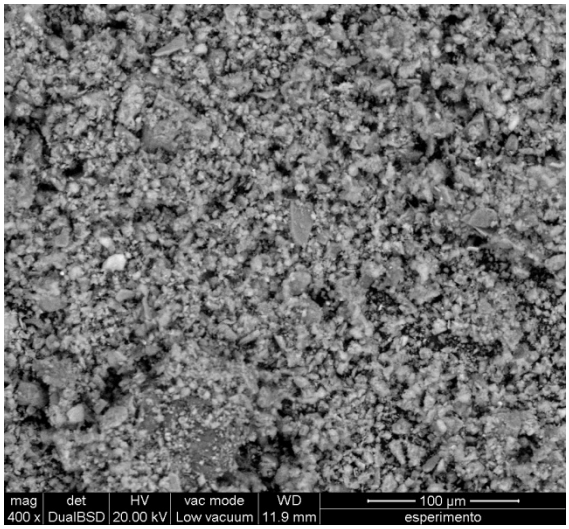

Figure 6.9.5. ESEM of the EXP.4: morphology.

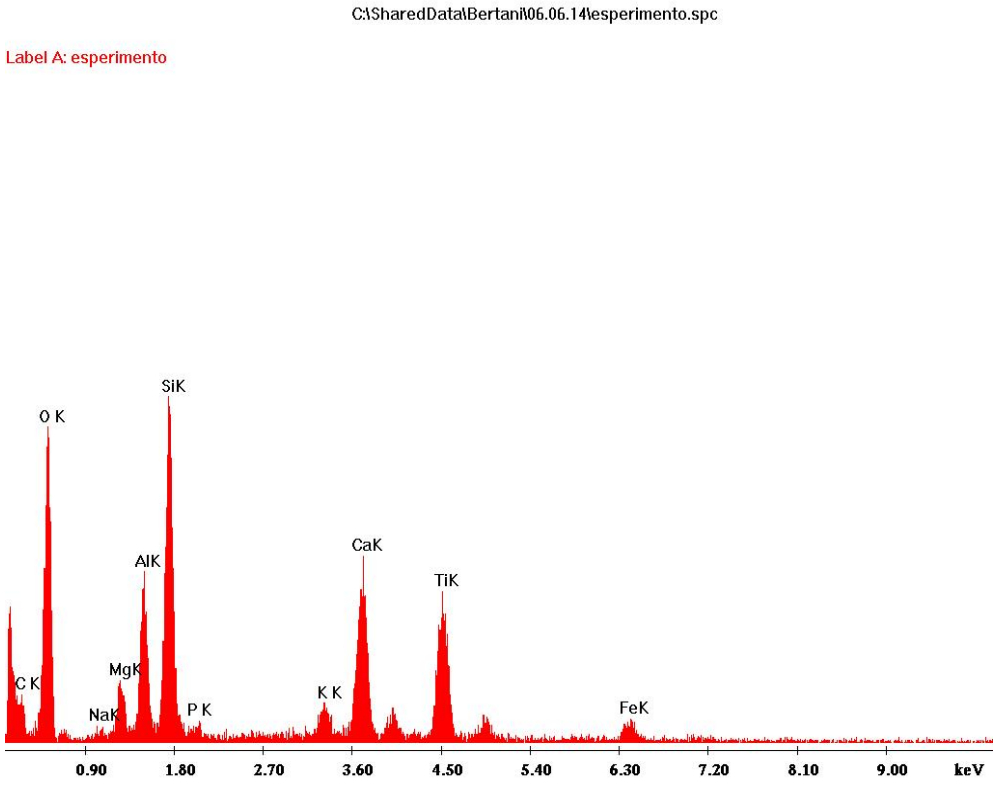

Figure 6.9.6. Spectra of elements of the EXP.4.

Elem	Wt %	At %
C K	8.58	14.75
O K	44.68	57.64
NaK	0.46	0.42
MgK	2.33	1.98
AlK	5.44	4.16
SiK	12.06	8.86
P K	0.35	0.23
K K	1.75	0.93
CaK	9.13	4.70
TiK	11.61	5.00
FeK	3.60	1.33
Total	100.00	100.00

Figure 6.9.7. ESEM characterization of the elements constituting EXP.4.

From the RFX data it can be observed that C content decreases from 24.55% to 8.58% w/w. It is noteworthy that the two methods gave different results (with GC – MS hydrocarbons reduction of 53% w/w, with RFX – ESEM hydrocarbons degradation of 65% w/w). Anyhow, both results are good being the two techniques completely different.

d) Evaluation of the degradation products

Assuming that the degradation process gives CO_2 as the most relevant final product, it has been tried to capture the CO_2 formed in a typical experiment (EXP.47) and compare its amount with the expected one.

EXP.47: 5g soil; 5mL deionized water, 15% w/w TiO_2; 24 h; UV lights.

The capture of CO_2 was carried out using the device shown in Figure 6.9.10.

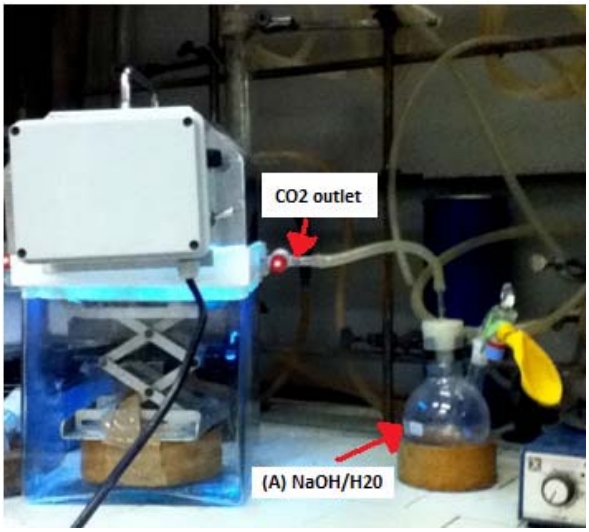

Figure 6.9.10. Device used to evaluate the CO_2 production from the process.

CO_2 was bubbled inside the flask containing a NaOH and water solution (2g NaOH in 10mL H_2O). It is known that the following reaction occurs:

$$CO_2 + 2\,NaOH \rightarrow Na_2CO_3 + H_2O$$

The suspension formed in (A) (see Figure 6.9.10) was dried for 24 hours at RT in the air.
Thus, the solid Na_2CO_3 was weighted (3.35 g) (Figure 6.9.11).

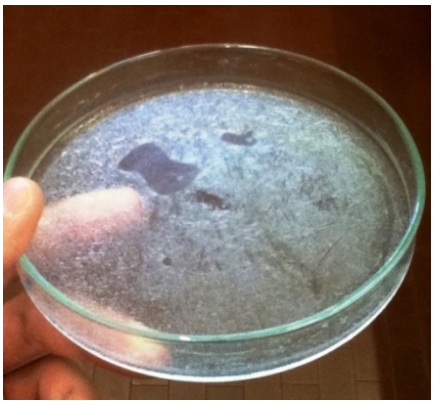

Figure 6.9.11. Solid Na_2CO_3 in Petri dish.

The same quantity of NaOH in 10mL of water was left in the air at RT for the same time. The solid Na_2CO_3 obtained by reaction with CO_2 of air alone was weighted (3.24 g).
Na_2CO_3 was identified on the basis of FT – IR spectra (Figure 6.9.12 and Figure 6.9.13).

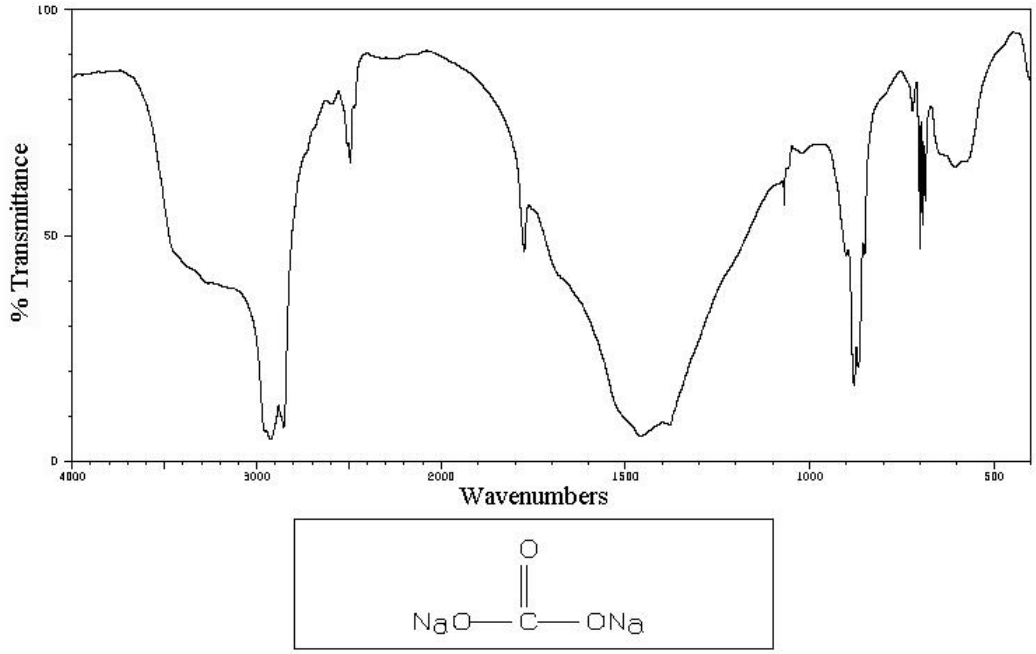

Figure 6.9.12. Reference FT-IR spectra for Na_2CO_3 (SDBS, Spectral Database for Organic Compounds).

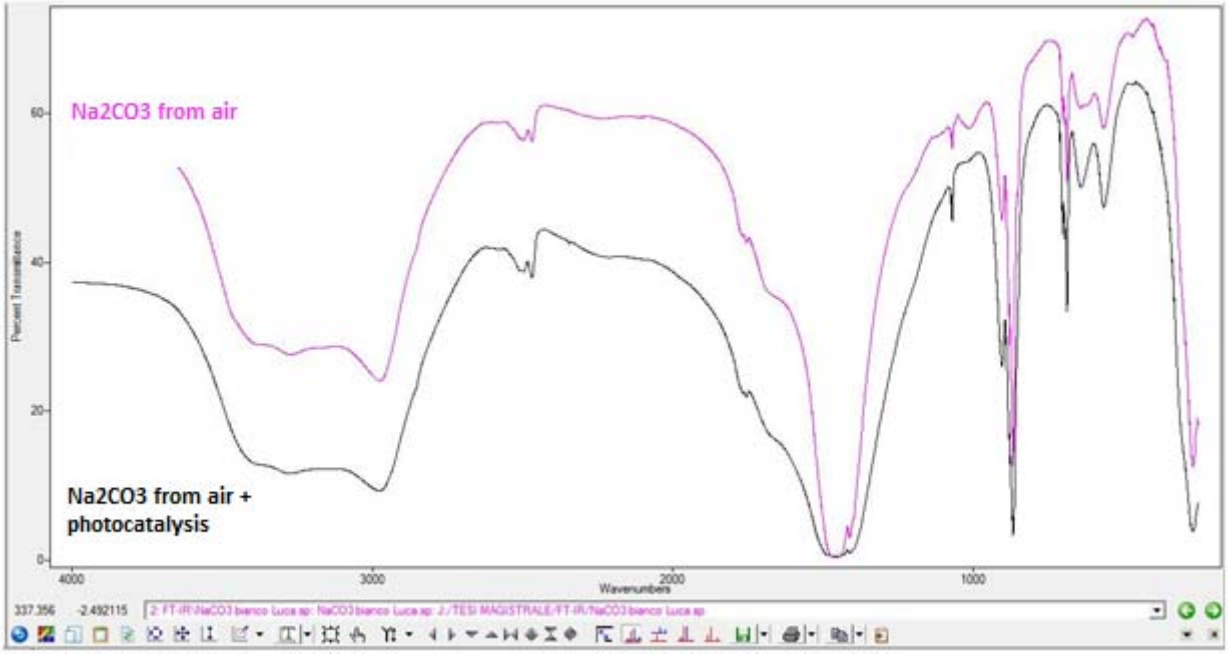

Figure 6.9.13. Spectra of the sample from the FT-IR analysis: $NaCO_3$ from air alone [pink] and $NaCO_3$ from air and after photocatalysis [black].

The Na_2CO_3 formed by a typical photocatalytic process is about 0.1 g corresponding to almost $1*10^{-3}$ moles. This value is of the same order of magnitude of the one found from the comparison of the data reported in Table 6.9.1 ($2*10^{-3}$ moles) of EXP.45 (starting soil) and EXP.46 (photocatalyzed soil).

6.10 COMPARISON WITH OTHER AOPs METHODS (FENTON AND PHOTO-FENTON)

a) Fenton oxidation processes

The Fenton reactions were carried out (EXP. 48, EXP.49) according to the procedure illustrated in Xu J. et al., 2011, due to its similar procedures in samples preparations and analysis.

EXP.48: 10g soil; 40mL H_2O; 10mL (6.98 mmol/L) $FeSO_4 \cdot 7H_2O$; 179mg citric acid; 2.5 mL 30% H_2O_2; closed and stirred flask; 3 days; RT.

EXP.49: 10g soil; 40mL H_2O; 10mL (6.98 mmol/L) $FeSO_4 \cdot 7H_2O$; 179mg citric acid; 2.5 mL 30% H_2O_2 (plus an addition at the 4th day); closed and stirred flask; 7 days; RT.

At the end of the reaction time the organic phase was extracted with hexane (100mL) with the same procedure used in the previous experiments. Both EXP.48 and EXP.49 were analyzed with the GC – MS and therefore compared with Exp.37, assumed as blank.
The results are reported in Table 6.10.

Table 6.10. Degradation degree % calculated for the hydrocarbons present in the EXP.48 and EXP.49.

		Degradation %	
Peak	**RetentionTime [min]**	**EXP.48**	**EXP.49**
tetrachloroethane	3.543	-	-
C13	8.078	7.62	79.62
C14	9.761	27.53	66.37
C15	11.328	6.69	56.53
C17	12.812	0.00	46.09
C18	14.196	0.00	28.75
C19	14.796	0.00	0.00
C20	15.513	0.00	3.79
C21	16.030	0.00	0.00
C22	16.747	0.00	0.00
C23	17.930	53.03	61.61
C24	19.047	0.00	0.00
C25	20.131	0.00	0.00
C25	21.164	0.00	0.00
C26	22.160	46.56	83.85
C27	23.177	0.00	72.58

b) Photo – Fenton oxidation processes

A photo-Fenton was carried out according to a similar procedure of the one illustrated in Sa da Rocha et al., 2012.

EXP.50: 10g soil; 40mL H_2O; 10mL (6.98 mmol/L) $FeSO_4 \cdot 7H_2O$; 179mg citric acid; 2.5 mL 30% H_2O_2 15% TiO_2; stirring; 8 hours ; UV lamps.

The system used to carry out the experiment is shown in Figure 6.10.

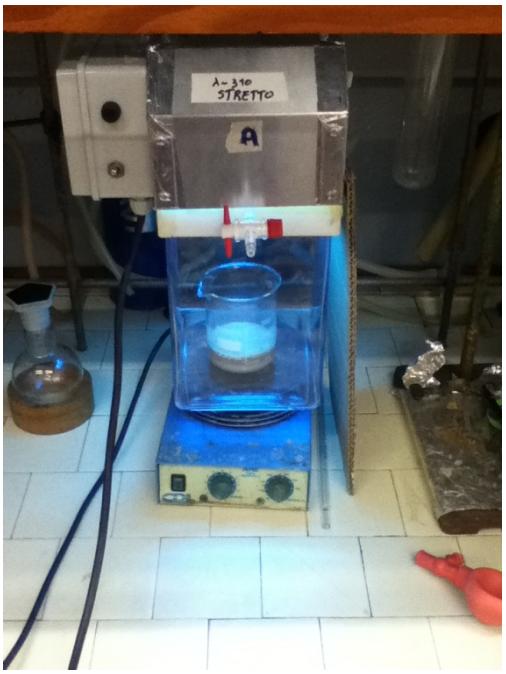

Figure 6.10. Device used to carry out the photo-Fenton reaction.

After 8 h of UV irradiation, the organic phase was extracted with hexane (100mL).
At the end the sample was analyzed with GC – MS and the results were compared with EXP.37 assumed as blank (Table 6.10.1).

Table 6.10.1. Degradation degree % calculated for the hydrocarbons present in EXP.50.

		Degradation %
Peak	**RetentionTime [min]**	**EXP.50**
tetrachloroethane	3.543	
C13	8.078	**19.22**
C14	9.761	**52.78**
C15	11.328	**48.91**
C17	12.812	**37.22**
C18	14.196	**13.03**
C19	14.796	**0**
C20	15.513	**0**
C21	16.03	**0**
C22	16.747	**0**
C23	17.93	**48.06**
C24	19.047	**0**
C25	20.131	**0**
C25	21.164	**0**
C26	22.16	**92.23**
C27	23.177	**86.73**

7. DISCUSSION

7.1 PROCESS PARAMETERS OPTIMIZATION

Initially, the evaluation of the process parameters was carried out.

7.1.1 Evaluation of the influence of reaction time

The first parameter to be optimized was the exposure time of the sample to UV lights, and it was chosen equal to 24 h (instead of 48 hours) due to the results obtained and summarized in the following table and figure (Table 7.1.1, Figure 7.1.1). These experiments (EXP.1 (blank), EXP.2 for 24 h and EXP.3 (blank), EXP.4 for 48 h) were done with 10% w/w of TiO_2 according to the results obtained from the previous work on this soil (Burigo, 2014).

Table 7.1.1. Results of the degradation of the recognized hydrocarbons species according to a 24h and a 48 h photocatalysis.

	24 h	48h
Specie	Degradation %	Degradation %
C12	100	100
C13	100	100
C14	73.35	97.28
C15	65.13	58.32
C16	31.49	41.11
C18	0.49	2.98
C19	10.64	8.04
C20	0	8.52

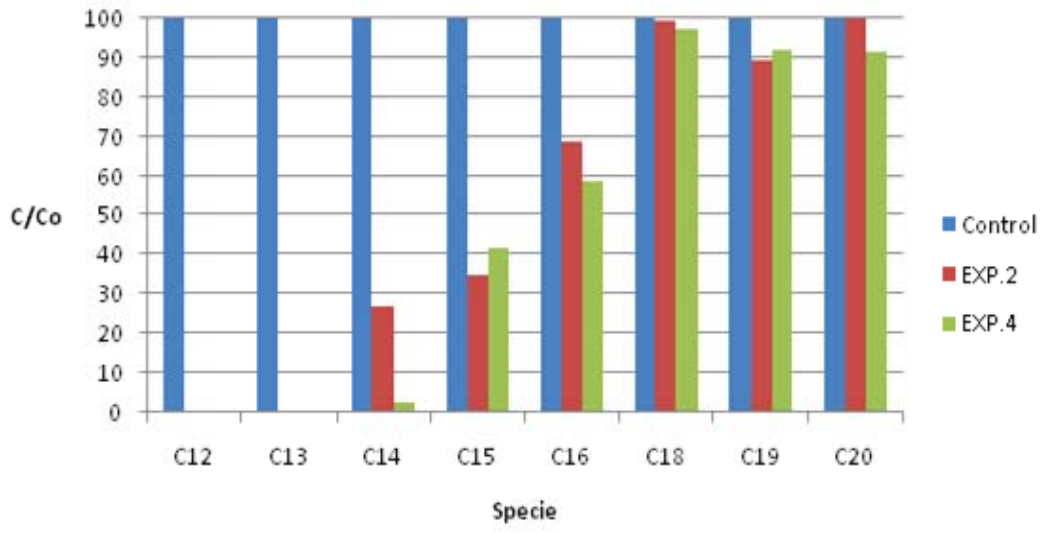

Figure 7.1.1. Degradation of the hydrocarbons after 24 and 48 hours of photocatalysis [10% TiO_2 w/w].

The histogram above shows that the degradation efficiency of the photocatalytic process occurring respectively for 24 h (EXP.1 (blank), EXP.2) and 48 h (EXP.3 (blank), EXP.4) is quite comparable, which leads to the choice of 24 hours as irradiation time of the sample. The results of the degradation percentages related to the species above C_{20} are not reported because they didn't degrade at all.

This time of exposure was used to evaluate the subsequent parameter, in order to reach, step by step, an optimized procedure.

Another observation should be done concerning the specific degradation of each hydrocarbons specie. In fact it is possible to see that the lightweight hydrocarbons, such as C_{12} and C_{13} are completely degraded, the medium weight ones (C_{14} to C_{16}) are averagely degraded and the heavyweight ones ($> C_{20}$) are not degraded. This is in agreement with the expected process performance, because the lighter chains are more easily degraded due to their simpler structure and their higher "compatibility" with water, while increasing the structural complexity the degradation efficiency is lower. Thus, it is possible to conclude that the photo degradation process, under these experimental conditions, is effective overall for the lightweight hydrocarbons chains.

7.1.2 Evaluation of the influence of TiO_2 amount

The second parameter optimized was the % w/w of the titania with the respect to the soil weight. Looking at the scientific literature, Dong et al., 2010 [a], in the scientific paper titled "Photocatalytic degradation of phenantrene and pyrene on soil surfaces in the presence of nanometer rutile TiO_2 under UV irradiation" , stated that the optimal catalyst dosage was 2% of TiO_2 in order to achieve the best degradation performances. In the previous study on this soil (Burigo, 2014) was instead shown that a % of 5% w/w of TiO_2 represented the optimal one. In this work higher titania percentages were tried in order to see if the process would be more effective. Therefore, two experiments with 5% TiO_2 w/w (EXP.5 (blank) and EXP.6) and 15% TiO_2 w/w (EXP.7 (blank) and EXP.8) were carried out. The results obtained were then compared with the ones from the experiment with 10% TiO_2 (w/w) (EXP.1 (blank) and EXP.2) (see Figure 7.1.2).

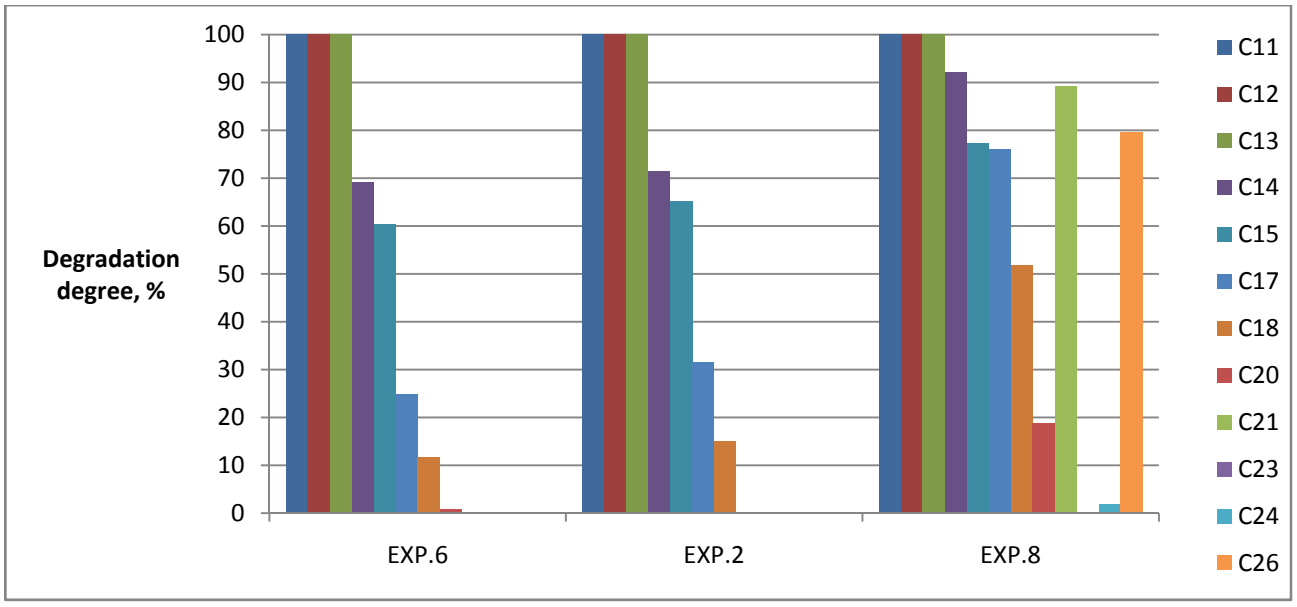

Figure 7.1.2. Degradation degree of hydrocarbons using the 5% (EXP.6),10% (EXP.2) and 15% w/w (EXP.8) of titania in the soil samples. In EXP.6 and 2 aren't reported the $>C_{20}$ hydrocarbons degradation because they were null .

It can be observed that the higher efficiency in the degradation process was obtained by using 15% w/w of TiO_2 (EXP.8). Higher titania percentages were not investigated due to the fact that too high increasing of the volume of the reactants is not practically implementable.

The degradation efficiency decreases with the increase of the hydrocarbons molecular weight, apart for the C_{24} and C_{26} species, in which is observed an increase. A reasonable explanation can be the fact that the species C_{24} and C_{26} are the branched isomers, more reactive towards radical process.

7.1.3 Temperature

Temperature effect was checked for two reasons:

- To achieve a preliminary evaluation concerning the exo or endothermal effect of the photocatalytic process. If the process is endothermic, for instance, it means that it absorbs energy (as heat), hence, increasing the temperature of the process would increase its efficiency.
- To evaluate the possible hydrocarbons evaporation. According to the paragraph 6.3, it is possible to observe that the starting temperature for the both two samples is about 24°C and rise up to an average of 43°C for the sample without the titania (EXP.11), and to 45°C for the sample with it (EXP.12).

Thus, as first observation, it can be noted that, even if the difference in the two system temperature is narrow, the sample with titania (EXP.12) develops a quite little increasing in the temperature

(≈2°C) with respect to the experiment without it (EXP.11). That could be explained as a very small exothermic effect. The detailed evaluation of the thermal balance of the process is suggested to be developed in a subsequent study.

As concerning the second task, according to the chemistry of the hydrocarbons, the boiling point increases with the molecular weight, thus with the chain length (Figure 7.1.3).

Name	*Molecular Formula*	*Boiling Point (°C)*
methane	CH_4	-164
ethane	C_2H_6	-89
propane	C_3H_8	-42
butane	C_4H_{10}	-0.5
pentane	C_5H_{12}	36
hexane	C_6H_{14}	69
heptane	C_7H_{16}	98
octane	C_8H_{18}	125
nonane	C_9H_{20}	151
decane	$C_{10}H_{22}$	174
undecane	$C_{11}H_{24}$	196
dodecane	$C_{12}H_{26}$	216
eicosane	$C_{20}H_{42}$	343
triacontane	$C_{30}H_{62}$	450

Figure 7.1.3. Typical boiling points of the hydrocarbons [Elmhurst.edu].

The figure below shows that the undecane, for instance, has a boiling temperature of 196°C. This is sufficient to prove that at 43-45°C occurs no hydrocarbons evaporation in the soil because the species of concern range between C_{11} to $C_{26\text{-}27}$.

7.1.4 Evaluation of the influence of H_2O_2 amount

The influence of the hydrogen peroxide (H_2O_2) effect was another parameter to optimize. It is recognized in fact that the H_2O_2 is a strong oxidant agent, therefore, should help the degradation.

In the literature, few and controversial results are reported concerning the influence of the presence of hydrogen peroxide.

In the case of decolouration of the anionic azo-dye Reactive Orange 16, the UV-C irradiation in the presence of H_2O_2/TiO_2 was almost 5 times faster than the one with only TiO_2, but was slower than the one with only H_2O_2 (Egerton et al., 2014).

In another case study, the photolytic degradation of microcystin-LR in aqueous solutions, the system $H_2O_2/TiO_2/UV$ removed completely the toxin together with many by-products (Cornish et al., 2000).

It was observed that a little amount of H_2O_2 was good enough to speed up the photo degradation with TiO_2 of 2-chloroaniline (Chu et al., 2007).

The photocatalytic degradation of 2,4-dichlorophenol in TiO_2 suspension was studied in the presence of additional oxidants, observing that H_2O_2 enhanced the photocatalytic process (Meliàn et al., 2013)

Thus, it was of interest to evaluate the influence of the presence of H_2O_2 under the described experimental conditions (paragraph 6.4)

In the photocatalytic reaction H_2O_2 acts as electron acceptor which is more efficient than oxygen.

It reacts with the conduction band electrons and it generates hydroxyl radicals which are necessary for photomineralisation of the organic pollutants, in accordance with the following equation (12):

$$H_2O_2 + e_{CB}^- \rightarrow HO\bullet + HO^- \qquad (12)$$

There are other reaction by which hydroxyl radicals can also be produced, although reaction only takes place at $\lambda < \approx 300$ nm with maximum absorption taking place at 220 nm (13, 14).

$$H_2O_2 + \bullet O_2^- \rightarrow HO\bullet + HO^- + O_2 \qquad (13)$$

$$H_2O_2 + h\nu \rightarrow 2HO\bullet + O_2 \qquad (14)$$

The results of the experiments described in the paragraph 6.4 are reported in the graphs below (Figure 7.1.4 , Figure 7.1.4.a).

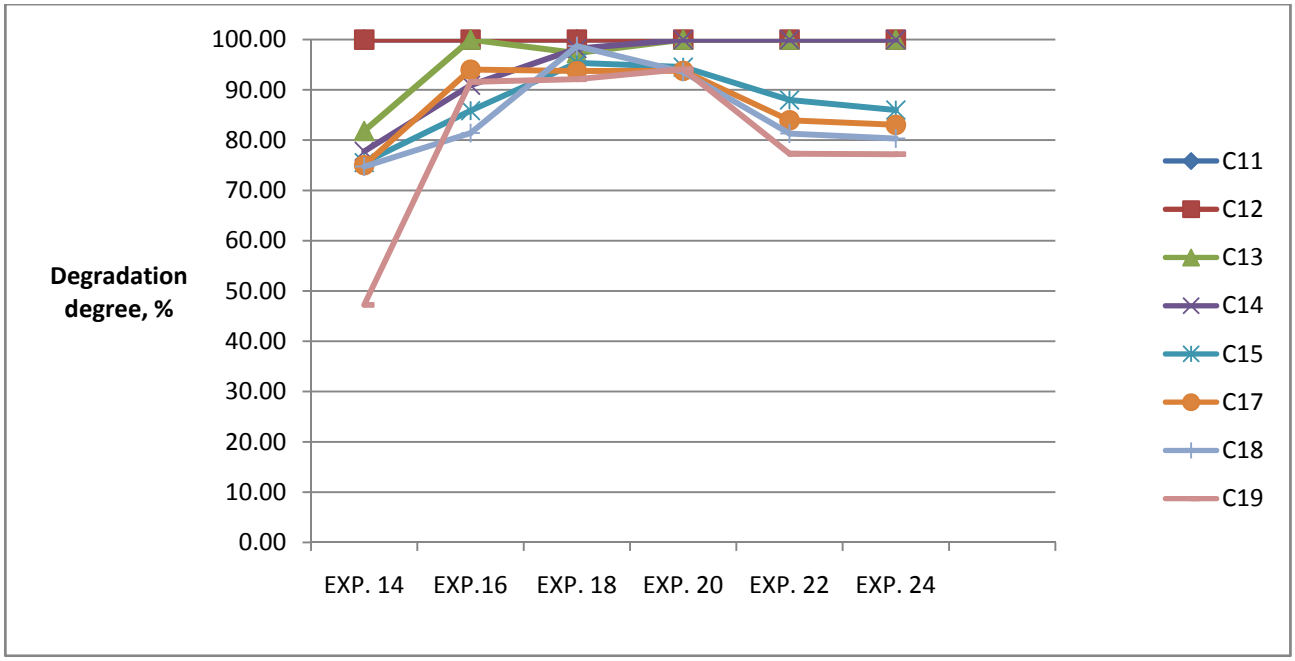

Figure 7.4.1. Degradation degree of hydrocarbons related to the different H_2O_2 concentrations for the species between C_{11} to C_{19} .

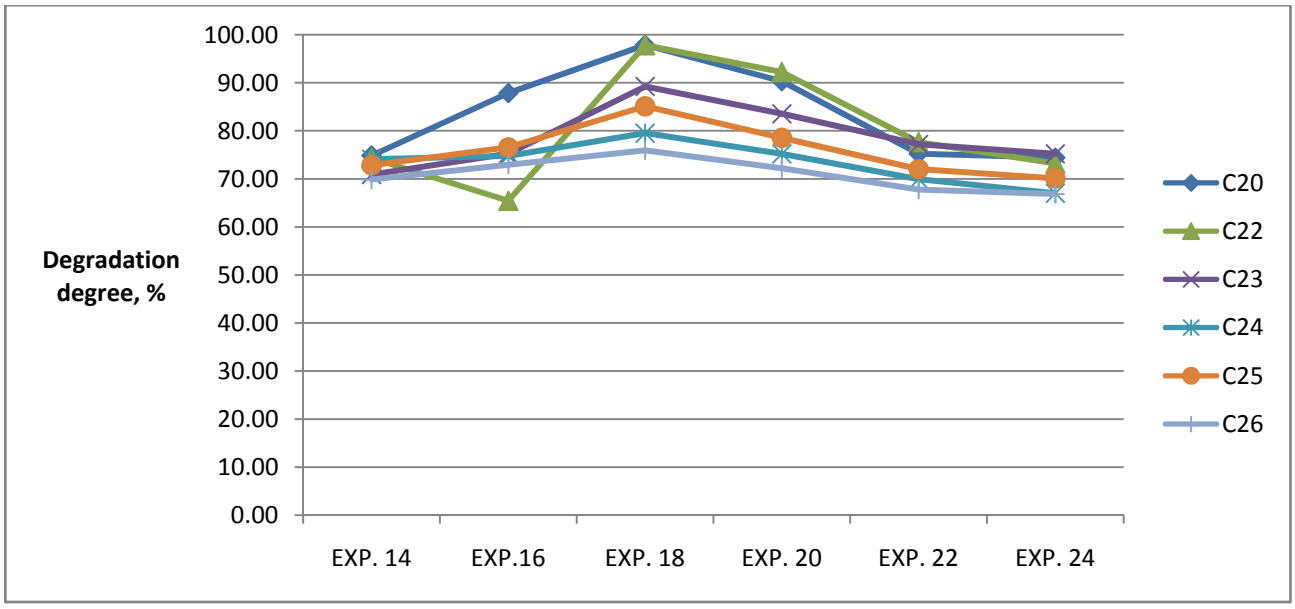

Figure 7.4.1.a. Degradation degree of hydrocarbons related to the different H_2O_2 concentrations for the species between C_{20} to C_{26}.

It can be observed from the reported graphs that for C_{13} and C_{14} complete degradation was achieved with a hydrogen peroxide concentration of $5*10^{-2}$ M (EXP.18).

For the heavier weight hydrocarbons, > C_{14}, hydrogen peroxide concentration of $5*10^{-2}$ M (EXP.18) represents the one giving the best degradation, which decreases at higher concentrations.
This result proved that the hydrogen peroxide concentration is not important in the degradation of the lightweight hydrocarbons chains, while became more significant for the medium weight ones; moreover, it is effective for the heavyweight chains but only at certain concentrations, because at low and high ones the degradation efficiency is not improved.
The H_2O_2 concentration of $5*10^{-2}$ M was utilized in all the optimized experiments. The trend is like the one observed in the literature, but more precise analyses should be conducted in a further study.
Considering the Figure 7.4.1 and Figure 7.4.1.a, it can be observed that the degradation of the hydrocarbons is almost above the 70% for all the recognized hydrocarbons species.

7.1.5 Evaluation of pH influence

The influence of pH in the degradation efficiency of the process was studied.
In literature are present few results on this regard.
In the case of the degradation of 2,4-dichlorophenol in TiO_2 suspensions, an optimum trend of the degradation for pH 5 was observed (Meliàn et al., 2013).
In another case of degradation of chlorinated aniline in a H_2O_2/TiO_2/UV system, a decrease of the degradation efficiency of the photocatalytic process was underlined in alkaline conditions.
It is remembered that, after having checked the soil pH in a slurry matrix with deionized water (ASTM D4972-01), the soil pH was adjusted by adding, to the deionized water used to feed the sample, an acid (H_2SO_4 96%) or a base (NaOH) respectively in order to obtain acidic or alkaline conditions in the sample.
Particularly, EXP.26 (EXP.25 as blank) and EXP.28 (EXP.27 as blank) were performed under acidic conditions, EXP.30 (EXP.29 as blank) under neutral conditions while EXP.32 (EXP.31 as blank) and EXP.34 (EXP.33 as blank) under alkaline conditions.
The results of the above experiments were therefore compared in the following Figure 7.1.5.

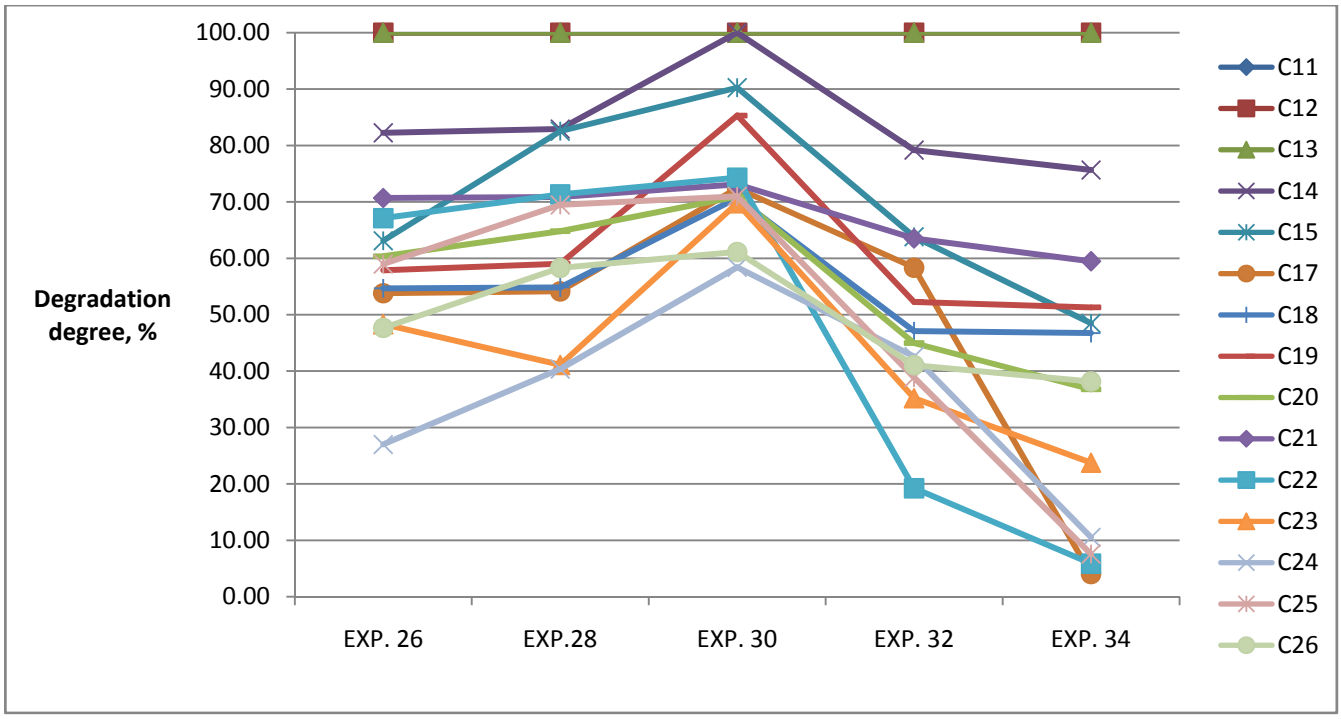

Figure 7.1.5. Degradation degree of hydrocarbons at different pH.

It is noticeable from Figure 7.1.5, that the degradation is complete for the C_{11}, C_{12} and C_{13} species at any pH conditions. From the C_{14} to the C_{26} specie, the largest degradation is observed at pH 7, thus indicating that the soil pH doesn't need to be adjusted to improve the photo degradation performance.

7.1.6 Optimized parameters

In Figure 7.1.5 the results of the hydrocarbons degradation carried out with all the optimized parameters are reported.

More precisely, the optimized conditions are summarized as follows:

- 24 hours of irradiation of the sample to the UV lights;
- 15% w/w of TiO_2 to be dosed;
- No temperature adjustment;
- H_2O_2 concentration of $5*10^{-2}$ M;
- pH 7 (No pH adjustment).

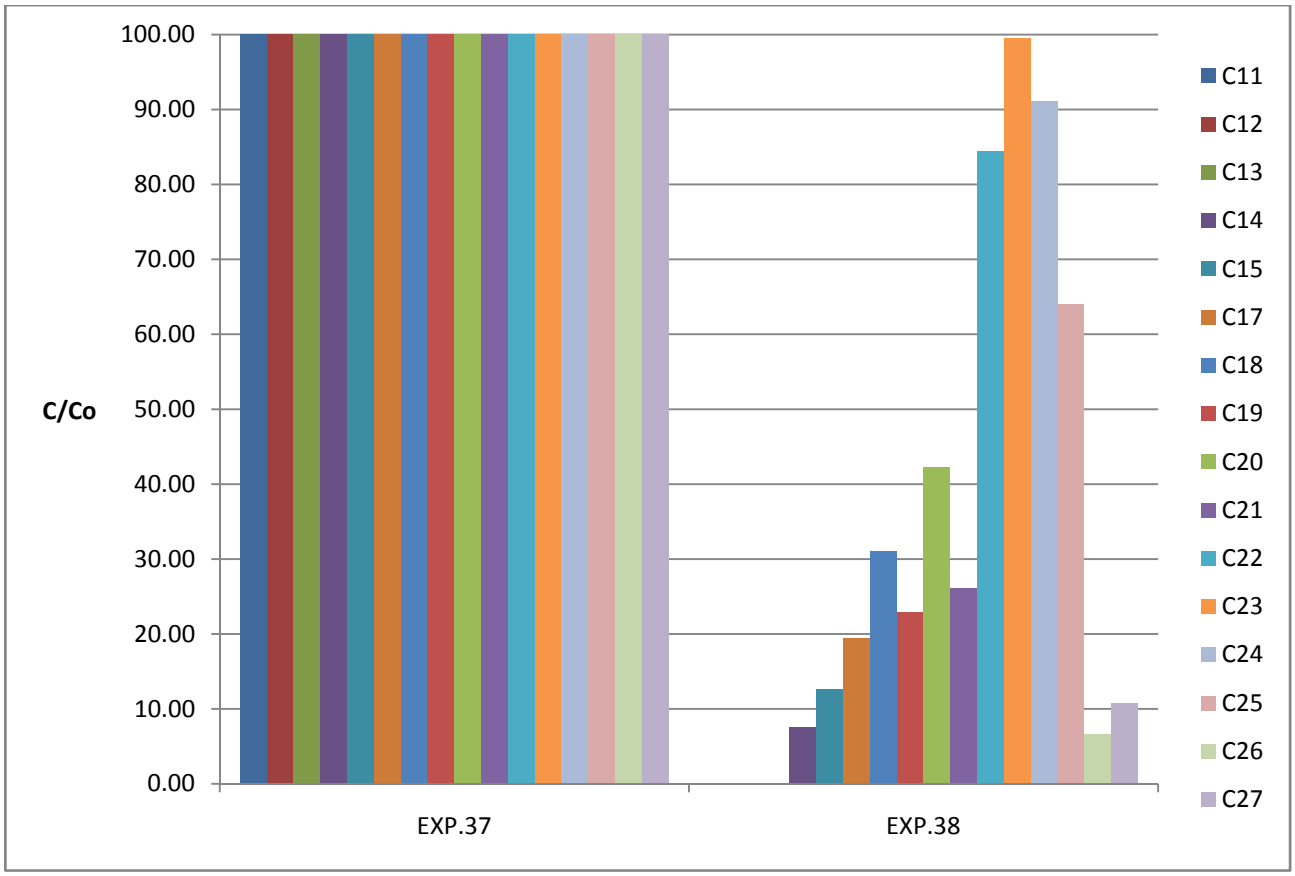

Figure 7.1.5. Degradation efficiencies of hydrocarbons in EXP.37 and EXP.38.

A degradation of more than 50% involves the majority of the hydrocarbons species, even for two of the heaviest ones (C_{26} and C_{27}) inside the sample.

For C_{22} – C_{25} the lower degradation with respect to the other hydrocarbons will be studied in the future.

7.2 EVALUATION OF THE DEGRADATION EFFICIENCY

The quantitative analysis described in paragraph 6.9 allowed to achieve relevant results:

- It was possible to measure the pollution degree of the soil: 1.23% w/w (in 5g) ("b"section);
- In this case, the soil contains about 13g/kg_{soil} of heavy hydrocarbons (> C_{12}) which, after the photocatalytic process, decreases to about 6g/kg_{soil}. Even if the final soil results to be extremely polluted with respect to the law limits (D.Lgs 152/2006), the photocatalysis can be proposed to be performed after a first cleaning treatment (i.e. soil washing). It is to remember that the efficiency of the photocatalytic process is strictly connected to the

concentration of the starting pollutants which, if too high, can saturate the catalyst (Dong et al., 2010 [a]).

- It was demonstrated that the degradation efficiency is about 53-65% ("c" section);
- It was proved that reasonably the most relevant degradation product is CO_2 ("d" section) in agreement with the observation that the GC – MS chromatograms of the post-photocatalysis samples do not show new signals with respect the starting ones.

7.3 COMPARISON WITH OTHER AOPs METHODS

With the previously described experiments a significant degradation of hydrocarbons having a carbon chain between C_{11} to C_{21} was recognized, while for the heavier weight ones the degradation was lower. Therefore, it was of interest to verify if other advanced oxidation processes (AOPs) could be more effective than the photocatalysis under experimental conditions.

In particular, were carried out experiments under Fenton and photo-Fenton conditions.

Fenton's reagent is a solution of hydrogen peroxide and an iron catalyst that is often used to oxidize contaminants or waste waters. Fenton's reagent can be used to destroy organic compounds such as trichloroethylene (TCE) and tetrachloroethylene (PCE) (Venny et al., 2012).

The oxidant species are •OH which are the primary reactive specie in degradation of organic pollutants such as PAHs (Gan et al., 2009, Xu J.et al., 2011).

A general scheme of the Fenton reaction is following reported (Fig.41, Venny et al., 2012).

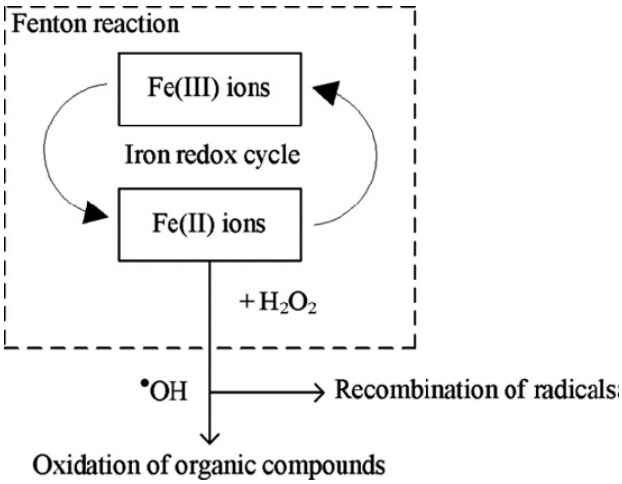

Figure 7.3. General scheme of a Fenton reaction.

The Fenton reaction is a process that involves many side reactions (Venny et al., 2012) among which principal radical initiation (Eqs. (15) and (16)), radical propagation (Eqs. (17) and (18)), termination (Eqs. (19)-(21)), reaction with intermediates (Eqs. (22)-(29)), carbonate species (Eqs. (30)-(35)) and natural organic matter (NOM) (Eq.(36)) are included.

$H_2O_2 + Fe^{2+} \rightarrow Fe^{3+} + \bullet OH + OH^-$ (15)

$Fe^{3+} + H_2O_2 \rightarrow Fe^{2+} + HO_2^\bullet + H^+$ (16)

$\bullet OH + RH \rightarrow R\bullet + H_2O$ (17)

$R\bullet + H_2O_2 \rightarrow ROH + \bullet OH$ (18)

$\bullet OH + Fe^{2+} \rightarrow Fe^{3+} + OH^-$ (19)

$\bullet OH + H_2O_2 \rightarrow H_2O + HO_2^\bullet$ (20)

$\bullet OH + \bullet OH \rightarrow H_2O_2$ (21)

$Fe^{2+} + HO_2^\bullet \rightarrow Fe^{3+} + HO_2^-$ (22)

$Fe^{3+} + HO_2^\bullet \rightarrow Fe^{2+} + O_2 + 2H^+$ (23)

$HO_2^\bullet + H_2O_2 \rightarrow H_2O + \bullet OH + O_2$ (24)

$HO_2^\bullet + HO_2^\bullet \rightarrow H_2O + O_2$ (25)

$O_2\bullet^- + Fe^{3+} \rightarrow Fe^{2+} + O_2$ (26)

$O_2\bullet^- + Fe^{2+} + 2H^+ \rightarrow Fe^{3+} + H_2O_2$ (27)

$HO_2^\bullet + O_2\bullet^- + H_2O \rightarrow H_2O_2 + O_2 + OH^-$ (28)

$\bullet OH + HO_2^\bullet \rightarrow H_2O + O_2$ (29)

$CO_2\,(g) + H_2O \leftrightarrow H_2CO_3\,(aq)$ (30)

$H_2CO_3\,(aq) \leftrightarrow HCO_3^- + H^+$ (31)

$HCO_3^- + \bullet OH \rightarrow CO_3\bullet^- + OH^-$ (32)

$CO_3\bullet^- + H_2O_2 \rightarrow HO_2^\bullet + HCO_3^-$ (33)

$2CO_3\bullet^- \rightarrow$ products (34)

$CaCO_3(s) + H^+ \leftrightarrow Ca^{2+} + HCO_3^-$ (35)

NOM + $\bullet OH \rightarrow$ products (36)

The Fenton reaction has been widely applied in the remediation of contaminated soil from organic pollutants due to its relative simplicity and operability at ambient pressure and temperature (Venny et al., 2012). Anyway, the conventional Fenton reaction (CF) is not applied for in situ intervention due to the low pH requirement (pH 2-4) and the low mobility by which the reagent is characterized. Also, narrow pH changes cause a sharp reduction of the Fe^{2+} - H_2O_2 efficiency.

From a practical point of view the reaction is modified by means of some catalysts addiction, excess of hydrogen peroxide and addiction of Fe chelator.

The reaction are therefore categorized as Conventional - Fenton (CF), Fenton - Like (FL) and Modified - Fenton (MF) oxidation, depending respectively on how much the reaction is modified from the conventional one.

The list of the advantages and the disadvantages of Fenton oxidation techniques can be summarized as follows (Venny et al., 2012):

Advantages:

- Applicable to a wide range of contaminants such as PCBs, PAHs, pesticides, pentachlorophenol (PCP), benzene, toluene, ethylene, xylene (BTEX);
- Iron is highly abundant and non-toxic, H_2O_2 is easy to handle and environmentally benign;
- Shorter treatment time than other technique e.g. bioremediation;
- Contaminants can be destroyed in situ, on-site or off-site;
- Insensitive to external disturbances e.g. contaminant load;
- Heat released from reactions enhance mass transfer, reaction rate and microbial activity;
- Reactions sub-products are usually more biodegradable and soluble than parent compounds;

Disadvantages:

- Harmless organic matters in the soils may also be oxidized during the course of the oxidation;
- Less economic than bioremediation when large quantity of oxidant is needed;
- Oxidant must be introduced near the contaminated zones;
- Natural oxidant demand may be high in some soil matrices;
- Wastage of oxidants may occur due to the presence of naturally occurring organic and inorganic oxidizable fraction in soils;
- Oxidant handling and delivery problems arise due to exothermic reaction and aquifer heterogeneities. Gas generated acts as a potential hazard;
- Cause immobilization of inorganics with reactive species in treatment wall;

The scientific literature is abundant in case studies of soil remediation by means of Fenton reaction, in particular the method proposed by Xu J. et al., 2011 which deals with an enhanced bioremediation of an oil contaminated soil by graded modified Fenton oxidation, was of interest.

Beside the bioremediation, this article was taken as a reference in this work because the preparation of the samples followed a similar procedure of the one used in this study.

After the Fenton reaction, it has been decided to test also a photo-Fenton process one by integrating the TiO_2 and the UV lights. In photo-Fenton type processes, where the reactions presented in the equations 1-4, 11, and 15-36 occur, additional sources of OH radicals should be considered: through photolysis of H_2O_2, and through reduction of Fe^{3+} ions under UV light (Eqs. 37 and 38):

$$H_2O_2 + h\nu \rightarrow \bullet OH + \bullet OH \quad (37)$$

$$Fe^{3+} + H_2O + h\nu \rightarrow Fe^{2+} + \bullet OH + H^+ \quad (38)$$

These reactions have been proven to be more efficient than the other photocatalytic processes but the disadvantages of the process are the low pH values required (iron precipitates at higher pH values) and the fact that iron has to be removed after treatment. Concerning the use of the photo-Fenton reaction for the soil remediation, in literature the state of the art is reported in Table 7.3.

Table 7.3. State of the art concerning the use of photo-Fenton process for soil remediation at lab scale.

Contaminant	System	Reference
Crude oil	Visible light (Philips 20 W) UV-A (Higuchi, F20T10 20W), UV-C (Philips 20W), $FeSO_4 \cdot 7H_2O$, H_2O_2, irradiation time 6,9,12 h	Sa da Rocha et al., 2012
PAHs	Sunlight, $FeSO_4 \cdot 7H_2O$, H_2O_2, irradiation time 8 h	de S. e Silva et al., 2008
TNT	Photo-reactor Heraeus TQ150 model plus water cooled mercury lamp (150 W), H_2SO_4 (to decrease pH), ferrous ions in solution, H_2O_2, irradiation time 70 min. (Coupled with soil flushing with cyclodextrin)	Yardin et al., 2006
DDT - DDE	Sunlight, FeSO4·7H2O, H2O2, irradiation time 6 h. (Coupled with soil washing with surfactants)	Villa et al., 2010

In Figure 7.3.1. the results of the degradation experiments described in paragraph 6.10 (EXP.49, EXP.50) are compared with one carried out under the optimized photocatalytic conditions (EXP.38).

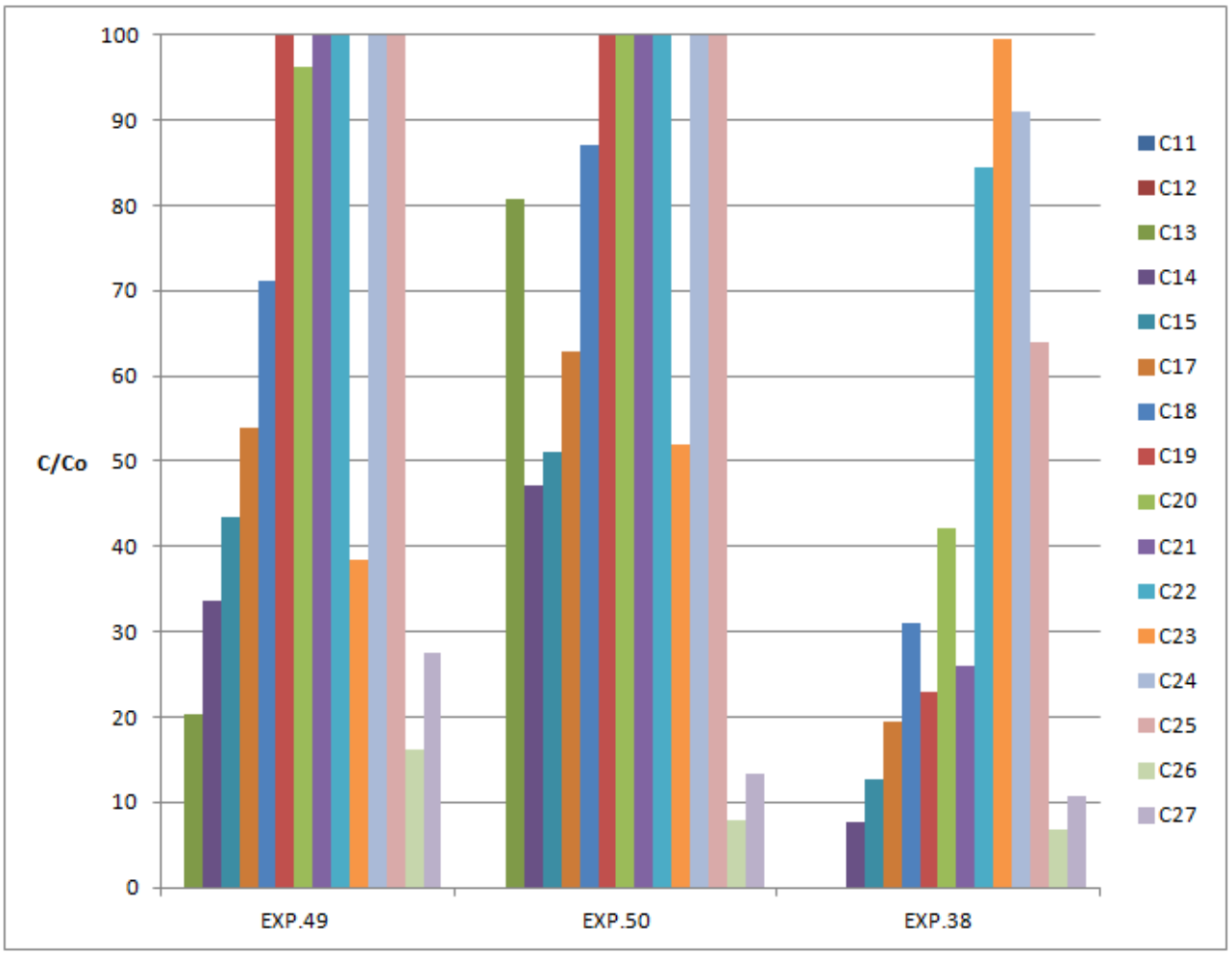

Figure 7.3.1. Degradation efficiencies of hydrocarbons in EXP.49, EXP.50 and EXP.38.

In general the efficiency of the photocatalysis (TiO_2 15% / H_2O_2) is higher than Fenton and photo-Fenton conditions.

As for C_{23}, these latter processes were more active.

8. CONCLUSIONS AND PERSPECTIVE

The experimental activity carried out in the thesis can be summarized in the following scheme:

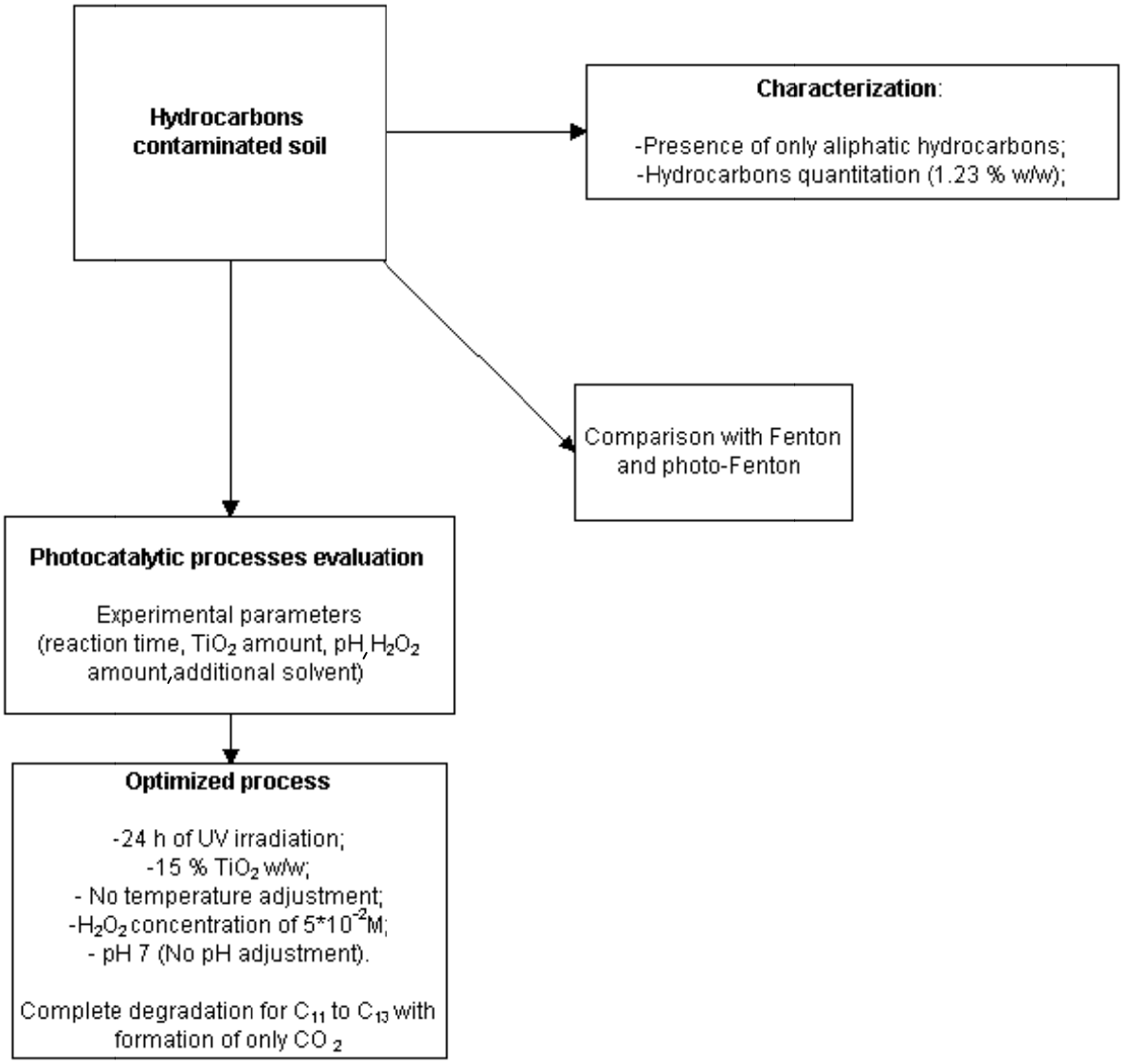

The most relevant results achieved along this study concern the optimization of the experimental conditions for the degradation of aliphatic hydrocarbons at a significant extent:

C_{11}, C_{12} and C_{13} degraded for 100%, C_{14} degraded for 92%, C_{15} degraded for 87%, C_{17} degraded for 80%, C_{18} degraded for 69%, C_{19} degraded for 77%, C_{20} degraded for 58%, C_{21} degraded for 74%, C_{26} degraded for 93% and C_{15} degraded for 89%.

A relevant result is represented by the identification as CO_2 of the most abundant degradation product containing carbon, without the formation of additional organic by-products.

Considering the comparison with other well known AOPs, photocatalysis under optimized experimental conditions demonstrates to be more active.

Nevertheless the results of the study strongly suggest further investigation concerning, in particular, the influence of the nature of the soil in terms of salts content, of the presence of additional semiconductors such as ZnO and Fe_2O_3 and surfactants.

Furthermore, the degradation of $C_{22} – C_{25}$ hydrocarbons requires deeper analysis, in particular C_{23}.

An important aspect to study in the future is the thermal balance of the whole process by means of a series of exothermic and endothermic reactions.

As for a large scale application two aspects must be improved: (i) The reaction rates by enhancing the catalyst activity and (ii) the use of sunlight. Reasonably, this task would be reached by the catalyst optimization (i.e. doping TiO_2).

The integration of the photocatalytic process with a traditional cleaning method (i.e. soil washing) could be an useful approach to let the soil comply with the law limits (D.Lgs 152/2006, Part IV, V, Annex 5 (Table 1)).

Bibliography

Adams W.A., Impellitteri C.A., 2009. *The photocatalysis of n,n-diethyl-m-toluamide (DEET) using dispersions of Evonik Degussa p-25 TiO2 particles*. J. Photochem. Photobiol. A, 202, 28–32.

Alvarez P.M., Jaramillo J., Lopez-Pinero F., Plucinski P.K., 2010. *Preparation and characterization of magnetic TiO2 nanoparticles and their utilization for the degradation of emerging pollutants in water*. Appl. Catal. B, 100, 338–345.

Amarjargal A., Tijing L.D., Yu M.H., Kim C.-H., Park C.-H., Kim D.-W., Kim C.-S., 2012. *Characterization and photocatalytic efficiency of TiO2/Ti beads fabricated by simple heat-treatment.* J. Mater. Sci. Technol., 28, 184–192.

An T.C., An J.B., Yang H., Li G.Y., Feng H.X., Nie X.P., 2011. *Photocatalytic degradation kinetics and mechanism of antivirus drug-lamivudine in TiO2 dispersion*. Journal of Hazardous Material, 197, 229–236.

An T.C., Yang H., Li G.Y., Song W.H., Cooper W.J., Nie X.P., 2010. *Kinetics and mechanism of advanced oxidation processes (AOPs) in degradation of ciprofloxacin in water*. Appl. Catal. B, 94, 288–294.

Antoniou M.G., Shoemaker J.A., de la Cruz A.A., Dionysiou D.D., 2008.*LC/MS/MS structure elucidation of reaction intermediates formed during the TiO2 photocatalysis of microcystin-LR.* Toxicon, 51, 1103–1118.

Araña J., Doña-Rodriguez J.M., Gonzàles-Diaz O., Tello Rendon E., Ilerrera Meliàn J.A., Colòn G., Navìo J.A. Perèz Peña J., 2004. *Gas – phase ethanol photocatalytic degradation study with TiO_2 doped with Fe, Pd and Cu.* J. Molec. Catal. A: chemical 215, 153-160.

Barrera-Diaz C.E., Lugo-Lugo V., Bilyeu B., 2012. *A reviwe and biological methods for aqueous Cr(VI) reduction.* J. Haz. Mater., 2012, 223, 1-12.

Binh N.D., Oanh N.T.K., Parkpian P., 2014. *Photodegradation of dioxin in contaminated soil in the presence of solvents and nanoscale TiO_2 particles*. Environmental Tec. Vol 35, 9, 1121.-1132.

Berry R.J. and Mueller M.R., 1994. *Photocatalytic decomposition of crude oil slicks using TiO_2 on a floating substrate.* Microchem. J. 50, 28-32.

Boroski M., Rodrigues A.C., Garcia J.C., Sampaio L.C., Nozaki J., Hioka N., 2009. *Combined electrocoagulation and TiO2 photoassisted treatment applied to wastewater effluents from pharmaceutical and cosmetic industries.* J. Hazard. Mater., 162, 448–454.

Bouzaza A., Laplanche A., 2002. *Photocatalytic degradation of toluene in the gas phase: comparative study of some TiO2 supports*. J. of Photochemistry and Photobiology A: Chemistry, 150, 207-212.

Brezová V., Blazková A., et al., 1997. *Phenol decomposition using Mn+/TiO2 photocatalysts supported by the sol-gel technique on glass fibres.* Journal of Photochemistry and Photobiology A: Chemistry 109(2): 177-183.

Canle M., Fernandez M.I. Martinez C., Santaballa J.A., 2012. *(Re)greening photochemistry: using light for degrading persistent organic pollutants.* Rev. Env. Sci. and Bio-Tec., 11 213-221.

Carp O., Huisman C.L., et al., 2004. *Photoinduced reactivity of titanium dioxide.* Progress in Solid State Chemistry 32(1-2): 33-177.

Chen Q., W.H. Ma., Chen C. C., Ji, H. W. Zhao, J. C., 2012. *Anatase TiO_2 mesocrystals enclosed by (001) and (101) facets: Synergistic effects between Ti^{3+} and facets for their photocatalytic performance.* Chem. Eur. J., , 18, 12584-12589.

Cheng Y., Sun H., Jin W., Xu N., 2007. *Photocatalytic degradation of 4-chlorophenol with combustion synthesized TiO_2 under visible light irradiation*. Chem. Eng. J. 128, 127-133.

Choi W., Termin A., et al., 2002. T*he role of metal ion dopants in quantum-sized tio2: correlation between photoreactivity and charge carrier recombination dynamics.* The Journal of Physical Chemistry 98(51): 13669-13679.

Choina J., Duwensee H., Flechsig G.U., Kosslick H., Morawski A.W., Tuan V.A., Schulz A., 2010. *Removal of hazardous pharmaceutical from water by photocatalytic treatment.* Cent. Eur. J. Chem., 8, 1288–1297.

Chung Y.C., Chen C.-Y., 2009. *Degradation of azo dye reactive violet 5 by TiO2 photocatalysis.* Environ. Chem. Lett. 7, 347–352.

Chu W., Choy W.K., So T.Y., 2007. *The effect os solution pH and peroxide in the TiO_2-induced photocatalysis of chlorinated aniline*. J. of Haz. Materials 141, 86-91.

Cong Y., Chen F., Zhang J., Anpo M., 2006. *Carbon and Nitrogen-codoped TiO2 with High Visible Light Photocatalytic Activity*. Chemistry Letters, 35, 800-801.

Cornish B., Lawton L.A., Robertson P.K.J., 2000. *Hydrogen peroxide enhaced photocatalytic oxidation of microstyn-LR using titanium dioxide.* Applied Catalyssis B: Environment 25, 59-67.

Dalrymple O.K., Isaacs W., Stefanakos E., Trotz M.A., Goswami D.Y., 2011. *Lipid vesicles as model membranes in photocatalytic disinfection studies*. J. Photochem. Photobiol. A, 221, 64–70.

Davezza M., Fabbri D., Pramauro E., Prevot A.B., 2013. *Photocatalytic degradation of chlorophenols in soil washing wastes containing Brij 35. Correlation between the degradation kinetics and the pollutant-micelle binding.* Env. Sci. and Poll. Res., 20, 5, 3224-3231.

de S. e Silva Paula Tereza, Locatelli Marco A.F., Jardim Wilson F., Neto Benìco B., da Motta Mauricio, de Castro Gabriela Ribeiro, da Silva Valdinete Lins, 2008. *Endogeneus iron as photo-Fenton reaction catalyst for the degradation of PAH's in soils*. Journal of the Brazilian Chemical Society, vol.19 no.2.

D.Lgs 3/04/2006, n. 152, in material di "Valori limite di conc. nel suolo e nel sottosuolo", Parte IV, Vol. V, All. 5 (Tab. 1).

Demeestere K., Dewulf J., De Witte B., Beeldens A., Van Langenhove H., 2008. *Heterogeneus photocatalytiv removal of toluene from air on building materials enriched with TiO2*. Build. and Environ. 43, 406-414.

Deveau. P.A., Arsac F., Thivel P.X., Ferronato C., Delpech F., Chovelon J.M., Kaluzny P., Monnet C., 2007. *Different methods in TiO2 photodegradation mechanism studies: Gaseous and TiO2-adsorbed phases*. J. Haz. Mater. 144, 692-697.

Dias M.G., Azevedo E.B., 2009. *Photocatalytic decolorization of commercial acid dyes using solar irradiation*. Water Air Soil Pollut., 204, 79–87.

Dong D. [a], Li P., Li X., Xu., Gong D., Zhang Y., Zhao Q., Li P., 2010. P*hotocatalytic degradation of phenanthrene and pyrene on sil surfaces in the presence of nanometer rutile TiO2 under UV-irradiation*. Chem. Eng. J., 158, 378-383.

Dong D. [b], Li P., Li X., Zhao Q., Zhang Y., Jia C., Li P.,2010. *Investigation on the photocatalytic degradation of pyrene on soil surfaces using nanometer anatase TiO2 under UV irradiation*. J. Haz. Mater. 174, 859-863.

Dvoranová D., Brezová V., et al., 2002. *Investigations of metal-doped titanium dioxide photocatalysts.* Applied Catalysis B: Environmental 37(2): 91-105.

Echavia G.R.M., Matzusawa F., Negishi N., 2009. *Photocatalytic degradation of organophosphate and phosphonoglycine pesticides using TiO2 immobilized on silica gel*. Chemosphere, 76, 595–600.

Egerton T.A., Purnama H., 2014. *Does hydrogen peroxide really accelerate TiO_2 UV-C photocatalyzed decolouration of azo-dyes such as Reactive Orange 16?*. Dyes and Pigments 101, 280-285.

Esparza P., Borges M.E., Diaz L., Alvarez-Galvan M.C., Fierro J.L.G., 2010. *Photodegradation of dye pollutants using new nanostructured titania supported on volcanic ashes*. Appl. Catal. A , 388, 7–14.

Fabbri D., Bianco Prevot A., Zelano V., Ginepro M., Pramauro E., 2008. *Removal and degradation of aromatic compounds from a highly polluted site by coupling soil washing with photocatalysis*. Chemosphere 71, 59-65.

Fabbri D., Crime A., Davezza M., Medana C., Baiocchi C., Bianco Prevot A., Pramauro E., 2009. *Surfactant-assisted removal of swep residues from soil and photocatalytic treatment of the washing wastes*. Applied Catalysis B: Environmental, 92, 318-325.

Fenoll J., Flores P., Hellin P., Hernandez J., Navarro S., 2014. *Minimization of methabenzthiazuron residues in leaching water using amended soils and photocatalytic treatment with TiO_2 and ZnO*. J. Env. Sci. China, Vol. 26, 4, 757-764.

Fenoll J., Sabater P., Navarro G., Vela N., Perez-Lucas G., Navarro S., 2013. *Abatement kinetics of 30 Sulfonylurea herbicide residues in water by photocatalytic treatment with semiconductor materials.* J. Env. Manag., 130, 361-368.

Gan S., Lau E.V., Ng H.K., 2009. *Remediation of soils contaminated with polycyclic aromatic hydrocarbons (PAHs).* J. Haz. Mater., 172, 532-549.

Ghaly M.Y., Jamil T.S., El-Seesy I.E., Souaya E.R., Nasr R.A., 2011. *Treatment of highly polluted paper mill wastewater by solar photocatalytic oxidation with synthesized nano TiO2*. Chem. Eng. J., 168, 446–454.

Giraldo A.L., Penuela G.A., Torres-Palma R.A., Pino N.J., Palominos R.A., Mansilla H.D., 2010. *Degradation of the antibiotic oxolinic acid by photocatalysis with TiO2 in suspension.* Water Res., 44, 5158–5167.

Graham D., Kisch H., Lawton L.A., Robertson P.K.J., 2010. *The degradation of microcystin-LR using doped visible light absorbing photocatalysts*. Chemosphere, 78, 1182–1185.

Hamerski M., Grzechulska J., Waldemar Morawski A., 1999. *Photocatalytic purification of soil contaminated with oil using modified TiO2 powders*. Solar Energy Vol. 66, No. 6, 395-399.

Hanzhong J., Zhao J., Fan X., Dilimulati K., Wang C., 2012. *Photodegradation of phenanthrene on cation-modified clays under visible light*. Applied Catalysis B: Environmental 2012, 123-124, 43-51.

Hapeshi E., Achilleos A., Vasquez M.I., Michael C., Xekoukoulotakis N.P., Mantzavinos D., Kassinos D., 2010. *Drugs degrading photocatalytically: Kinetics and mechanisms of ofloxacin and atenolol removal on titania suspensions*. Water Res., 44, 1737–1746.

Herrmann J. M., Tahiri H., et al., 1997. *Characterization and photocatalytic activity in aqueous medium of TiO2 and Ag-TiO2 coatings on quartz"* Applied Catalysis B: Environmental 13(3-4): 219-228.

Higarashi M., Jardim W.F., 2002. *Remediation of pesticide contaminated soil using TiO2 mediated by solar light*. Catalysis today, 76, 201-207.

Huang X., Wang H., Yin S., Chen X., Chen W., Yang H., 2009. *Sterilization system for air purifier by combining ultraviolet light emitting diodes with TiO2*. Wiley Interscience.

Ioannou L.A., Hapeshi E., Vasquez M.I., Mantzavinos D., Fatta-Kassinos D., 2011. *Solar/TiO2 photocatalytic decomposition of beta-blockers atenolol and propranolol in water and wastewater.* Sol. Energy, 85, 1915–1926.

ISPRA, 2011. *Procedura per l'analisi degli idrocarburi > C_{12} in suoli contaminati*. Manuali e linee guida n. 75/2011.

Kaneko M., Okura I., 2002. *Photocatalysis: Science and Technology,* Springer.

Karaka G., Tasdemir Y., 2013. *Effects of temperature and photocatalysts on removal of polycyclic aromatic hydrocarbons (PAHs) from automotive industry sludge*. Polycyclic aromatic compounds, 33, 380-395.

Karaca G. [a], Tasdemir Y., 2014. *Application of various methods for removal of polycyclic aromatic hydrocarbons from synthethic solid matrices*. Envir. Tec. J. Vol 35, 14, 1840-1850.

Karaka G. [b], Cindoruk S.S. Tasdemir Y., 2014. *Migration of polycyclic aromatic hydrocarbons (PAHs) in urban treatment sludge to the air during PAH removal applications*. J. of air & waste management association Vol.64, 5, 568-577.

Karam F.F., Hussein F.H., Baqir S.J., Halbus A.F., Dilelrt R., Bahnemann D., 2014. *Photocatalyitic Degradation of Anthracene in Closed System Reactor*. Int. J. of Photoenergy, Art. 503825.

Kim B., Murayama M., Colman B.P., Hochella M.F., 2012. *Characterization and environmental implications of nano-and larger TiO_2 particles in sewage sludge, and soils amended with sewage sludge*. J. Env. Monit.m 14, 1129-1137.

Keshmiri M., Troczynski T., Mohseni M., 2006. *Oxidation of gas phase trichloroethylene and toluene using composite sol-gel TiO2 photocatalytic coatings*. J. Haz. Mater. B128, 130-137.

Lazar A.M., Varghese S., Nair S.S., 2008. *Photocatalytic Water Treatment by Titanium Dioxide: Recent Updates;* Catalysts, 572-601.

Li F.B., Chen J.J., Liu C.S., Dong J., Liu T.X., 2006. *Effect of iron oxides and carboxylic acids on photochemical degradation of bisphenol-A*. Biol. Fertil. Soils, 42, 409-417.

Li F.B., Li X.Z., Liu C.S., Liu T.X., 2007. *Effect of alumina on photocatalytic activity of iron oxides for bisphenol-A degradation*. J. Haz. Mater., 149, 199-207.

Li G.Z., Park S., Kang D.W., Krajmalnik-Brown R., Rittmann B.E., 2011. *2,4,5-trichlorophenol degradation using a novel TiO2-coated biofilm carrier: Roles of adsorption, photocatalysis, and biodegradation*. Environ. Sci. Technol., 45, 8359–8367.

Li W., Guo C., Su B., Xu J., 2012. *Photodegradation of four fluoroquinolone compounds by titanium dioxide under simulated solar light irradiation*. J. Chem. Technol. Biotechnol., 87, 643–650.

Licciulli A., Rocca A., Leopardi A., 2006. *Materiali foto catalitici;* Università di Salento.

Lin Y.X., Ferronato C., Deng N.S., Chovelon J.M., 2011. *Study of benzylparaben photocatalytic degradation by TiO2*. Appl. Catal. B, 104, 353–360.

Lopez L., Daoud W.A., Dutta D., 2010. *Preparation of large scale photocatalytic TiO2 films by the sol-gel process*. Surf. Coat. Technol., 205, 251–257.

Lopez-Vasquez A., Ramirez L.N., Benavides-Contreras E., Lopez-Vasquez R., 2013. *Photocatalytic reduction of hexavalent chromium in contaminated soil.* World Congress on Engineering and Computer Science, Vol. II, 632-635.

Medana C., Calza P., Dal Bello F., Raso E., Minero C., Baiocchi C., 2011. *Multiple unknown degradants generated from the insect repellent deet by photoinduced processes on TiO2*. Journal of Mass Spectrometry, 46, 24–40.

Meliàn E.P., Dìaz Gonzàles O., Rodrìguez Dona J.M., Arana J.,Pena P., 2013. *Adsorption and photocatalytic degradation of 2,4.dichlorophenol in TiO_2 suspensions. Effect of hydrogen peroxide, sodium peroxodisulphate and ozone*. Applied Castalysis A: General 455, 227-233.

Ministry of transportation, Ontario. *Ontario's transportation technologies transfer digest* – Summer 2011 – Vol.17, Isuue 3.

Miranda-Garcia N., Maldonado M.I., Coronado J.M., Malato S., 2010. *Degradation study of 15 emerging contaminants at low concentration by immobilized TiO2 in a pilot plant*. Catal. Today, 151, 107–113.

Miranda-Garcia N., Suarez S., Sanchez B., Coronado J.M., Malato S., Maldonado M.I., 2011. *Photocatalytic degradation of emerging contaminants in municipal wastewater treatment plant effluents using immobilized TiO2 in a solar pilot plant.* Appl. Catal. B, 103, 294–301.

Mohseni M., 2005. *Gas phase trichloroethylene (TCE), photooxydation and byproduct formation: photolysis vs. titania/silica based photocatalysis*. Chemosphere 59, 335-342.

Moon J., Takagi H., et al., 2001. *Preparation and characterization of the Sb-doped TiO2 photocatalysts.* Journal of Materials Science 36(4): 949-955.

Moulis F., Krysa J., 2013. *Photocatalytic degradation of several VOC's (h-hexane, n-butyl acetate and toluene) on TiO2 layer in a closed-loop reactor*. Catalysis today, 209, 153-158.

Noguchi D., Kawamata Y., Nagatomo T., 2005. *The Response of TiO_2 Photocatalysts Codoped with Nitrogen and Carbon to Visible Light.* The Electrochemical Society, 152, 9, D124-D129.

Obee T. N., Brown R. T., 1995. *TiO2 photocatalysis for indoor air applications: Effect of humidity and trace contaminant levels on the oxidation rate of formaldehyde, toluene, and 1,3-butadiene*. Environ Sci Technol 29: 1223-1231.

Palanivelu K., Im J.S., Lee Y.S., 2007. *Carbon Doping of TiO2 for Visible Light Photo Catalysis - A review*. Carbon science, 8, 3, 214-224.

Pelentridou K., Stathatos E., Karasali H., Lianos P., 2009. *Photodegradation of the herbicide azimsulfuron using nanocrystalline titania films as photocatalyst and low intensity black light radiation or simulated solar radiation as excitation source*. J. Hazard. Mater., 163, 756–760.

Pereira J., Vilar V.J.P., Borges M.T., Gonzalez O., Esplugas S., Boaventura R.A.R., 2011. *Photocatalytic degradation of oxytetracycline using TiO2 under natural and simulated solar radiation*. Sol. Energy, 85, 2732–2740.

Pichat P., Disdier J., Hoang-Van C., Mas D., Goutailler G., Gaysse C., 2000. *Purification/deodorization of indoor air and gaseous effluents by TiO2 photocatalysis*. Catalysis today 63, 363-369.

Qiu Z.P., Yang Q.C., Liu W.K., 2013. *Photocatalytic degradation of phytotoxic substances in waste nutrient solution by various immobilized levels of nano-TiO_2*. Water and soil pollution, 224, 2, 1461.

Qourzal S., Barka N., Tamimi M., Assabbane A., Nounah A., Ihlal A., Ait-Ichou Y., 2009. *Sol-gel synthesis of TiO2-SiO2 photocatalyst for beta-naphthol photodegradation*. Mater. Sci. Eng. C, 29, 1616–1620.

Radjenovic J., Sirtori C., Petrovic M., Barcelo D., Malato S., 2009. *Solar photocatalytic degradation of persistent pharmaceuticals at pilot-scale: Kinetics and characterization of major intermediate products*. Appl. Catal. B, 89, 255–264.

Rizzo L., Meric S., Guida M., Kassinos D., Belgiorno V., 2009. *Heterogenous photocatalytic degradation kinetics and detoxification of an urban wastewater treatment plant effluent contaminated with pharmaceuticals*. Water Res, 43, 4070–4078.

Rosenberg I., Brock J.R., Heller A., 1992. *Collection optics of TiO_2 photocatalyst on hollow glass microbeads floating on oil slicks.* J. Phys. Chem., 96, 3423-3428.

Sà da Rocha Otidene Rossiter, Dantas Renato F., Bezerra Duarte Matra M.M., Lima Duarte Màrcia Maria., da Silva Valdinete Lins., 2012. *Remediation of petroleum contaminated soil by photo-Fenton process applying black, white and germicidal light*. Universidade Federal de Pernambuco.

Saien J., Ojaghloo Z., Soleymani A.R., Rasoulifard M.H., 2011. *Homogeneous and heterogeneous AOPs for rapid degradation of Triton X-100 in aqueous media via UV light, nano titania hydrogen peroxide and potassium persulfate*. Chem. Eng. Journal 167, 172-182.

Sanchez M., Rivero M.J., Ortiz I., 2010. *Photocatalytic oxidation of grey water over titanium dioxide suspensions*. Desalination, 262, 141–146.

Sharma V.K., Triantis T.M., Antoniou M.G., He X.X., Pelaez M., Han C.S., Song W.H., O'Shea K.E., de la Cruz A.A., Kaloudis T., et al., 2012. *Destruction of microcystins by conventional and advanced oxidation processes: A review.* Sep. Purif. Technol., 91, 3–17.

Silverstein R.M.,Francis X. Webster F.X., David J. Kiemle D.J., 2005. *Spectrometric identification of organic compounds.* John Wiley & Sons Inc.

Skoog A.D., Holler J.F., Crouch S.R., 2009. *Chimica analitica strumentale*. Edises.

Teodorescu V. S., Blanchin M.G., et al., 1999. *XTEM study of Al doped TiO2 anatase epitaxial films deposited on MgO by pulsed laser deposition.* Journal of Materials Science 34(22): 5469-5476.

Tobaldi D.M., 2009. *Materiali ceramici per edilizia con funzionalità foto catalitica*.

Triantis T.M., Fotiou T., Kaloudis T., Kontos A.G., Falaras P., Dionysiou D.D., Pelaez M., Hiskia A., 2012. *Photocatalytic degradation and mineralization of microcystin-LR under UV-A, solar and visible light using nanostructured nitrogen doped TiO2*. J. Hazard. Mater., 211, 196–202.

Turchi C.S., Mehos M.S., 1992. *Solar photocatalytic detoxification of groundwater: Developments in reactor design*. Proceedings of the Second International Symposium "Chemical oxidation Technologies for The Nineties" , Vanderbilt University, Nashville, Tennessee, Vol. 2, 301-314 , Technomic Publishing AG, Basel, Switzerland.

Turchi C.S., Kalausner J.F., Goswami D.J., 1993. *Field test results for the solar photocatalytic detoxification of fuel-contaminated groundwater*. Proceedings of the Third International

Symposium "Chemical oxidation Technologies for The Nineties" , Vanderbilt University, Nashville, Tennessee, Vol. 3, 216-224 , Technomic Publishing AG, Basel, Switzerland.

Venkatachalam N., Vinu A., Anandan S., Arabindoo B., Murugesan V., 2006. *Visible light active photocatalytic degradation of bisphenol-A using nitrogen doped TiO2.* J. of Nanoscience and Nanotechnology, Vol.6, 2499-2507.

Venny, Gan S., Ng K.H., 2012. *Current status and prospects of Fenton oxidation for the decontamination of persistent organic pollutants (POPs) in soils*. Chem. Eng. Journal, 213, 295-317.

Villa R.D., Trovò A.G., Nogueira R.F.P., 2010. *Soil remediation using a coupled process: soil washing with surfactant followed by photo-Fenton oxidation*. J. Haz. Mater., 174, 770-775.

Wang Y., Cheng H., 1999. *Preparation, characterization and photoelectrochemical behaviors of Fe(III)-doped TiO2 nanoparticles.* Journal of Materials Science 34(15): 3721-3729.

Wang Y., Hong C-S., 1998. *Effect of hydrogen peroxide, periodate and persulfate on photocatalysis of 2-chlorobiphenyl in aqueous TiO_2 suspensions.*Wat. Res. Vol. 33, No.9 2031-2036.

Wang X., Liu C., Li X., Li F., Zhou S., 2008. *Photodegradation of 2-mercaptobenzothiazole in the γ-Fe_2O_3/oxalate suspension under UVA light irradiation*. J. Haz. Mater., 153, 426-433.

Wang Y., Wilkins D.P., Neburchilov V., Song C., Guest A., Zhang J.,2014. *Ta and Nb co-doped TiO_2 and its carbon-hybrid materials for supporting Pt–Pd alloy electrocatalysts for PEM fuel cell oxygen reduction reaction*. J. Mater. Chem. A, 2014,2, 12681-12685.

Xu Q.C., Wellia D.V., Yan S., Liao D.W., Lim T.M., Yang Tan T.T., 2011. *Enhanced photocatalytic activity of C–N-codoped TiO2 films prepared via an organic-free approach*. J. Haz. Mater., 188 (1-3), 172-180.

Xu J., Xin L., Huang T., Chang. K., 2011. *Enhanced bioremediation of oil contaminated soil by graded modified Fenton oxidation*. J. of Env. Science, 23(11), 1873-1879.

Yamashita H., Harada M., et al., 2001. *Application of ion beam techniques for preparation of metal ion-implanted TiO2 thin film photocatalyst available under visible light irradiation: metal ion-implantation and ionized cluster beam method.* Journal of Synchrotron Radiation 8(2), 569-571.

Yang X.P., Xie L.X., Tang J., Lin J., 2014. *Removal and degradation of phenanthrene and pyrene from soil by coupling surfactant washing with photocatalysis*. Adv.Res in Mat. Sc. and Mech. Eng., PTS 1 and 2, Vol 446-447, 1485-1489.

Yardin G., Chiron S., 2006. *Photo-Fenton treatment of TNT contaminated soil extract solutions obtained by soil flushing with cyclodextrin.* Chemosphere 62, 1395-1402.
Young C., Lim T.M., Chiang K., Scott J., Amal R., 2008. *Photocatalytic oxidation of toluene and trichloroethylene in the gas-phase by metalized (Pt, Ag) titanium dioxide.* Applied Catalysis, 78, 1-10.

Zhang L., Peijun L., Gong Z.Q., Oni Adeola A., 2006. P*hotochemical behavior of benzo[a]pyrene on soil surfaces under UV light irradiation*. J. Env.Sci., 18, 6, 1226-1232.

Zhang L., Peijun L., Zongqiang G., Xuemei L., 2008. *Photocatalytic degradation of polycyclic aromatic hydrocarbons on soil surfaces using TiO2 under UV light.* Journal of Hazardous Materials Volume 158, Issues 2–3, 478–484.

Zhang L., Xu C., Chen Z., Li X., Li P., 2010. *Photodegradaton of pyrene on soil surfaces under UV light irradiation*. J. Haz. Mat. 173, 168-172.

Zhang L., Jia N., Xu C., Li X., 2011. *Photocatalytic degradation of policy clic aromatic hydrocarbons on soil surfaces using Fe_2O_3 under Uv light*. Adv. Mater. Res. Vols. 189-193, 420-423.

Zhang W., Li, Y., Su, Y., Mao, K., Wang, Q., 2012. *Effect of water composition on TiO2 photocatalytic removal of endocrine disrupting compounds (EDCs) and estrogenic activity from secondary effluent*. J. Hazard. Mater., 215, 252–258.

Zhang Y.X., Wang H.T., 2014. *Study of PCP photodegradation by TiO_2 catalyst based on different properties of soil washing effluents*. Selected proceedings of the eight international conference on waste management and technology, Vol. 878, 791-796.

Zhao X., Quan X., Zhao Y.Z., Zhao H.M., Chen S., Chen J.W., 2004. *Photocatalytic remediation of γ-HCH contaminated soil induced by α-Fe_2O_3 and TiO_2*. J. Env. Sci., 16, 6, 938-941.

Zhu X.D., Zhou D., Wang Y., Cang L., Fang G., Fan J., 2012. *Remediation of polychlorinated biphenyl-contaminated soil by soil washing and subsequent TiO2 photocatalytic degradation*. J. Soils Sediments 12:1371–1379.

Zhuang J.D., Dai W.X., Tian Q.F., Li Z.H., Xie L.Y., Wang J.X., Liu P., Shi X.C., Wang D.H., 2010. *Photocatalytic degradation of rhb over TiO2 bilayer films: Effect of defects and their location.* Langmuir, 26, 9686–9694.

Zou L., Luo Y., Hooper M., Hu E., 2006. *Removal of VOCs by photocatalysis process using adsorption enhaced TiO2-SiO2 catalyst*. Chem. Eng. and Process. 45, 959-964.

AKNOWLEDGEMENT

I miei ringraziamenti vanno al Prof. Roberto Raga per la suo interesse a questo lavoro e la sua supervisione e alla Prof.ssa Roberta Bertani per la sua costante disponibilità, i suoi consigli ed il suo aiuto.

Questi ultimi mesi sono stati i più belli di questi 5 anni e questo grazie anche ai mitici Flavio, Fabio e Paolo con i quali ho condiviso mille risate e bei momenti, siete stati unici. Nondimeno, ringrazio i miei indispensabili compagni di laboratorio: la cara Elisa, il comico Riccardo, il super Ivo, la pazza Bianca e la sorridente Ana. Aggiungo alla lista Mirto ed Alessandro.

Il ringraziamento più grande va alla mia Famiglia: Mamma, Papà, Nonna Teresa, Nonno Carlo (anche se non più qui) e Gloria, costantemente presenti. Grazie per il vostro sostegno, la vostra presenza e per avermi permesso di arrivare sino a qui, questo traguardo è anche un vostro successo. Un ringraziamento particolare anche allo Zio Virginio.

Ringrazio ancora la Famiglia Parelli al completo per avermi sempre supportato ed incoraggiato, in particolare la mia cara Francesca, indispensabile compagna di vita negli ultimi 8 anni, senza di te non sarei qui.

Infine ringrazio i miei compagni d'università, Michele e Simone in particolare, i parenti, gli amici, la crew e tutte le persone che hanno accompagnato la mia vita ed hanno contribuito a fare di me la persona che sono.

Vi voglio bene.